63-3-4

LO-TEMP THERMIONIC PLASMA STUDY

FORD INSTRUMENT CO.
DIVISION OF SPERRY RAND CORPORATION
31-10 THOMSON AVE., LONG ISLAND CITY 1, NEW YORK

Contract No. NONR 3416(00)
Task No. NR 099-356

FINAL REPORT
January 31, 1963

POWER BRANCH
OFFICE OF NAVAL RESEARCH
WASHINGTON 25, D.C.

OFFICE OF NAVAL RESEARCH

Contract Nonr 3416(00)

Task No. NR 099-356

FINAL REPORT

LO-TEMP THERMIONIC PLASMA STUDY

FORD INSTRUMENT COMPANY

Division of Sperry Rand Corporation

Long Island City 1, N.Y.

January 31, 1963

FOREWORD

This report was initiated by the Power Branch, Office of Naval Research, Washington 25, D.C. The research and development work upon which this report is based was accomplished by the Nuclear Development Division, Ford Instrument Company, Division of Sperry Rand Corporation, Long Island City, New York, under the Office of Naval Research Contract Nonr 3416(00), Task No. NR 099-356, "Lo-Temp Thermionic Plasma Study."

The research and development was directed by M. Silverberg - Engineering Department Head, and L. L. Haring - Project Supervisor. The bulk of the experiments and theoretical analysis were performed by W. G. Stenzel - Principal Engineer. The electrical circuitry was designed and set up by Walter Oppen - Project Supervisor and M. Cosenza - Senior Engineer. W. Franklin - Principal Engineer, J. McInally - Senior Engineer and R. Mercer - Assistant Engineer were responsible for device fabrications. Commander John J. Connelly Jr. monitored the project for the Power Branch.

ERRATA

LO-TEMP THERMIONIC PLASMA STUDY - FINAL REPORT 1/31/63

CONTRACT NO. Nonr 3416 (00)

TASK NO. NR 099-350

Page	Line	Error	Correction
Cover	9	Final Report	Annual Summary Report
vi	5	velicity	velocity
5	last	1959)	1959))
6	16	cm.$^{-3}$	electrons/cm^3
9	19	Chopman and Hull, Std.	Chapman and Hall, Ltd.
11	3	probe pulse	probe cell
23	Table 9	10^{-13}	10^{+13}
24	Table 10	V = 0.2	V = -0.2
24	Table 11	V = 0.3	V = -0.3
24	Table 12	J -7.0	J = 7.0
34	19	Profits	Profiles
37	Equation 8	add = 2.66 in second line	
42	Equation 1	I ( )	I (ν)
43	Equation 3	$C_2/\lambda T$)	($C_2/\lambda T$)
43	Equation 5	I (T)	I(λ,T)
54	7, 20	Figure 38	Figure 40
62	7	anode-glow	"anode-glow"
65	Equation 12	$\frac{J_p}{J_e} = \frac{(m_p\ T_p)}{(m_e\ T_e)}\ \frac{(T_p)^{1/2}}{(T_e)}$	
	9	cathode	emitter
70	2	$\phi_c-\phi_e-V-JR_p$	$\phi_c=\phi_e-V-JR_p$
71	7, 8	T_c	T_{ec}
74	Equation 4, 5	$e^{e\phi/kT}$	$e^{-e\phi/kT}$
79	11	Cathode	Emitter
80	4	making	taking
Fig. 5		284°C	248°C
Fig. 27		(cup anode, flange anode (cup cathode, cathode	(cup collector, flange collector (cup emitter, emitter

ABSTRACT

Measurements of electron temperature, electron concentration and space potential in the plasma region of low temperature thermionic converters were determined by means of a pulsed Langmuir probe technique. The spatial distributions of these parameters, in parallel plate geometry, were measured with the aid of movable probes within these operating converters. The experimental values are shown to be consistant with reasonable physical models.

Spectroscopic measurements were made in both the visible and infrared regions and the validity and applicability of the results are discussed.

Results obtained from converters, in which small amounts of oxygen were present in the discharge region, are explored. The effects of cesium and "patch effects" on the surface characteristics of impregnated tungsten emitters are discussed on the basis of a theoretical analysis and experimental results with numerous test cells.

NOMENCLATURE

A	Richardson constant
A_{nj}	Einstein coefficient of spontaneous emission
α	Ionization coefficient
a_o	Smallest Bohr radius
C_1	First radiation constant
C_2	Second radiation constant
c	Velocity of light
d	Random distance travelled by electron
E	Electron Field strength
E_n	Energy of excited level
e	Charge on electron
F	Helmholtz free energy
f_i	Fractional area of spot i
f_{nj}	Oscillator strength
g_j	Statistical weight of state j
h	Planck's constant
I_c	Collector current
I_s	Saturation current
I_{nj}	Intensity of emitted line
J	Output current density
J_e	Emitter current density
J_p	Ion current density
J_ϵ	Electron current density
k	Boltzmann's constant
L	Mean free path of electrons

NOMENCLATURE (cont'd)

ℓ	Length of Discharge
M_a	Mass of atom
m	Mass of electron
m_p	Mass of ion
N_n	Concentration of atoms in excited state n
N_e	Concentration of atoms in ground state
n_m	Quantum number
p	Pressure
R_L	Load resistance
R_p	Plasma resistance
r	Reflection coefficient
S	Area of emitting surface
T	Absolute temperature
T_c	Collector temperature
T_e	Emitter temperature
T_{ex}	Excitation temperature
T_g	Gas temperature
T_p	Ion temperature
T_ϵ	Electron temperature
t_{cs}	Cesium temperature
V	Output potential
V_c	Collector sheath potential
V_d	Potential difference between surfaces of emitter and collector
V_e	Emitter sheath potential
V_{ext}	Externally applied potential

NOMENCLATURE (cont'd)

V_i	Ionization potential
V_m	Minimum potential in emitter sheath
V_p	Plasma potential drop
V_{sp}	Space potential
$\bar{v}$	Average random electron velicity
v_d	Electron drift velocity
α	Temperature coefficient of work function
$\alpha(\lambda,T_c)$	Absorptivity
$\epsilon(\lambda,T_e)$	Emissivity
λ	Wavelength
μ	Chemical potential
$\bar{\mu}$	Electrochemical potential
ν_{nj}	Frequency of emitted light
ρ_p	Ion concentration
ρ_ϵ	Electron concentration
$\bar{\Phi}$	Electrostatic potential
ϕ_c	Collector work function
ϕ_e	Emitter work function

TABLE OF CONTENTS

TABLE OF CONTENTS (cont'd)

LIST OF ILLUSTRATIONS

Figure

LIST OF ILLUSTRATIONS (cont'd)

Figure

SECTION 1. PURPOSE OF INVESTIGATION

In order to improve the operating characteristics of the low temperature cesium vapor thermionic converter and to find possible avenues leading to better devices, it is necessary to understand the conditions actually prevailing within the body of the discharge, and to uncover the physical mechanisms governing these conditions. A complete understanding of the converter also requires knowledge of conditions prevailing at or near the surface of the emitter and the collector during, before, and after operation. In addition, a smaller level of effort was directed at determining the effects of additives (in particular, oxygen) on the operation of the low temperature thermionic converter.

The present investigation was undertaken to shed light on some of the above problems. In particular, the following areas were studied:

a. The space potentials, electron temperatures, and electron concentrations within the body of the discharge under various modes of operation of a pure cesium vapor device.

b. The effect on performance of adding oxygen to the system.

c. The variation of the work functions of the emitter material with temperature and with cesium vapor pressure.

d. The amount of patchiness and its effect on the emitter material (i.e., impregnated tungsten).

e. Finally a useful physical model was to be suggested on the basis of the results of this investigation.

SECTION 2. SUMMARY OF RESULTS

2.1 Specific Program Accomplishments

1. The first and only reported measurements of the spatial variation of electron temperature, electron concentration, and space potential were accomplished in an operating and practical thermionic plasma diode. These were achieved with a movable Langmuir probe utilizing pulse techniques in both hard glass and metal ceramic constructions.

2. Spectrographic studies were carried out in the infrared as well as the visible region of the emitted spectrum. The value of such measurements for determining plasma characteristics is analyzed in detail.

3. Theoretical models of the originally puzzling ultra low voltage arc in cesium are developed and verified on the basis of a mechanism which maintains adequate ion generation for space charge neutralization.

4. It was demonstrated that the plasma in a wide spacing converter spills over beyond the limits of the emitter, thus providing a ratio of collector to emitter greater than one, a factor which results in increased performance.

5. The dependance of the impregnated tungsten emitter work function on temperature and cesium pressure is demonstrated and explained thermodynamically.

2.2 Conclusions

1. The discharge is shown to consist of three distinct regions. The first is the emitter sheath where the electrons are accelerated to energies sufficient to provide neutralizing ions , the second is the plasma region where the positive and negative charge densities are essentially equal

and the third is the collector sheath where there is a decelerating field.

2. In the plasma region of an operating low temperature thermionic converter, the electron distribution is definitely of the Maxwell-Boltzmann type. The average electron temperature along the axis of the plasma lies between 5000 and 8000°K. The higher value is obtained with small area emitters (3 mm diameter) while the lower value is obtained with an emitter with a diameter of 0.25".

3. The apparent electron temperature drops in the radial direction outward from the axis. The drop is larger for smaller emitters so that outside the luminous region the apparent electron temperature is about 4000°K for all emitter sizes.

4. If the current density is increased above the value corresponding to maximum power output there is an increase in electron concentration as is expected from the developed flow equation.

5. Spectrographic techniques are useful only for obtaining distribution of excited cesium energy levels in the discharge. Theoretically these distributions could be related to electron distributions, but such correlation requires exact knowledge of the magnitude of electron-atom excitation cross-sections which is not available at present. The results verify that the original emphasis on probe techniques was well justified due to the limited value of the spectrographic determination of electron temperature from an assumed maxwellian distribution of excited states.

6. The required ionization level can be explained by single collision process with the high energy tail of the electron distribution in conjunction with molecular ionization enhanced by "radiation entrapment" phenomena.

7. The variation of emitter work function with temperature and cesium pressure corresponds very well with known theoretical mechanisms.

SECTION 3. EXPERIMENTAL SECTION

3.1 SELECTION OF METHOD OF MEASUREMENT

Various methods have been used for obtaining plasma data. Three that have possible application are:

a. Spectrographic techniques

b. Microwave methods

c. Langmuir probes

The advantages and disadvantages of these experimental methods were studied in order to select a technique best suited for the present purposes. Spectrographic techniques are theoretically capable of measuring electron and gas temperatures, and electron concentrations without disturbing the discharge itself. In long column discharges spatial distribution of the quantities can also be obtained. These measurements depend on two basic phenomena: first, the population of excited states in a gas depends on the temperature (i.e., the total internal energy); second, the free electron concentration perturbs the discharge thus widening the width of a given emission line.

It can be seen that these measurements require the use of a spectrograph that has sufficient resolution to isolate individual emission lines and to accurately show their width, that then gives the absolute as well as the relative intensities of each line, that covers the spectral region covering the lines of interest. For short period discharges or discharges of rapidly varying intensity, only an optical spectrograph can be used; for steady discharges, a scanning spectrograph is more convenient and gives rapid accurate results. However, the most valid equations used in interpreting spectrographic data depend on the existence of "local thermal equilibrium," (i.e., the electron, ion and gas temperatures must be essentially equal (J. M. Somerville, The Electric Arc, Wiley, 1959). This condition prevails in high-pressure arcs, but

in low-pressure arcs the electron temperature is much higher than the gas or ion temperature; hence, spectrographic data become difficult to interpret without the use of rather extreme assumptions. Also, spectrographic data do not permit the determination of space potentials or electron distribution functions.

Microwave techniques are used for determining electron concentration in plasmas. In general, these methods require that the plasma be confined in a cavity of known dimensions; but a more recent method, permits the measurements to be carried out essentially at definite points (Levitskii and Shasharin, Soviet Physics-Technical Physics 6; 315, 1961). This method measures the dielectric constant of a plasma with the aid of a shorted transmission line, the bare end of the line being inserted at the required point. The resonant frequencies of a definite length of the line depend on the dielectric constant which in turn is determined by the plasma concentration. Measurements have been carried out in the 3 cm. and the 10 cm. regions. The 3 cm. microwaves gives better agreement with Langmuir probe results. Densities from 10^{10} to 10^{13} cm. $^{-3}$ can be measured.

Finally, the Langmuir probe (G.E. Rev. 27: 449, 538, 1924 G.E. Rev. 28: 727, 1926) can be applied to plasmas which do not have a very high gas or ion temperature (i.e., low pressure discharges). The probe essentially consists of a thin insulated wire with the bare end inserted into the plasma. A positive potential is applied to the probe, and the current drawn is measured. The "probe characteristic" is a semilogarithmic plot of the probe current vs. the potential applied to the probe. In general, this characteristic consists of a straight line which has a distinct break at a definite value of the potential. At this break saturation electron current is drawn since the probe potential is then equal to the plasma potential. The slope of the characteristic is equal to $\frac{5034}{T_e}$, where T_e is the electron "temperature" in degrees Kelvin.

The electron current density is equal to $\rho_\epsilon e \sqrt{\frac{kT}{2\pi m}}$, where ρ_ϵ is the electron concentration, e and m the charge and mass of an electron, respectively and k the familiar Boltzmann constant. Thus, the probe characteristic permits the determination of the space potential, the electron temperature, and the electron concentration at the point where the end of the probe is inserted.

Furthermore, if the characteristic is strictly rectilinear, the electron distribution is completely Maxwellian. The "electron temperature" is the equivalent electron temperature corresponding to a Maxwellian distribution. If the characteristic is not a straight line, Druyvesteyn (Z. Phys. 64: 781, 1930) has shown that the actual electron distribution can be obtained by an appropriate numerical integration. Medicus (J. Ap. Phys. 27: 1242, 1956) has developed a particularly simple method for performing this integration.

It was concluded that the method that could obtain the maximum information from our low temperature low voltage arc was the Langmuir probe technique. Spectrographic techniques were also utilized with due regard for the assumptions of interpretation.

3.2 LANGMUIR PROBE METHOD

Once the Langmuir probe method was chosen as the principal tool it was necessary to select the best technique for recording the data. The simplest way is to apply a DC voltage to the probe and record the probe current with an ammeter. However, the surface of the probe can become contaminated by substances evaporated from the emitter during the measurement. This changes the work function of the probe material; thus the contact potential

between emitter and probe. Since the probe potential must be corrected by the contact potential to determine the absolute potential, serious errors may occur. This is particularly true when using impregnated tungsten emitters that evaporate large amounts of barium. Some investigators have overcome this problem by cleaning the probe by electron bombardment before each dc measurement. Such a technique is very tedious and does not completely eliminate the problem since contamination can occur during the several seconds required for each dc measurement.

Waymouth (J. Ap Phys. 30; 1404, 1956) has developed a special method in which a large positive triangular pulse is applied at intervals to a probe maintained at a potential of -45 volts with respect to the emitter. During the off-pulse time the probe is kept clean by ion bombardment. The total pulse is applied for adjustable periods in the microsecond ranges at intervals of 1/60 of a second. Since the probe is thus positive for only a few microseconds, little contamination can occur during the measurement. Brodie, Jenkins and Trodden (J. Elect. and Control 6: 149, 1959) have shown that an impregnated tungsten emitter give off less than 0.8 monolayer of barium per second at 1500°K (the normal operating temperature). Thus in 2 microseconds at most 1.6×10^{-6} monolayers of barium can evaporate from the emitter and be deposited on the probe surface.

If we consider the cesium impinging on the probe, the flux, $\frac{\bar{n}\bar{v}}{4}$, is equal to about 10^{22} atoms per m^2 per second. Thus, during the time the probe is positive, about 2×10^{16} atoms of cesium will impinge on 1 m^2 of the probe. Since a monotomic layer of cesium is about 5×10^{18} atoms per m^2, only .004 monolayer could be deposited on the probe during this period.

Thus, Waymouth's method for obtaining probe characteristics was adopted for our studies. The I-V characteristics of the probe can be displayed on an oscilloscope and a picture can be made rapidly and studied at leisure. It must be noted that it is an integral part of Waymouth's circuitry that the emitter be grounded and thus all voltages are measured with respect to the emitter.

The Waymouth method was particularly well suited for use in our experiments. In the experiments with glass cells an electrically heated emitter was employed and it was necessary to make all measurements when no voltage was applied to the heater. The heater was thus energized with a half-wave a-c current and the probe pulse was applied during the off-cycle. The relationships are shown in Figure 1.

In addition, the method makes possible the measurement of the contact potential between the probe and emitter surfaces under actual operating conditions. None of the other standard methods of measuring contact potential potential which were considered (i.e., the Kelvin method, the Zisman method, the intersection method or the magnetic method), offer this advantage. (Herrmann and Wagener, The Oxide-Coated Cathode, Vol. 2, p.82, Chopman and Hull, Std., London, 1951).

3.3 EXPERIMENTAL RESULTS WITH LANGMUIR PROBES

In order to test the applicability of and gain experience with the Waymouth technique as well as to obtain useful preliminary results, the first test cells built were made with fixed probes. All the probes used in the present investigation consisted of .015 inch diameter tungsten wire insulated by a thin layer of glass (.005 inch). The end of the probe was ground flat to expose a plane section of the wire. As mentioned in the

previous section, all voltages are measured with respect to the emitter.

Fixed Probes. The first probe tube was TC-94. The base assembly is shown in Figure 2. The probe extends in from the radial direction and the end is situated about half-way between the emitter and the collector. The total pulse width was varied from several microseconds up to 20 microseconds. No significant difference in the results were observed; hence, the widest pulse was used in all subsequent tests because it gave the least difficulty in obtaining reproducible traces. Some results were obtained with this tube by operating at the minimum collector-emitter voltage possible. These results are given in Table 1.

Table 1. RESULTS WITH TC-94

Cesium Temperature, t_{cs} °C	Emitter Temperature T_e °K'	Electron Temperature T_e °K	Electron Concentration ρ_e cm^{-3}
190	1280	14,100	4.6×10^{12}
190	1450	17,100	6.4×10^{11}
210	1220	13,600	1.1×10^{13}
210	1270	15,600	6.5×10^{12}
210	1420	17,600	6.6×10^{11}

Several probe tubes were made with a longitudinal probe passing through the collector (Figure 3). Some trouble was encountered with glass melting or splitting from the probe. Attempts were made to spray coat the probe with alumina using jet-spray methods. Although it was possible to obtain a uniform white coating, this coating did not exhibit a good adhesion to the base metal. Also, it was too brittle to hold the probe wire with the necessary

rigidity. The probes used in the latter tests with glass cells were coated with a uniform coating of uranium glass and no trouble was encountered.

Fixed probe pulse TC-106 was used to obtain characteristics at different operating conditions. Table 2 gives the results obtained at various cesium pressures with the emitter maintained at 1500°K. Table 3 gives the results with the emitter maintained at 1450°K. Figures 4 and 5 reproduce the probe characteristics corresponding to these measurements. The origin of the probe voltage axis is displaced for each curve so that the characteristics are clearly separated to show their properties.

Table 2.

RESULTS WITH FIXED PROBE CELL TC-106

T_e = 1500°K

Cesium Temp.	Output Potential	Externally Applied Potential	Output Current Density	Probe Measurements		
				Space Potential	Electron Temp.	Electron Conc.
t_{Cs} °C	V volts	V_{ext} volts	J amps/cm^2	V_{sp} volts	T_ϵ °K	ρ_ϵ cm^{-3}
203	-	1.4	2.1	3.0	13,600	1.51×10^{12}
228	-	0.06	2.4	0.4	10,100	1.21×10^{12}
248	0.07	-	2.3	0.1	9,300	1.31×10^{12}

Table 3

RESULTS WITH FIXED PROBE CELL TC-106

T_e = 1450°K

Cesium Temp.	Output Potential	Externally Applied Potential	Output Current Density	Probe Measurements		
				Space Potential	Electron Temp.	Electron Conc.
t_{Cs} °C	V Volts	V_{ext} volts	J amps/cm^2	V_{sp} volts	T_ϵ °K	ρ_ϵ cm^{-3}
203	-	1.4	1.8	2.4	11,600	0.95×10^{12}
228	-	0.3	4.8	0.6	10,100	1.22×10^{12}
248	-	0.3	8.5	0.1	9,500	1.19×10^{12}

Because of a poisoned emitter the test cell had a rather low activity; its saturation current density was below 1 amp/cm^2. Only one of the measurements was made with an output voltage actually present (Cs temp. 248°C, T_e 1500°K). The other measurements were made with the minimum applied voltage required to sustain the discharge. The discharge under these conditions always consisted of a purplish glow within a cylindrical volume extending longitudinally from close to the emitter up to the collector and with a diameter approximately equal to that of the emitter surface (0.3 cm.).

The end of the probe was inserted into the center of the discharge and thus all the probe data refer to this point. Under the normal operating conditions (t_{cs} 200°C, T_e 1500°K), the measured space potential was 1.6 volts more positive than the supply potential. The measured electron temperature of 13,600°K corresponds to an average accelerating voltage of 1.2 volts. An increase in cesium pressure improved the activity, permitting the supply voltage to be lowered. This is to be expected since the cesium coverage of the emitter will increase and thus lower the work function. The space potential drops almost to zero at the point of measurement. The electron temperatures also drop, but an accelerating voltage of at least 1 volt must be present in front of the emitter since the measured electron temperatures remain close to 10,000°K. The electron concentrations seem to remain fairly constant at about 10^{12} electrons per cm^3.

Lowering the emitter temperature by 50°K does not affect the results greatly except to reduce the performance of the cell somewhat, as is to be expected. This reduced performance is exhibited in either a lower output current or a higher external voltage required to maintain the discharge.

Otherwise the results are not significantly different than at the normal emitter temperature.

The actual probe characteristics shown in figures 4 and 5 all have one very significant feature: the characteristic is a straight line in every case. This shows that, within the limits of the measurement accuracy, the electron distributions at the center of the discharge were strictly maxwellian. This shows that the electron velocities have become completely randomized, "thermalized", at this position which also shows that the concept of "electron temperature" is very valid in all these measurements.

ADJUSTABLE PROBES:

Table 4.

Results with a movable probe (Run A) - TC-158

T_e = 1500°K V = .10 volt
t_{Cs} = 192°C J = 4.2 amps/cm^2

Distance from cathode inches	Space Potential V_{sp} volts	Electron temp. T_e °K	Electron conc. ρ_e cm^{-3}
.029	1.30	10,400	0.35×10^{13}
.043	1.23	8,900	0.68×10^{13}
.057	1.30	8,350	0.84×10^{13}
.072	1.48	8,050	0.63×10^{13}
.086	1.33	6,500	0.58×10^{13}
.100	1.25	6,150	0.54×10^{13}

Table 5

RESULTS WITH A MOVABLE PROBE (RUN B) - TC-158

T_e = 1500°K V = .13 volt

t_{Cs} = 193°C J = 4.2 amps/cm^2

Distance from cathode inches	Space Potential V_{sp} volts	Electron temp. T_ϵ °K	Electron conc. ρ_{ϵ} cm^{-3}
.029	1.05	8,800	0.51×10^{13}
.043	1.10	7,600	1.09×10^{13}
.057	1.10	6,800	1.03×10^{13}
.072	1.10	6,500	0.91×10^{13}
.086	1.05	6,400	0.71×10^{13}
.100	0.98	5,500	0.69×10^{13}

Table 6

AVERAGE RESULTS WITH A MOVABLE PROBE TC-158

T_e = 1500°K V = 0.12 ± .02 volt

t_{Cs} = 195 ± 3°C J = 4.5 ± 0.3 amps/cm^2

Distance from cathode inches	Space Potential V_{sp} volts	Electron Temp. T_ϵ °K	Electron Conc. ρ_{ϵ} cm^{-3}
.029	1.50 ± 0.33	9,700 ± 600	$.47 \pm .06 \times 10^{13}$
.043	1.37 ± 0.27	8,500 ± 500	$.84 \pm .16 \times 10^{13}$
.057	1.36 ± 0.21	7,900 ± 700	$.91 \pm .08 \times 10^{13}$
.072	1.41 ± 0.16	7,700 ± 600	$.78 \pm .10 \times 10^{13}$
.086	1.42 ± 0.20	6,400 ± 100	$.65 \pm .05 \times 10^{13}$
.100	1.31 ± 0.19	5,600 ± 400	$.57 \pm .08 \times 10^{13}$

The results given in tables 4, 5 and 6, were obtained with a fairly active adjustable probe tube TC-158 (figures 6 and 7) which had a saturation current density of 10 amps/cm^2. Tables 4 and 5 give the results obtained with two typical runs taken on different days while table 6 gives the average results of all runs made with this test cell. All measurements were made under normal operating conditions.

The cell operated as a thermionic converter in all these measurements and had an output voltage of about 0.1 volt with an output current density of 4.5 amperes per square centimeter. The discharge was a cylindrical

purplish glow as described previously in the case of the fixed probe cell and it was confined within the same spatial limits.

Figures 8 and 9 plot the variation of the space potential with position. It can be seen that there is an initial increase in the potential of 1.1 to 1.5 volts near the emitter, i.e. there definitely is a "virtual collector" very close to the emitter. In the remainder of the space the potential remains essentially constant in the longitudinal direction up to the actual collector, although, as will be shown later, there must be a definite decrease at the surface of the collector. This shows that there is practically no longitudinal electric field within the plasma region of the discharge. Figure 9 shows that this result holds true for the individual runs as well as for the average results.

Figures 10 and 11 show plots of the spatial variation of electron temperature. The electron temperature reaches a maximum of about 10,000°K near the emitter and then gradually drops to about 6000°K near the collector. Again the curve is essentially the same in each individual run as in the average.

Figures 12 and 13 show the spatial variation of the electron concentration. The distribution is parabolic or sinusoidal within the plasma and reaches a maximum near the center of the discharge. Here too this behavior holds for the individual runs as well as for the average values.

Figure 14 shows a typical set of probe characteristics obtained with the test cells where the position at which each characteristic was obtained is indicated on the individual curves. As was true for the fixed probe characteristics, the origin of the probe potential axis is displaced for each separate characteristic in order to keep each of them from overlapping.

It is important to note that, except for the exact magnitude of the slopes and for the exact points where the break occurs, all the sets of characteristics exhibited the same properties so that the following discussion of these properties is generally valid for all the results obtained.

It can be seen that before the knee of the curve each characteristic has a long linear section. The slope of this line is the one used for determining the "electron temperature". Since the length of the straight line portion is fairly long, the distributions are all at least mainly maxwellian so that the concept of temperature has reasonable validity. In those cases where the characteristic is not completely a straight line the observed electron current is always larger than it would be along the extension of the straight line. Thus, in these cases, there always is an excess of electrons with higher kinetic energies as compared with a pure maxwellian distribution.

Although theoretically it would be possible to apply the method of Medicus (J. Ap. Phys. 27, 1242 (1956)) and thus obtain exact electron energy distributions, it did not appear warranted to attempt to find such an exact distribution since the values corresponding to the higher electron energies represent increasingly smaller probe currents with greatly increasing percentage errors. Since in our measurements the measurements only encompass a few volts in range, no valid conclusions can be drawn as to how the distributions behave at very high electron energies particularly since all methods for obtaining the distributions actually depend on second order graphical differentiations of the characteristics.

Thus it can be said that up to a distance of .029", at least, from

the emitter the distribution is not maxwellian and as is to be expected there is a definite excess in high energy electrons since it appears that the electrons have not been completely thermalized up to this point. In the center of the plasma between .043" and .072" from the emitter the distribution seems to be completely maxwellian which agrees with the results obtained with the fixed probes. More than .086" from the emitter the distribution again becomes non-maxwellian and up to the energies measured there is an excess of electrons compared with a maxwellian distribution. However, it must be mentioned that at points beyond those shown (beyond the collector) the probe electron current was too low to be measured so that it may well be that at the higher energies there may actually be a deficit of electrons. The results only indicate that there is a definite perturbation in the distribution near the collector.

Results were also obtained with two other probe tubes, TC-150 and TC-155. While the results are interesting, the tubes design and operating conditions were different from our standard thermionic converters. TC-150 had an interelectrode spacing of 0.050 inch, only half that of the smallest spacing used in experimental thermionic converters. The color of the discharge was distinctly whitish indicating that at least some air was present in the tube. However, the tube did operate in the thermionically active region, and the characteristics were obtained in this region.

Table 7 and Figures 15 and 16 show the results obtained with TC-150. As with TC-158, the space potential is essentially constant between 1.4 and 1.5 volts in the discharge region, but rises sharply near the emitter.

The collector current of 0.60 amperes was greater than the saturation (extrapolated zero field) current of 0.30 amperes; hence, an accelerating field must be present near the emitter, and correspondingly no potential minimum exists. The electron temperature is much higher than in TC-158, but this is easily explained by the higher maximum space potential; furthermore, there is a distinct drop as the collector is approached. The electron concentration distribution increases markedly near the collector. Figure 16 shows that (as in TC-158) the electron distribution is quite maxwellian in the body of the discharge, but high energy electrons increase as the collector is approached.

TC-155 had the same spacing as TC-158, 0.100 inch, but this tube definitely contained air. It had a distinctly whitish discharge and became inoperative due to air leakage through a cracked base after one set of results had been obtained. These results are given in Table 8 and Figures 17 and 18.

As with the other cells the space potential is about 1.5 volts in the body of the discharge, but it increases considerably near the collector (Figure 17A). The space potential must have a minimum of about -0.16 volts near the emitter since the saturation current is 0.74 amperes while the collector current is only 0.20 amperes. Figure 17 shows that the electron temperature falls in the direction of the collector. The magnitude of the electron temperature is close to that in TC-150, but higher than in TC-158. It exhibits a distinct minimum before coming close to the collector. The curve of the electron concentration distribution (Figure 17c) approximates that of TC-158 except that the maximum seems to occur closer to the collector. The magnitude is about 1/10 that in TC-158, although it is about the same as

in TC-150.

The probe characteristics shown in Figure 18 corroborate the results with TC-158 and TC-150. The distribution is definitely maxwellian in the body of the discharge while there is an increase in high energy electrons both towards the collector and toward the emitter.

Table 7

RESULTS WITH TC-150

T_e = 1500°K V = .12 volt

t_{Cs} = 196°C J = 8.4 amps/cm^2

Distance From Emitter	Space Potential V_{sp} volts	Electron Temp. T_e °K	Electron Conc. ρ_e cm^{-3}
.017"	2.80	16,800	.38x10^{12}
.025"	1.40	14,500	.50
.033"	1.22	15,300	.47
.042"	1.35	15,700	.57
.050"	1.70	13,100	1.38

Table 8

RESULTS WITH TC-155

T_e = 1500°K

t_{Cs} = 195°C

Distance from Emitter	Collector Voltage V Volts	Collector Current J Amps/cm^2	Space Potential V_{sp} Volts	Electron Temp. T_e °K	Electron Concentration ρ_e cm^{-3}
.025"	.16	2.8	1.50	15,600	.62x10^{12}
.038"	.12	2.8	1.45	13,900	1.08
.050"	.08	2.8	1.43	12,000	1.47
.063"	.06	2.8	1.53	10,000	1.82
.075"	.01	2.8	1.88	11,100	1.95
.088"	.03	2.8	1.85	11,400	1.61
.100"	0	2.8	2.18	13,600	1.26

After this series of cells a new voltage pulsing circuit was developed for use in the testing of the cells. This circuit is capable of delivering an almost perfect triangular pulse with equal rise and fall time. The rise and fall times are adjustable within wide ranges while maintaining a constant or controllable height. This circuit has been used to obtain I-V characteristics curves and with some modifications was used for the probe characteristic in all the remaining experiments. Another advantage of this circuit is that the pulse has an adjustable delay, enabling it to occur at any point in the heater off cycle.

Test cell TC-171 was first used with the new pulsing circuit to obtain I-V characteristics at different rise times, different emitter and cesium temperatures and with the pulse occurring at different times during the off-cycle of the heater current.

Figures 19 through 24 give some of the I-V characteristics thus obtained. In each case, the relationship of the heater pulse and the collector voltage pulse is shown below the I-V curve.

Figures 19 through 22 were obtained with the cesium maintained at 200°C and the emitter kept at a brightness temperature of 1100°C. There was a load resistance of 1 ohm in the collector circuit. The rise and fall times of the collector pulse were 1 millisecond each.

It can be seen that as long as the collector pulse occurs two or more milliseconds after the heater current stops, there is essentially no current flowing (uptrace) in the collector circuit before the arc is struck.

Figures 23 and 24 were obtained with rise and fall times of 0.5 milliseconds each under otherwise the same conditions. Here a somewhat larger current is drawn during the uptrace as the pulse is moved close to the

beginning of the heater off-cycle. This larger current apparently is due to the fact that the pulse starts only 0.5 milliseconds after the heater current stops. These results show that heater interaction effects vanish within 10^{-3} seconds after the heater current is shut off.

The results with longer rise times and different emitter and cesium temperatures did not alter the results significantly. Also the I-V curve of the probe was the same as the uptrace and on the downtrace. This result had been expected as the rise time of the pulse was long enough for dynamic equilibrium.

The pulsing circuit was modified so that it can deliver up to 100 milliamperes at a positive voltage of 10 volts. Figure 25 shows the shape of the pulse which was fed to the tube. The base level below the zero line can be adjusted from any value between 0 and 50 volts. The total width of the pulse can be adjusted from below 0.1 milliseconds to about 2 milliseconds. The height of the triangular portion can also be adjusted down to the base line. In the tests run the pulse was made to occur at the end of the heater off cycle. However, it can be set at any point from about 1 millisecond after the start of the heater off-cycle into the on-cycle of the heater.

Test cell TC-193 (axial-probe) was used mainly to check the operation of the new pulsing circuit. However, it also was used to test the effects of a wider emitter to collector spacing since it was made with a .150" separation instead of the .100" separation used in most of the previous test cells.

Probe characteristics were obtained with pulse widths of 0.2, 0.5 and 1 millisecond. The probe was even with the surface of the collector, the oven temperature was 205°C and the emitter had a skirt brightness temperature

of 1423°K. With the 0.5 and 1 milliseconds width the curves obtained during the upswing and the downswing portions of the pulse essentially coincided except above the knee of the characteristics. However, with the 0.2 milliseconds width, the curves departed markedly. In all the measurements made, the results were calculated from the curve obtained in the downswing part of the pulse since equilibrium could be expected by then. The calculated results with the three different widths are given in Table 9.

Table 9.

EFFECT OF PULSE WIDTH ON PROBE RESULTS

t_{Cs} = 205°C

T_e = 1500°K

Pulse Width Milliseconds	Electron Temperature °K	Electron Conc. cm^{-3}
0.2	5540	$.94 \times 10^{-13}$
0.5	5300	1.03×10^{-13}
1.0	5140	1.10×10^{-13}

The results are very similar and well within the experimental errors. Thus it is felt that any width between 0.5 and 1 millisecond is suitable for the measurement.

Tests were now run at different positions of the probe with various cesium pressures and emitter temperatures. The results are given in Tables 10 through 12.

Table 10

PROBE MEASUREMENT WITH TC-193

t_{Cs} = 205°C V = 0.2 volts

T_e = 1500°K J = 7.0 amps/cm^2

Distance from Emitter	Space Potential V_{sp}, Volts	Electron Temp. T_e, °K	Electron Conc. ρ_e cm^{-3}
.060"	1.4	7,100	0.67×10^{13}
.075"	1.6	6,400	0.88×10^{13}
.090"	1.7	5,800	1.43×10^{13}
.120"	1.7	6,100	0.84×10^{13}
.150"	1.6	5,000	0.63×10^{13}

Table 11

PROBE MEASUREMENTS WITH TC-193

t_{Cs} = 205°C V = 0.3 volts

T_e = 1400°K J = 8.4 amps/cm^2

Distance from Emitter	Space Potential V_{sp}, Volts	Electron Temp. T_e, °K	Electron Conc. ρ_e cm^{-3}
.060"	2.0	11,300	0.32×10^{13}
.090"	2.0	9,200	0.70×10^{13}
.120"	2.1	8,000	0.65×10^{13}
.150"	2.1	6,900	0.56×10^{13}

Table 12

PROBE MEASUREMENTS WITH TC-193

t_{Cs} = 230°C V = 0 volts

T_e = 1400°K J - 7.0 amps/cm^2

Distance from Emitter	Space Potential, V_{sp} Volts	Electron Temp. T_e °K	Electron Conc. ρ_e cm^{-3}
.060"	0.5	5,400	0.10×10^{13}
.090"	0.9	5,000	0.25×10^{13}
.120"	1.1	5,400	0.39×10^{13}
.150"	1.1	3,700	0.39×10^{13}

Table 10 gives the results obtained with an emitter temperature of 1500°K and a cesium temperature of 205°C. The results are very close to those obtained previously under approximately the same conditions with test cell TC-158, which had an emitter-collector spacing of .100". The shape of the distributions of the space potentials, the electron temperatures and the electron concentration is not noticeably different. The values coincide quite well except that the magnitude of the electron temperatures is slightly lower. It thus appears that a change in spacing does not significantly alter the operating parameters of this type of thermionic converter in the active region.

Tables 11 and 12 give the results with an emitter temperature of 1400°K. Table 11 shows data obtained at an oven temperature of 205°C while table 12 gives the data at 230°C. At the lower cesium pressure (Table 11), the arc could not be operated in the active region and a small voltage V_{ext} (0.3 volts) was applied.

It can be seen that the higher cesium pressure shows decreased values for all the parameters measured. The lower electron temperature indicates a closer approach to thermal equilibrium at higher cesium pressures, as is to be expected.

Measurements were also carried out to determine radial distribution of the converter parameters. Thus test cells were constructed in which the probe was introduced into the periphery of the discharge. The arrangement is shown in Figure 26.

Radial probe tube TC-194 was subjected to test. Right at the commencement of the test the character of the discharge; i.e., a whitish

rather than a purple color, indicated the probable presence of air. Nevertheless, a set of useful data was obtained before the air pressure increased to severe poisoning levels.

Table 13

TEST RESULTS WITH RADIAL TEST CELL TC-194

Radial** Probe Distance cm	Collector Potential V_{ext}	Collector Current J Amperes/cm^2	Space Potential V_{sp} volts	Electron Temperature T_e °K	Electron Concentration ρ_e cm^{-3}
0	.40	2.9	0.8	7900	$.99 \times 10^{13}$
.04	.51	2.9	1.1	7100	1.29×10^{13}
.08	.65	2.9	0.8	6100	1.57×10^{13}
.11	.75	3.6	1.1	5000	2.93×10^{13}
.15*	.90	4.2	1.1	5000	0.50×10^{13}
.19	1.16	4.2	1.1	4400	0.53×10^{13}
.23	1.65	4.2	0.9	3600	0.40×10^{13}

*Outer edge of 3mm emitter
**Measured from emitter axis

It must be noted that these results represent only a single run. It can be seen that a time increasing positive voltage had to be applied to collector so that the cell was not thermionically active during the tests. This voltage had to be increased during the course of the test most probably due to an increasing amount of emitter poisoning by air leakage.

Nevertheless, the results are interesting particularly since they indicate that the electron temperature at the edge of the discharge is considerably below that prevailing in the center of the discharge.

Figures 27 and 28 show the details of the metal-ceramic adjustable probe tube which was constructed at Ford to be able to make probe measurements along radii as well as along the axis of the same thermionic converter. Except for the addition of the adjustable probe assembly this cell is similar to other metal-ceramic cells which have been operated successfully at Ford

Instrument Company for many thousands of hours. The output characteristics were similar to the cells without a probe assembly thus showing that the addition of the probe did not significantly affect the operating conditions of the thermionic converter.

Tables 14 and 15 give the results of probe measurements made with the converters operating with a power output of 1.3 watts per square centimeter. Table 14 gives the variation of the parameters along a radius outward from the axis near the middle of the discharge. These results are plotted in Figures 29 through 31.

Figure 29 shows the space potential values along a radius. The potential drops fairly rapidly near the center and reaches a plateau near the edge of the discharge only to drop again outside of the visible arc region.

Table 14

RESULTS OBTAINED ALONG RADIUS OF METAL CERAMIC CELL TC-230

$V = 0.20$ volt $\qquad T_e = 1500°K$

$J = 6.5$ amps/cm^2 $\qquad t_{Cs} = 200°C$

Radial Distance from Center inches	Space Potential V_{sp} volts	Electron Temp. T_e °K	Electron Conc. ρ_e cm^{-3}
0	1.32	5194	1.32×10^{13}
.023	1.25	5037	1.29
.045	1.20	4644	1.20
.068	1.02	4171	1.09
.091	1.045	4407	.83
.114	1.00	4564	.69
.136	0.95	4876	.47
.159	0.82	4725	.37
.182	0.73	4564	.30

Table 15

RESULTS OBTAINED ALONG CENTRAL AXIS OF METAL CERAMIC CELL TC-230

$V = 0.20$ volt $\qquad T_e = 1500°K$

$J = 6.5$ amps/cm^2 $\qquad t_{Cs} = 200°C$

Distance from Emitter inches	Space Potential relative to emitter V_{sp} volts	Electron Temp. T_e °K	Electron Conc. ρ_e cm^{-3}
.022	1.42	9051	1.21×10^{13}
.029	1.38	8422	.75
.044	1.26	7555	.78
.058	1.20	6926	1.06
.088	1.23	5666	1.28
.117	1.15	5510	1.30
.131	1.08	4956	1.11
.146	1.10	5037	.92
.163	0.95	4956	.80

Figure 30 shows the radial course of the electron temperature. It drops from a value of about 5200°K at the center to about 4500°K outside of the visible discharge region. The variation seems to follow the space potential curve to a great extent in that the electron temperature drops near the center and falls again outside of the visible region. However, there is an apparent increase in temperature near the edge of the arc, but there also is an indication of a similar increase of the space potential.

Figure 31 gives the electron concentrations along the radius. Here the values steadily drop from the center outward except that the drop seems at a smaller rate outside of the arc.

It must be noted here that as in the case of glass test cell TC-194 the electron temperature is lower at the outside of the discharge than at the center. The central temperature of the glass cell is higher than that measured with the metal ceramic cell. However, the emitter area of the glass cell is smaller and as will be discussed later a higher temperature is to be expected in this case. The glass cell gave an increase in electron concentration near the edge of the visible arc, but this result is very possibly caused by the change in applied field strength during the time of measurement as noted previously. However, both types of cells show a drop outside the luminous region. The same comments can be made about the space potential.

Figure 32 reproduces actual probe characteristics obtained in these measurements. It can be seen that while at the center the electron distribution is maxwellian within the limits of the measurements, the distributions deviate from a maxwellian as one proceeds outward. The temperature values given correspond to the slope of the straight line portions before the "knee" of the curve.

Table 15 gives the values obtained along the axis of the discharge and figures 33 through 35 plot the results. Figure 33 shows that the space potential rises to over 1.3 volts near the emitter and then drops to an almost constant value near 1 volt in the body of the discharge only to drop again slightly near the collector.

Figure 34 shows that near the emitter the apparent electron temperature is about 9000°K and then drops rapidly to a value of about 5000°K. The electron concentration as given by figure 35 shows a sinusoidal variation in the body of the discharge with a maximum near the center of the discharge, but there seems to be an increase near the emitter.

Figure 36 reproduces the probe characteristic obtained along the axis. Again the distribution appear to be essentially maxwellian in the body of the discharge. Near the emitter, as is expected, the distribution is definitely non-maxwellian. Approaching the collector there is an indication of a non-maxwellian distribution, nevertheless the characteristic obtained closest to the collector reverses this trend.

TABLE 16

RADIAL RESULTS WITH METAL CERAMIC CELL TC-230 WITH VARIOUS OUTPUT CURRENT DENSITIES

T_e = 1500°K

t_{Cs} = 200°C

Radial Distance from Central Axis inches	Output Current Density J amps/cm^2	Output Potential V volts	Space Potential V_{sp} volts	Electron Temperature T_e °K	Electron Concentration ρ_4 cm^{-3}
0	1.6	0.30	0.43	4564	0.61×10^{13}
	6.5	0.21	0.85	5586	1.34
	12.8	0	0.90	5747	1.33
.034	1.6	0.30	0.40	3934	0.59×10^{13}
	6.5	0.20	0.80	5274	1.11
	12.8	0	1.03	5747	2.32
.062	1.6	0.31	0.32	3622	0.64×10^{13}
	6.5	0.24	0.70	5666	1.10
	12.8	0	0.55	5274	1.16
.108	1.6	0.34	0.06	3073	0.58×10^{13}
	6.5	0.20	0.70	5586	0.77
	12.8	0	0.50	5666	1.03
.136	1.6	0.32	0.15	4251	0.39×10^{13}
	6.5	0.16	0.40	4800	0.61
	12.8	0	0.46	5037	0.81
.170	1.6	0.36	0.12	3385	0.39×10^{13}
	6.5	0.10	0.34	4880	0.66
	12.8	0	0.30	4407	0.39

Another set of values were obtained with metal-ceramic cell TC-230 in which the radial variation of the parameters were obtained under three operating conditions; maximum output voltage (J=1.6 amps/cm^2), maximum output current (J=6.5 amps/cm^2) and short circuit, i.e. V=0, (J=12.8 amps/cm^2). Table 16 lists the values obtained in this set of measurements while figures 37 through 39 plot these values.

Although the measured space potential are somewhat lower than those obtained in the first set of measurements, figure 37 shows that the variation is very similar, i.e. a rapid drop near the center, followed by a plateau and finally a decrease outside of the luminous zone. The values for the two highest current outputs are close together, but the lowest current gives considerably lower potentials at all points.

Figure 38 shows that the curves of the electron temperatures roughly follow the space potential curves except that they are flatter. Again, the two highest current densities give closely the same values for the electron temperature; it drops from about 5500°K at the center to about 4000°K at the outside. The lowest current gives appreciably lower values dropping from about 4500°K at the center to about 3000°K at the outside.

In the case of the electron concentrations figure 39 shows that the magnitudes vary with the output current density, i.e. the highest current gives the highest electron concentration and the lowest current the lowest concentration. It is also noteworthy that as the current decreases, the electron concentration variation becomes flatter; with the lowest current (1.6 amps/cm^2), the electron concentration is essentially constant in the luminous discharge region.

3.4 SPECTROSCOPIC METHODS

Supposedly, an examination of the emission and absorption spectrum of a cesium arc should permit the quantitative measurement of the following parameters:

Electron Temperature
Ion Temperature
Neutral Atom Temperature
Electron Number Density
Ion Number Density
Neutral Atom Number Density

The types of examination which are involved are the following:

Emission Line Intensities
Intensity of Continuum
Reversal Temperatures
Line Broadening

There is no question that spectrographic methods of measuring temperatures and number densities represent elegant techniques of great theoretical importance. They also are probably the only methods which do not disturb the conditions present in a thermionic converter. However, on the other hand they cannot be used in every type of converter since it is quite apparent that the walls of the converter must be transparent to the particular radiation to be observed. If special windows must be provided, these may change the character of the discharge to some extent and they lead to other complications. Thus, for example, beside the structural modifications necessary for adding a window, the window itself is subject to attack by the cesium (this is particularly true of quartz at high temperatures).

The results obtained are subject to many restrictions. In general, the numerical values have their main use as checks of other methods of measurement. In fact, in some cases, spectrographic methods require other types of measured results in order to be applied. Thus it may be necessary to find ion or gas temperature in order to find their number densities or vice versa.

Spectrographic techniques also require a good advance knowledge of the concentrations and temperatures to be expected. The validity of most of the methods depends on proof of equilibrium conditions being present and usually it is necessary that only one type of exciting mechanism be present or at least that all other mechanisms are completely negligible. If this knowledge is not at hand, spectroscopic techniques can be very questionable in value.

Finally, it is also true that the type of spectrographic equipment must be adapted to a particular measurement. Thus, the measurement of relative line intensities can be carried out with relatively simple apparatus. Such spectrographs do not require very high dispersion or resolution. They should, however, cover fairly wide spectral regions; in the case of cesium a coverage of 2,000 - 10,000 angstroms is advisable. Furthermore they should not have stray light to mask individual intensities and they should have high sensitivity so weak lines can be measured.

Measurements of intensity distributions in the continua may also be carried out with such simple spectrographs. However, since the continua of interest are very weak, it is probably necessary to use more expensive devices to obtain accurate results. It is particularly necessary to have excellent gratings to give good intensity profits and to reduce the effect of "ghosts" or false lines.

The exact widths of lines requires an unusually sensitive and accurate spectrograph. Determinations must be made within a thousandth of an angstrom or better in order to give meaningful results. The aberrations of the instrument must be very small in order not to give false readings.

Various methods will be discussed in the following paragraphs. A bibliography is given at the end of this section.

3.4.1 Emission Line Spectra

The absolute intensity I_{nj} of a line emitted by an atom due to a transition from energy levels n to level j is given by (cf. Ref. 1):

$$I_{nj} = C\, A_{nj}\, \nu_{nj}\, N_n = C\, N_o\, A_{nj}\, \nu_{nj}\, \frac{g_n}{g_o}\, \exp -\left(\frac{\varepsilon_n}{k\, T_{ex}}\right) \qquad (1)$$

where

C = instrument constant

N_n = concentration of atoms in excited state n

N_o = concentration of atoms in the ground state

A_{nj} = Einstein coefficient of spontaneous emission

ν_{nj} = frequency of emitted line

g_n, g_j = statistical weights of states n and j respectively

k = Boltzmann's constant

h = Planck's constant

T_{ex} = "excitation" temperature

E_n = energy of upper excited level n

Thus, in theory, a measurement of the absolute intensity of a spectral line makes possible the determination of the number of atoms N_n in the upper state n or, the excitation temperature T_{ex} could be determined if a maxwellian distribution is known to be present. In practice this is virtually impossible since the constant C is difficult to determine and the absolute value of the transition probabilities usually cannot be determined.

It is a customary practice in spectrographic work to use the "oscillator strength" or Ladenberg f instead of the Einstein A coefficient since this corresponds to classical concepts. The relationship between the two is given by[22]

$$A_{nj} = \frac{g_j}{g_n}\, \frac{8\pi^2 e^2 \nu_{nj}^2}{mc^3}\, f_{nj} \qquad (2)$$

If, furthermore, we consider the intensities of two separate lines I_{nj} and I_{mk}, we can write

$$\frac{I_{nj}}{I_{mk}} = \frac{g_j f_{nj} \nu^3_{nj}}{g_k f_{mk} \nu^3_{mk}} \exp -\left(\frac{E_n - E_m}{k T_{ex}}\right) \tag{3}$$

In this equation only relative intensities and relative oscillator strength need be known and thus T_{ex} can be determined by the measurement of the intensities of two lines.

By taking logarithms (Equation 3) can be expressed as

$$\ell n \left(\frac{I_{nj}}{g_j f_{nj} \nu^3_{nj}}\right) = -\left(\frac{E_n - E_m}{k T_{ex}}\right) + \ell n \left(\frac{I_{mk}}{g_k f_{mk} \nu^3_{mk}}\right) \tag{4}$$

Thus, a plot of the log $\left(\frac{I}{gf\nu^3}\right)$ vs. E_n should give a straight line whose slope is $\frac{1}{k T_{ex}}$ so that T_{ex} can easily be obtained. The advantage of making this plot is that, since the graph depends on several intensity measurements, the value of T_{ex} thus determined will be more accurate. Furthermore, if a straight line plot is not obtained, the exciting particles cannot be in thermal equilibrium. However, the converse is not true, i.e. a straight line plot could result without a thermal equilibrium[2].

It will be noted that the temperature determined by the above method is designated as excitation temperature. In order for the given equation to be valid there must be a Maxwellian distribution of excited states. The temperature thus obtained will refer to the type of excited state.

If "local thermal equilibrium" permits, the measured temperature will obviously be the same for all particles. However, in the case of the thermionic converter there is no reason to assume equilibrium. Thus the current density J is given by

$$J = \rho e v_d \tag{4}$$

where v_d is the drift velocity, i.e. the average directed velocity of the electrons

from the emitter to the collector and n_e is the electron concentration. The average random velocity $\bar{v}$ is given by

$$\tfrac{1}{2} m \bar{v}^2 = \tfrac{3}{2} k T_e$$

$$\text{or} \quad \bar{v} = \left(\frac{8k}{\pi m}\right)^{\frac{1}{2}} T_e^{\frac{1}{2}} \tag{5}$$

Thus the average distance d travelled by an electron in traversing the space between emitter and cathode is

$$d = \frac{\bar{v}}{v_d} \ell \tag{6}$$

where ℓ is the separation between emitter and collector. The average number of collisions C made by an electron is then

$$C = \frac{d}{L} \tag{7}$$

where L is the mean free path for collision.

According to Compton and Langmuir the fraction of energy f lost in collision with an atom of mass M_a is given by

$$f = 2.66 \frac{m M_a}{(m + M_a)^2} \left(1 - \frac{U_a}{U_e}\right)$$

$$2.66 \frac{m}{M_a} \left(1 - \frac{U_a}{U_e}\right)$$

(since $M_a \gg m$) (8)

where U_a, U_e = average kinetic energies of atoms and electrons, respectively.

Using this equation it can be shown that the number of collisions D required to have the electrons and atoms come into thermal equilibrium, i.e. for U_a U , will be equal to

$$D = \frac{m}{2.66 M_a} \tag{9}$$

for cesium atom $D = 9 \times 10^4$

Putting in representative values corresponding to conditions prevailing in the thermionic converter, i.e.

$$L = .03 \text{ cm}$$

$$T = 4000\ ^{o}K$$

$$J = 10 \text{ amps/cm}^2$$

$$\ell = .45 \text{ cm}$$

$$P_\epsilon = 10^{13} \text{ electrons/cm}^3$$

we find that

$$C \simeq 30$$

Thus the average electron will make only .033% of the number of collisions required for thermal equilibrium and conditions in the thermionic converter will be far from such thermal equilibrium. However, as long as there is a Maxwell-Boltzmann distribution of excited cesium atoms, spectrographic measurements will give an excitation temperature T_{ex}, but this temperature cannot be equated directly to the electron temperature T_ϵ unless it would be possible to show that the distributions of electron kinetic energies and of the excited cesium levels are the same. When thermal equilibrium is not present this requires that all or essentially all the excitation is due to electrons and also that the excitation cross-sections are very sharp, i.e., for example, a 2eV electron will excit a 2eV state, but not the states below or above it. These excitation cross-sections have not been measured to any appreciable extent for cesium, but hydrogen cross-sections, which are similar in form, do not exhibit such sharp resonance values. It must also be noted, however, that, if the excited cesium levels are non-maxwellian, this does not, for the same reasons, immediately imply that the electrons are non-maxwellian.

In addition to the assumption of thermal equilibrium, other assumptions must be made in deriving the basic equations required for the spectrographic methods.

Thus it must be assumed that induced emission is negligible. This means that the particular line or lines used must not be absorbed by the gas it goes through, i.e. the lines must not be "resonance lines", they must be "optically thin". In the case of thermionic converters using cesium only the resonance lines representing transitions to the ground level are strong. The other "optically thin" lines are quite weak which means that measurements with these lines suffer rather large experimental errors, especially since energy scattered within the spectrograph from the strong lines may cause a false increase in apparent intensity of these lines. In fact, these lines must be weak since they must not carry away enough energy to affect the thermal equilibrium which should exist between the electrons and the atoms, if electron temperature is to be measured.

Another basic assumption is that in the observed region conditions are homogeneous. The concentration of atoms in the lower state and the temperature must be constant in all regions which contribute to the observed light. Usually the temperature is hottest within the center of the discharge and drops toward the outside. The results will express, therefore, some kind of average over the various temperatures existing along the line of sight. Moreover, the light coming from the more distant, hotter portions will be modified by absorption and scattering during its passage through the nearer and cooler regions.[2]

3.4.2 Intensity of Continuum

Several authors have measured temperatures by using the continuum spectra. Thus, Jurgens,[1] used the continuum of the Balmer series in hydrogen in the same manner as the discrete lines in this series for determining the temperature in a hydrogen arc column. Dickerman[10] used the absolute intensity of the

continuum based on the following equation of Unsöld.

$$I = B \frac{c}{4\pi\lambda^2} \gamma \frac{128\pi^3}{3\sqrt{3}} \left(\frac{e^2}{hc}\right)^3 Z^2_{eff} P \exp\left(\frac{eV_i}{kT_g}\right) \quad (1)$$

where B = instrumental constant

c = velocity of light

e = electronic charge

h = Planck's constant

I = emission per cm^3 per steradian per unit wavelength

k = Boltzmann's constant

P = pressure of the gas

T_g = absolute temperature of the gas

V_i = reduced ionization potential of the gas

Z_{eff} = effective nuclear charge

γ = ratio of statistical weight of the high levels to that of the general level of the atom

λ = wavelength of light

This equation is based on the thesis that free-discrete and free-free transition of electrons ("Bremsstrahlung") are responsible for the greater part of this radiation. Donohue and Majkowski[5] use a somewhat different equation in which the ion and electron densities appear on the right side instead of the gas pressure. They use this method for obtaining the electron density after obtaining the excitation temperature by a different method, i.e. line of intensity.

Finally, Agnew and Summers[9] use the intensity distribution in the continuum for obtaining electron temperatures and concentrations. Apparently they assume this continuum is due almost entirely to recombination radiation and thus the intensity distribution is proportional to the electron energy distribution which in turn depends on the electron temperature according to the

Maxwell-Boltzmann equation. Thus according to the Bohr theory[7] if the recombination of electrons with atomic ions is the cause of the continuum radiation, electrons with kinetic energies $1/2\ mv^2$ could fall into vacant orbits in the energy level diagram. The emitted frequency could then be given by

$$h = 1/2\ mv^2 + h\nu_x \qquad (2)$$

where ν_x is the frequency with which an electron with zero kinetic energy falls into the potential level.[11] Thus, all lines correspond to capture into the vacant orbits (the ion will have frequencies ν which are greater than ν_x by the continuum spectra of electron energies $1/2\ mv^2$, modulated by the capture probability from the kinetic energy state. This probability is greater with smaller $1/2\ mv^2$).

Several difficulties are present in the analysis of continuum spectra. In the first place, the intensities of the continuum are very low, in general. Thus, Dickerman states".the lower temperature limit for this method is about 10,000°K. At this temperature, the continuum level approaches the level of scattered light present from the intense line spectra...". This would make absolute or relative intensity measurements quite inaccurate.

Another difficulty is that when molecular ions are present, according to Loeb[7], "most recombinations as observed in such plasmas is dissociation molecular recombination, where emitted spectra often cannot be predicted". Loeb makes particular note that in cesium, molecular Cs_2^+ ions are present to a large degree and have given rise to erroneous values. In particular, recombination coefficients were found to be too large by a factor of ten.

Thirdly, it is apparent that it would be difficult to show whether recombination or "Bremsstrahlung" is the major source of the continuum. Thus, the validity of this type of measurement is very dependent on the conditions in the cesium plasma; electron concentration, arc current,cesium pressure and actual electron temperature. In addition, of course, the comments made at the line spectra also hold.

The continuum must be optically thin. The problem of inhomogeneities is just as important.

3.4.3 Reversal Temperatures

The methods discussed up to now only apply to "optically thin" spectral lines, i.e., the emitted radiation is not appreciably absorbed by the gas itself. If some self absorption is present, according to Diecke[2], it is possible to correct for the different relative amounts of absorption occurring with the different lines. However, if the gas layer is very thick, there will be an equilibrium condition and the emitted radiation will be independent of the nature of the gas and its frequency distribution will be given by Planck's law:

$$I(\ ) = \frac{2(kT)^3}{h^2 c^2} \quad \frac{\alpha^3}{e^{\alpha}-1} \quad \alpha = \frac{h}{kT} \tag{1}$$

The temperature can then be determined from the position of the maximum radiant energy λ max. of the black body curve by Wien's displacement law:

$$T = \frac{ch/k}{4.9656\,\lambda\,\text{max.}} = 0.2898\,\lambda\text{max.} \tag{2}$$

Usually such continuous radiation will only be observed with gases under relatively high pressure. However, even under low pressure some lines, corresponding to transitions to the lowest level, will be absorbed very greatly, leading to the phenomenon known as "imprisonment of resonance radiation". The intensity of such lines will then be subject to Planck's law. The excitation temperature can then be determined by passing the light emitted from a hot source through the gas. If the temperature of the source is low, the line in question will appear as a bright line, superimposed on the continuous spectrum. Above a definite temperature, the line appears as a dark line. Thus as the source is heated, the line from the gas will turn from bright to dark. The temperature at which this change, or reversal takes place, is known as the "reversal temperature" and can be related to the excitation temperature

of the line. By Planck's law, I (, T), the observed radiant energy per unit time per unit wavelength of a black body at wavelength and temperature T is:

$$I(\lambda, T) = A\lambda^{-5} (\exp C_2/\lambda T) - 1)^{-1} \quad (3)$$

A is a constant, depending upon the first radiation constant,

$$C_1 = 2 h c^2;$$

on the instrument, including the area observed, the solid angle subtended, on the transmission and response characteristics; and on the wavelength interval used for observation. C_2 is the second radiation constant and is equal to ch/k. When the product of λT is less than 0.312 cm°K (λ 8% longer than λ max.), the Wien approximation

$$I(\lambda,T) = A\lambda^{-5} \exp(-C_2/\lambda T) \quad (4)$$

is accurate to better than 1%.

For any emitter with an intensity I_e and an absorptivity at a given wavelength λ, Kirchoff's law gives:

$$\frac{I_e(\lambda,T_e)}{I(,T_e)} = \epsilon_e(\lambda,T_e) = \alpha_e(\lambda,T_e) \quad (5)$$

where I_e is the radiant energy of the given emitter at temperature T_e.

At the reversal temperature the gas neither adds to (bright line) nor subtracts from (dark line) the observed intensity of the source. Thus,

$$I_s(\lambda,T_s)\left[1 - \alpha_g(\lambda,T_g)\right] + I_g(\lambda,T_g) = I_s(\lambda,T_s) \quad (6)$$

where the subscripts s and g refer to the source and the gas respectively.

Substituting equations (3) and (5) into (6) and assuming $A_s = A_g$ we get

$$T_g = \frac{C_2/\lambda}{\ln\left[1 + \frac{\exp(C_2/\lambda T_s)^{-1}}{\epsilon_s}\right]} \quad (7)$$

or when Wien's approximation is

$$T_g = \frac{T_s}{1 - \frac{\lambda T_s}{C_2} \ell n\, \epsilon_s} \tag{8}$$

We note that in the case of a black body source where $\epsilon_s = 1$

$$T_g = T \tag{9}$$

or, if a black body source is used, the reversal temperature is equal to the excitation temperature of the gas. However, if any other source is used, e.g. a tungsten lamp, the source temperature is <u>not</u> the same as the excitation temperature, even though Mohler[6] makes this statement.

Several difficulties are present in this method. First, we note that the assumption is made that $A_s = A_g$. This is not usually the case and according to Broida[4] the differences between the A's "can be a large source of error". Furthermore, Broida[4] states that while reversal "temperature" can be reproducible within a few degrees, the accuracy of the method may not be high unless proper precautions are taken with the optical path to insure reliable measurements. In addition to problems connected with the optical path and the hot gases, there are difficulties in the measurement of the temperature and emissivity of the source used for comparison.

Mohler[6] used this method in measuring electron temperatures in cesium arcs and Johnson[11] adopted the same idea in measuring electron temperatures in a cesium converter. In the case of tungsten lamps the maximum temperature is 3,100°K.[21] Carbon arcs can be used for somewhat higher temperatures.

Again this method assumes a homogeneous region of observation, which is not present in practice. Complete equilibrium must exist between the photons and the exciting processes at the energy of the spectral lines used.[19] Thus, the validity of this method requires proof of such complete equilibrium as well as analysis of the effects of non-homogeneity.

3.4.4 Spectral Line Widths

If most of the broadening is due to the Doppler effect, i.e. due to the relative motion v of the emitting atom, then the shift in frequency at a given frequency ν will be proportional to $\nu v/c$ (c = velocity of light). The numerical value of the width Δ at half maximum intensity is given by:

$$\frac{\Delta\nu}{\nu} = \sqrt{\frac{(2 \ln 2)\, k}{c^2}} \sqrt{\frac{T}{M}} \qquad (1)$$

In this case, T is the temperature of the emitting species. Thus, if Doppler broadening is the most significant cause of the line width, the temperature of the gas can be measured by this means. In fact, ion temperature could be determined by measuring the widths of the ionic lines.

Unfortunately, very often other causes of broadening (collision broadening, internal Stark effects, etc.) overshadow the Doppler effect and thus make the determination of temperature by this method impossible. In order to determine the validity of any measurement of line width it is necessary to calculate the relative magnitudes of each possible cause of line broadening.

The natural line width and broadening due to collisions (Pressure broadening) can be found from the Heisenberg uncertainty principle in the form:

$$\Delta E \, \Delta t \geq h/2\pi \qquad (2)$$

Here Δt is the time available for making the measurement of energy E and ΔE is the fundamental uncertainty in the value of W. In the present case, W is the difference in energy between the two levels giving rise to the emission of a particular line while Δt is the mean time, τ, involved in the transition.

Thus
$$W = h\nu \qquad (3a)$$

$$\Delta W = h \Delta\nu \qquad (3b)$$

We thus find that

$$A = \frac{1}{2\pi\tau} \qquad (4)$$

where $\Delta\nu$ is the frequency width of a line. The line width $\Delta\lambda$ is then

$$\Delta\lambda = \frac{\lambda^2}{2\pi c} \qquad (\text{since } \lambda\nu = c) \qquad (5)$$

where c is the speed of light. Since in the visible region $\lambda \simeq 6 \times 10^{-5}$ cm and $\tau \simeq 10^{-8}$ sec. for spontaneous emission, the natural line width $\Delta\lambda$ will be approximately 2×10^{-12} cm = 2×10^{-4} angstroms. If collisions occur more frequently than 10^8 sec. $^{-1}$, the time for emitting will be correspondingly increased. Thus, if the average time between collision is only 10^{-10} sec., the width of the line will be widened to 2×10^{-2} angstroms. Thus, increased pressure can cause considerable line broadening.

If large numbers of charged particles are present, the "microfields" of these particles will give rise to Stark splitting and, if these field are not great enough to actually separate the lines, the lines will appear to be broadened. The presence of foreign atoms or ions causes a polarization of the radiating atom giving rise to line broadening and an asymmetry or pressure shift effect [15]. The pressure shifts can be in either direction depending both on the particular energy levels involved and in the type of foreign atoms. Thus, the principal series lines of rubidium are displaced to the violet by helium and argon, but to the red by argon.

In general the amount of energy shift ΔW due to an electric field E can be represented by

$$\Delta W = A E + B E^2 + C E^3 + \qquad (6)$$

The A, B and C are constants referred to as first-order, second-order and third-order coefficients. The three terms in the equations are called the linear term, the quadratic term and the cubic term, respectively.

The linear term will only appear, if the energy levels are degenerate, e.g. hydrogen [14]. Since in the case of hydrogen the constant A is larger than B by a factor of about 10^{11} and larger than C by a factor of almost 10^{+20}, the linear term is the only important term. Thus for hydrogenic atoms the Stark effect varies as the first power of E.

In the case of non-degenerate emitters, the linear term will be absent and the quadrator term will be dominant. This depends on E^2, but the magnitude will be much less due to the small value of B. It will give rise to asymmetry broadening.

For the alkali metals, the lower energy levels are non-degenerate, but with larger quantum number the alkali levels become hydrogenic and thus the linear Stark effect is effective. The Coulomb approximation can thus be used to calculate the appropriate A. This will then be given by (ΔW in ergs)

$$A = \frac{3\ h^2}{8\ \pi^2\ m\ e\ (300)}\ n_{eff}\ n_F \qquad (7)$$

where n_{eff} is the "effective" quantum numbers and n_F is the "electric" quantum number (see references 5 and 15).

If the electric microfield is due to ions, then the field of each ion is proportional to e/r^2. Since the average distance of neighboring ions is proportional to ρ_1 -1/3, where ρ_i is the number of ions per cm^3, the average electric field would be proportional to $e\rho_i^{2/3}$. According to Holtsmark[12] in a plasma where $\rho_i = \rho_e$ (the electron concentration) the average field strength is given by

$$F = 2.61\, e\rho_e^{2/3} \qquad (8)$$

Thus, in degnerate emitters the change in energy is found to be

$$\Delta E = 2.61\ A\rho_e^{2/3} \qquad (9)$$

Since the half-width of a Stark-broadened line will enable one to calculate ΔW, ρ_e can be found.

The Stark effect will also cause the continuous spectrum of a hydrogenic emitter to extend past the series limit and thus overlap the highest discrete lines. Inglis and Teller[16] have shown that in hydrogen the electron density ρ_e can be found from the number of lines which can be observed as separate lines in the Balmer series by the equation

$$2 \rho_e = 0.027 \, a_o^{-3} \, n_m^{-7.5} \qquad (10)$$

where a_o is the smallest Bohr radius and n_m is the quantum number of the last line to be observed as a separate one near the series limit. This equation can be applied to the alkali metals simply by replacing (n_m) by the corresponding effective quantum number[5].

Outside of the obvious difficulties in calculating the required constants to a fair degree of accuracy, the actual experimental errors must be quite large since the line which would have to be used for cesium, including the continuum, are quite faint. This makes the measurement of exact line widths very difficult and the spectrographs itself will introduce erroneous apparent line widths. Any scattered light, as, for example, is present in Littrow spectrographs, would cause large errors in measurement.

SPECTROGRAPHIC REFERENCES

1) J. M. Somerville, The Electric Arc, Wiley 1959

2) G.H. Diecke, High Gas Temperatures, 19; TEMPERATURE, IT'S MEASUREMENT AND CONTROL IN SCIENCE AND INDUSTRY, Vol. II, Reinhold 1955

3) C. Payne-Gaposchkin, Astrophysical Temperatures, 31; Temperature, etc. Vol. II, Reinhold 1955

4) H.P. Broida, Experimental Measurements in Flames and Hot Gases, 256; Temperature, etc., Vol. II, Reinhold 1955.

5) R.J. Donohue and R.F. Majkowski, Spectroscopic Measurement of Temperatures and Densities in a Cesium Plasma, J. Ap. Phys. 33, 3 (1962)

6) F. Mohler, Collisions of the First and Second Kind in the Positive Column of a Cesium Discharge, Bur. of Standards, J. of Res. 9, 493,(1932)

7) L.B. Loeb, Basic Processes of Gaseous Electronics, Univ. of Calif. Press 1960

8) G.R. Harrison, R.C. Lord and J.R. Loofbourow, Practical Spectroscopy, Prentice-Hall 1957

9) L. Agnew and C. Summers, Experimental Cesium Line Shapes, Paper IV-7, Symposium on Thermionic Power Conversion, Colorado Springs, Colorado, May 14-17, 1962

10) P.S.Dickerman, Intensity Ratio of Continuum, Symposium on Optical Spectrometric Measurements of High Temperatures, Univ. of Chicago, March 23-25, 1960

11) F.M. Johnson, Optical Studies of the Cesium Arc, Paper IV-9, Symposium on Thermionic Power Conversion, Colorado, 1962

12) W. Lochte-Holtgreven, Ionization Measurements at High Temperature, 413, Temperature, etc., Vol. II, Reinhold 1955.

13) L. Spitzer, Physics of Fully Ionized Gases, Interscience 1956

14) L.I. Schiff, Quantum Mechanics, McGraw-Hill 1955

15) J.R.McNally, Jr., Atomic Spectra Including Zeeman and Stark Effects, 7-25, Handbook of Physics, McGraw-Hill 1958

16) D. Inglis and E. Teller, Ionic Depression of Series Limit in One-Electron Spectra, Astrophys. J. 90, 439 (1939)

17) F.K. Richtmeyer, E.M. Kennard and T. Lauritser, Introduction to Modern Physics, 5th Edit., McGraw-Hill 1955

SPECTROGRAPHIC REFERENCES (cont'd)

18) S.S. Penner, Optical Methods for the Determination of Flame Temperatures I. Two-color and Line-reversal Techniques, Am. J. Phys. 17, 422 (1949)

19) F. Henning and C. Tingwaldt, Die Temperatur der Acetylen-Sauerstoffflamme, Z. Physik, 48, 805 (1928)

20) L. Bernard and G. von Elbe, Combustion Flames and Explosions of Gases, Academic Press, 1951

21) S.G. Gaydon and H.G. Wolfhard, Flames, Their structure, radiation and temperatures, Chapman and Hull 1960

22) D.H. Menzel, Fundamental Formulas of Physics, Vol. 2, Dover Publications, New York, 1960

23) K.T. Compton and I. Langmuir, Rev. Mod. Phys 2, 211 (1930)

3.5 Spectroscopic Measurements

A regular metal-ceramic converter, TC-222, (which was identical to figure 27 except for the probe assembly) was used for obtaining various infrared spectrograms with a Perkin-Elmer Model 112 Infrared Spectrometer. A number of recordings were made at different emitter temperatures, cesium pressures and output current densities. Relative intensities were determined from these spectrograms using the 1.47μ as a reference. These intensities are the amounts above the background continuous spectrum. There was a relatively high noise level so that weak lines were masked by the noise level. Thus these values are subject to relatively high errors in measurement.

The results observed with various lines are given in table 17. Other lines were observed, but these did not appear as frequently as the one's given and some could not definitely be identified as being cesium lines.

TABLE 17

RELATIVE INTENSITIES OF INFRA-RED LINES OBSERVED WITH TC-222
(Intensity of 1.47 μ line used as reference)

Emitter Temp T_e	Cesium Temp t_{cs}	Output Current Density J	Relative Observed Intensity								
^oK	^oC	Amp/cm^2	.80 μ	.85 μ	.89 μ	.92 μ	1.00 μ	1.36 μ	1.47 μ	2.4 μ	3.4 μ
1500	200	2.4	-	.460	.794	.167	.103	.381	1	.587	-
		3.2	-	.978	.740	.259	.340	1.370	1	-	-
		3.2	-	.632	.735	-	.162	1.000	1	-	-
		3.2	-	.677	.787	.244	.401	.502	1	-	-
		4.0	-	.222	.236	.0684	.111	.474	1	.139	-
		4.8	-	.683	.417	.275	.337	1.950	1	.258	.437
		5.0	-	-	.562	.315	-	1.129	1	-	-
		5.2	-	.377	.428	-	.193	.719	1	-	.719
		5.5	-	.659	.775	-	.450	1.101	1	-	-
		8.3	-	.307	.313	.176	.119	1.060	1	.176	-
		9.5	-	.827	1.333	-	1.000	1.507	1	-	1
		19.0	-	.324	.216	.270	.378	.838	1	.326	-
	225	4.0	-	.054	.215	.129	.247	.473	1	.129	.570
		5.1	-	.284	.412	.0823	.239	.817	1	.171	.540
		8.3	-	.170	.247	.138	.216	.604	1	.0814	.224
		9.5	-	.479	.427	.103	.278	1.137	1	.150	.551
		19.0	.089	.132	.206	.295	.530	1.000	1	.266	.295
	250	4.0	-	.0851	.0851	.128	.340	.680	1	.213	.681
		8.3	.0524	.0653	.1167	.182	.469	.740	1	.078	.545
		19.0	.082	.0668	.134	.261	.483	.910	1	.119	.446
1550	200	2.1	-	.434	.347	.215	.306	.740	1	.194	-
		2.2	-	.411	.364	.138	.091	.775	1	.091	.385
		4.0	-	.413	.394	.130	.224	.886	1	.189	-
		5.1	-	.568	.450	.144	.117	1.239	1	.189	.523
		8.3	-	.269	.239	.195	.439	.646	1	.181	-
		9.5	-	.337	.270	.202	.270	.674	1	.156	.404
		19.0	.150	.250	.138	.227	.642	.628	1	.126	-

TABLE 18

INFRA-RED LINES USED IN TEMPERATURE MEASUREMENT

Observed Line μ	Theoretical Lines Angstroms	Transition A → B	E_A eV	$gf\nu^3$ $\times 10^{10}$	$\ell n\, gf\nu^3 - \ell n\, 10^{10}$
.80	8079.02	$5F \longrightarrow 5D_{5/2}$	1.811	144.73	4.9749
	8015.71	$5F \longrightarrow 5D_{3/2}$	1.799	94.36	4.5471
.85	8521.10	$6P_{3/2} \longrightarrow 6S_{1/2}$	0	263.13	5.5726
.89	8931.0	$8P_{3/2} \longrightarrow 5D_{5/2}$	1.811	184.04	5.2152
	8943.50	$6P_{1/2} \longrightarrow 6S_{1/2}$	0	110.15	4.7018
.92	9172.24	$6D_{5/2} \longrightarrow 6P_{3/2}$	1.456	172.20	5.1487
	9208.46	$6D_{3/2} \longrightarrow 6P_{3/2}$	1.456	20.34	3.0126
1.00	10025.4	$4F \longrightarrow 5D_{3/2}$	1.799	119.96	4.7872
1.35	13589.1	$7P_{3/2} \longrightarrow 5D_{3/2}$	1.799	34.38	3.5346
	13603.9	$7P_{3/2} \longrightarrow 5D_{5/2}$	1.811	365.34	5.9008
1.47	14697.7	$7S_{1/2} \longrightarrow 6P_{3/2}$	1.456	26.20	3.2658
2.4	24253.8	$7D_{5/2} \longrightarrow 7P_{3/2}$	2.723	7.906	2.0676
	24377.7	$7D_{3/2} \longrightarrow 7P_{3/2}$	2.723	0.9388	-0.06315
3.4	34898.7	$5D_{5/2} \longrightarrow 6P_{3/2}$	1.456	1.922	0.6534

Table 18 gives the transitions involved in the various observed lines as well as the function $gf\nu^3$. The oscillator strengths used were obtained by P.M. Stone (Phys. Rev. 127, 1151 (1962)). It can be seen that several of the observed lines are composed of at least two lines due to different transitions. The relative intensities of each observed line was calculated at various temperatures taking into account the composition of each observed line and the results are plotted in Figure 38. As noted above the 1.47 micron line was used as the reference line. This line was chosen since it was observed in each case; it was definitely due only to one transition (cf. Table 18) and it was not a "resonance line", i.e., it was not a result of a transition to the ground level. The .85 μ and .89 μ lines were not used further since they are resonance lines and thus subject to a large amount of self-absorption.

Table 19 gives the electronic excitation temperatures (i.e. necessarily assuming a maxwellian ratio of the lines used) corresponding to the observed intensities obtained by use of Figure 40. It can be seen that there is a wide spread in the "temperatures" from values below the emitter temperature to values far above it. Whereas part of this discrepancy is due to the experimental errors of measurement, it must be noted that those lines which give low values are consistently low while the high valued lines give consistently high temperatures. Furthermore, a study of Figure 38 reveals that in order to have all lines yield the same temperature the measured intensities for some lines would have to be changed by factors of 20 or 30, a value far above possible experimental error.

It can be noted, however, that higher output currents tend to give higher excitation "temperatures".

TABLE 19

ELECTRONIC EXCITATION TEMPERATURES OBTAINED BY TWO-LINE RELATIVE INTENSITY METHOD (1.47 μ used as reference)

Emitter Temp T_e	Cesium Temp t_{cs}	Output Current Density J	Electronic Excitation Temperature °K					
°K	°C	Amps/cm²	.80 μ	.92 μ	1.00 μ	1.36 μ	2.4 μ	3.4 μ
1500	200	2.4	-	1550	1802	1075	∞	-
		3.2	-	1739	2410	1695	-	-
		3.2	-	-	2000	1493	-	-
		3.2	-	1724	2532	1163	-	-
		4.0	-	1258	1835	1143	12,500	-
		4.8	-	1786	2410	2041	33,333	3125
		5.0	-	1869	-	1563	-	-
		5.2	-	-	2083	1316	-	2439
		5.5	-	-	2632	1538	-	-
		8.3	-	1575	1869	1527	16,667	-
		9.5	-	-	3448	1786	-	2128
		19.0	-	1770	2500	1389	100,000	-
	225	4.0	-	1449	2198	1143	11,111	2703
		5.1	-	1316	2183	1389	15,385	2778
		8.3	-	1481	2128	1242	7,692	4878
		9.5	-	1376	2283	1575	13,333	2740
		19.0	2632	1828	2778	1493	45,455	3922
	250	4.0	-	1449	2410	1481	23,810	2788
		8.3	2353	1587	2667	1333	7,407	2740
		19.0	2564	1764	2695	1435	10,526	3030
1550	200	2.1	-	1667	2353	1330	12,821	-
		2.2	-	1475	1754	1351	8,333	3333
		4.0	-	1453	2151	1422	20,000	-
		5.1	-	1493	1852	1626	20,000	2801
		8.3	-	1621	2597	1266	18,868	-
		9.5	-	1631	2262	1285	13,888	3205
		19.0	2959	1689	2941	1258	11,111	-

Another similar metal-ceramic thermionic converter was examined spectrographically in the visible region with the aid of a Jarrell-Asch 0.5 meter Scanning Ebert Spectrograph at the Sperry Rand Research Center, Sudbury, Massachusetts. The work was carried out by Ronald H. Curry and Avram A. Kalisky of the Research Center.

Fourteen lines in the cesium spectrum were selected and the function $\ell n \left(\frac{gf\nu^3}{I}\right)$ was plotted versus the energy of upper level of the transition. As discussed before such a plot should yield a straight line with a slope equal to 1/T, provided that the distribution of excited cesium states follows a maxwellian pattern. A straight line could not be drawn directly through the plotted points, but a "least squares fit" yielded lines whose slopes corresponded to "temperatures" of about 1300°K. When one of the lines corresponding to 6723 $(7D_{3/2} \rightarrow 6P_{1/2})$ was omitted similar least square lines gave values of about 1100°K.

In another set of runs in which the emitter temperature was increased 300°K above regular operating temperature, similar methods gave a "temperature" of 2100°K when all fourteen lines were used and 1600°K when only thirteen lines were used.

The results in the visible region thus give values which are quite similar to the infrared study. The term "temperature" is only defined for a Maxwell-Boltzmann distribution of excited levels and thus any consistent deviation from a straight line would indicate the presence of non-maxwellian distribution.

3.6 EFFECT OF ADDITIVE GASES

Experiments conducted at Ford Instrument Company as early as 1960 have indicated that improved performance can be obtained in cesium vapor thermionic converters when foreign gases are added. These experiments consisted of devices in which alumina specimens were indirectly heated with tungsten wire up to 1800°C. After heating the alumina piece marked improvements in output were noted repeatedly. Mass spectrometer studies at the Microwave Division of Sperry Gyroscope Company showed that various gases are evolved during such heating (oxygen with lesser amounts of hydrogen, water, carbon monoxide and carbon dioxide).

A number of glass enveloped planar cesium diodes have been constructed with a 3mm Philips Type B impregnated tungsten emitter with spacings of 0.100". In one of these devices the addition of alumina outgassing additives increased the minimum sustaining output voltage by 10%, the short circuit current by 15% and the maximum power density by 30%.

Some effects of the addition of air as an additive were noted during the probe studies, particularly in cells TC-150 and TC-155 in which air was leaked during testing. The data, although limited, indicates as much as a 50% increase in electron temperature of the plasma and a decrease in electron concentration by almost a factor of 10. Almost identical changes in plasma parameters have been noted for non-additive devices when operating with increased applied voltages across the diodes. In the additive case, a decrease in collector work function would provide the necessary simulated increase in applied voltage. The emphasis on electrode surface effects is strengthened further when one considers the chemically reactive properties of the additive gases. Contributing evidence is also available from the extensive technology which has been developed on photo-emissive oxide surfaces.

SECTION 4. THEORETICAL DISCUSSION

4.1 GENERAL THEORY OF THERMIONIC CONVERTERS

One of the reasons for undertaking the present study was to try to achieve a better insight into the basic processes taking place in a low temperature, low pressure cesium thermionic converter. It was felt that with sound experimental data a better physical and mathematical model would ultimately lead to the design of more efficient thermionic converters.

In any thermionic converter there is an emitter which is heated by an external source to a temperature T_e and a collector which in equilibrium is maintained at a temperature T_C. These are connected through an external circuit with a load resistance R_L. In a very simple theoretical model, electrons inside of the emitter are raised from the Fermi level to the potential just outside the emitter (i.e., this potential energy is increased by $e\phi_e$ where ϕ_e is the work function of the emitter). Upon reaching the collector they fall into its Fermi level (i.e., their potential energy is decreased by $e\phi_C$ where ϕ_C is the work function of the collector). If $\phi_C < \phi_e$, there is an amount of energy equal to $e(\phi_e - \phi_C)$ which can perform external work. Such a converter acts as a battery with an e.m.f. of $\phi_e - \phi_C$ volts.

Even in such a simple converter there are losses which reduce the maximum efficiency. In the first place there is a direct heat radiation from the emitter to the collector which depends directly on the difference $T_e^4 - T_C^4$ and on the emissivities of the emitter and collector. Secondly, there is a considerable amount of loss from direct heat conduction through leads and supports. A third heat loss is due to the fact that the emitted electrons are not given off with zero kinetic energy, but rather with a distribution of energies such that their average kinetic energy is $2kT_e$. The useful converted energy will thus be related to the electron current reaching the collector Fermi level, I_C. The energy $I_C^2R_L$ is the actual output energy. The I^2r energy, where r is the resistance of the leads, is another loss.

The maximum electron current, I_S, which can be obtained at a given emitter temperature is given by Richardson's equation:

$$I_S = AST^2 \exp -\left(\frac{e\phi_e}{kT_e}\right) \tag{1}$$

where S is the effective emission area of the emitter. Unfortunately, in a vacuum diode the electrons in transit between the electrodes will cause a negative space charge to accumulate causing a minimum potential $-V_m$ to be formed which restricts the electron current I_e to a value:

$$I_e = I_S \exp -\left(\frac{eV_m}{kT_e}\right) \tag{2}$$

Such a space charge potential rapidly restricts the electron flow to such low values that thermionic converters have a very low output. It is thus very essential, if a useful converter is to be achieved, to overcome this space charge effect.

One of the more practical methods of reducing the space charge is the neutralization of the electronic charge by ions of an element with a low ionization potential, e.g. cesium. If at every point between the electrodes the ion density (assuming a unit positive charge per ion) equals the electron density, there will be a zero net charge, and thus the space between emitter and collector is field-free.

Fortunately, in order to maintain such a charge neutrality the number of ions generated need not equal the number of electrons emitted. If both electrons and ions are emitted at the emitter with the same energy distribution into a field-free region, their density ρ is given by

$$\rho = \frac{J}{v},$$

where J is the current density per unit area and v is the particle velocity.

The average kinetic energies of electrons and ions would be equal

$$1/2 m_e v_e^2 = 1/2 m_p v_p^2 \quad \text{or} \quad \frac{v_e}{v_p} = \frac{m_p}{m_e}^{1/2},$$

where subscript e refers to electrons, p to ions. Since

$\rho_e = \rho_p$, we obtain that

$$\frac{J_e}{v_e} = \frac{J_p}{v_p}$$

or

$$\frac{J_e}{J_p} = \frac{v_e}{v_p} = \frac{m_p}{m_e}^{1/2}$$

Thus, for Cs^+ ions the ratio of electron to ion current will be $(2.423 \times 10^5)^{1/2} \simeq 490$ under these assumed circumstances.

4.2 SURFACE IONIZATION OF CESIUM ATOM

It is perfectly possible for electrons and ions to be emitted from a single emitter. Langmuir (I. Langmuir, Phys. Rev. 33:954, 1929) found that all cesium atoms striking a heated tungsten surface will be converted into ions. In fact cesium atoms will be ionized at any surface as long as its work function remains above the ionization potential (3.89 volts). Thus, with a cesium pressure of about 0.1 torr a thermionic converter can easily operate with a heated tungsten emitter kept at 2000°K.

There are several difficulties encountered in surface ionization. When a gas is introduced into the interelectrode space there will be losses due to inelastic collision with the gas atoms. Secondly, an emitter with such a high work function has a low electron emissivity; thus, high temperatures are required to achieve reasonable current densities (10 amperes per cm^2 and above). Thirdly, if the temperature is reduced, there will be an increase in cesium coverage so

that the work function of increasing portions of surface falls below 3.89 volts. Then, although the electron emissivity will increase, the surface ionization is rapidly decreasing.

4.3 VOLUME IONIZATION OF CESIUM ATOMS

Another way of achieving a production of ions is by having the ionization take place throughout the volume of the interelectrode space. Normally in order to obtain such volume ionization the collector must be maintained at a potential which is positive with respect to the emitter by at least the ionization potential of the gas between the electrodes. Such a high potential would make thermionic conversion practically impossible.

However, it has been known for many years that under certain conditions an arc can be maintained at potentials far below the ionization potential. Such arcs were first analyzed by Compton and Eckart (Phys. Rev. 25:139, 1929) and by Druyvesteyn (Z. Physik 64: 78, 1930). It was soon discovered that such arcs (known as "low voltage arcs") have a "virtual anode" in the interelectrode space whose potential with respect to the emitter is considerably higher than the collector potential.

The equations of space charge limited discharges were developed by Langmuir (Phys. Rev. 21: 419, 1923) who also made a thorough study of the neutralization of space charge by positive ions (I. Langmuir, Phys. Rev. 33: 954, 1929). Auer and Hurwitz (J. Ap. Phys. 30: 161, 1959) have expanded this last work.

Whereas "normal" discharges have been fairly well analyzed, the analysis of the low voltage arc presents several special difficulties. Originally Compton and Eckart made measurements which indicated that the maximum space potential was equal to the ionization potential. It was found difficult to explain how the electrons which had caused the ionization could obtain sufficient energy to

overcome the potential barrier to reach the collector. Druyvesteyn (Z. Phys. 64:781, 1930) gave an explanation in having the electrons, coming into the plasma region, share energy with the "ultimate" electrons present giving them the required energy. Also a large concentration gradient had to be present in order to the required "drift current".

Malter, Johnson and Webster (RCA Rev. 12: 415, 1951) discuss various arcs and the transition, in the case of noble gas discharges, from the anode-glow discharge through the "ball-of-fire" mode or low voltage arc to the "Langmuir mode" and then to the temperature limited case where full saturation current is drawn. According to Johnson (RCA Rev. 16: 498, 1955) in the case of the low voltage arc the maximum space potential is far below the ionization potential. In this case it was a prevalent assumption that cumulative ionization was the dominant mechanism. However, Johnson shows that direct ionization by the high energy tail of the Maxwellian distribution is sufficient to explain the effect.

However, other mechanisms can help maintain the required degree of ionization. Thus photoionization experiments have shown (K. Freudenberg, Z.F. Physik 67, 417 (1931)) that collisions between excited cesium atoms and neutral atoms or between two excited atoms can result in an ionized cesium molecule. This process is aided by the binding energy (.35 volts) of the molecule and the fact that only 3.2 volts is required to ionize a cesium molecule. Thus only about 2.9 volts need be supplied to produce a cesium molecular ion versus about 3.9 volts for a cesium atomic ion.

This process is aided by the well-known "imprisonment of resonance radiation", i.e., resonance lines will tend to be absorbed within the plasma and thus maintain a high level of excited states. Even the 8521 line, corresponding to 1.45 volts, can excite atoms which are able to combine to give a molecular ion.

4.4 EMITTER SHEATH

For practical purposes the discharge can be divided into three regions: the emitter sheat, the plasma, and the collector sheath. We can take the emitter sheath to be the region between the surface of the emitter and the potential maximum. We assume that practically no collisions occur in this region and that the plasma is the source of an ion current density J_p. By applying Langmuir's method to a Maxwellian distribution of electrons emitted at the emitter at a temperature T_e, we find that there will be a potential minimum in this region with a value $-V_m$. The electron current density J_e into the plasma is given by

$$J_\epsilon = J_s \exp -\left(\frac{eV_m}{KT_e}\right) \tag{3}$$

where J_s is the saturation electron current density found by Richardson's equation:

$$J_s = AT_e^2 \exp -\left(\frac{e\phi_e}{KT_e}\right) \tag{4}$$

In equation (4), A is a constant (= 120 amperes cm^{-2} $sec^{-1}deg^{-2}$), ϕ_e is the work function of the emitter, k is Boltzmann's constant and e the electron charge. Between the emitter surface and the potential minimum the electron concentration

$$\rho_\epsilon = \frac{J_e}{e}\left(\frac{\pi m_\epsilon}{2kT_e}\right)^{1/2}\left[1 + \text{erf}\left(\frac{eV}{kT_e}\right)^{1/2}\right]\exp\left(\frac{eV}{kT_e}\right) \tag{5}$$

Past the potential minimum

$$\rho_\epsilon = \frac{J_\epsilon}{e}\left(\frac{\pi m_\epsilon}{2kT_e}\right)^{1/2}\left[1 - \text{erf}\left(\frac{eV}{kT_e}\right)^{1/2}\right]\exp\left(\frac{eV}{kT_e}\right) \tag{6}$$

where m_ϵ is the mass of an electron and V the potential at the point in question

with respect to V_m. The positive ion density

$$\rho_p = \frac{J_p}{e}\left(\frac{\pi m_p}{2kT_p}\right)^{1/2}\left[1 - \text{erf}\sqrt{\frac{e}{kT_p}(V_p - V)}\right] \exp\left\{\frac{e}{kT_p}(V_p - V)\right\} \tag{7}$$

where m_p is the mass of the ion, T_p the ion temperature in the plasma and V_p the maximum space potential (with respect to V_m). By applying Poisson's equation,

$$\frac{d^2V}{dx^2} = \frac{(\rho_\epsilon - \rho_p)e}{\epsilon_o} \tag{8}$$

(ϵ_o = permittivity of freespace), and integrating once by applying the condition that at the potential minimum $\frac{dV}{dx} = 0$ and $V = 0$, we obtain:

$$\begin{aligned}\left(\frac{dV}{dx}\right)^2 = \frac{J_\epsilon}{e\epsilon_o}(2\pi m_\epsilon kT_e)^{1/2} \Bigg\{ & \left(1 \pm \text{erf}\sqrt{\frac{eV}{kT_e}}\right)\exp\left(\frac{eV}{kT_e}\right) \mp \frac{2}{\pi^{1/2}}\left(\frac{eV}{kT_e}\right)^{1/2} - 1 \\ & + \frac{J_p}{J_\epsilon}\left(\frac{m_p T_p}{m_\epsilon T_e}\right)^{1/2}\Bigg[\left(1-\text{erf}\sqrt{\frac{e}{kT_p}(V_p - V)}\right)\exp\left(\frac{e}{kT_p}(V_p - V)\right) \\ & + \frac{2}{\pi^{1/2}}\sqrt{\frac{e}{kT_p}(V_p - V)} - \left(1-\text{erf}\sqrt{\frac{eV_p}{kT_p}}\right)\exp\left(\frac{eV_p}{kT_p}\right) \\ & - \frac{2}{\pi^{1/2}}\left(\frac{eV_p}{kT_p}\right)^{1/2}\Bigg]\Bigg\}\end{aligned} \tag{9}$$

where the top sign is valid before the potential minimum and the bottom sign after. At the potential maximum $\frac{dV}{dx} = 0$, $V = V_p$ and we obtain

$$\frac{J_p}{J_\epsilon}\left(\frac{m_p T_p}{m_\epsilon T_e}\right)^{1/2} = \frac{1-\left(1-\text{erf}\left[\frac{eV_p}{kT_e}\right]^{1/2}\right)\exp\left(\frac{eV_p}{kT_e}\right)-\frac{2}{\pi^{1/2}}\left(\frac{eV_p}{kT_e}\right)^{1/2}}{1-\left(1-\text{erf}\left[\frac{eV_p}{kT_p}\right]^{1/2}\right)\exp\left(\frac{eV_p}{kT_p}\right)-\frac{2}{\pi^{1/2}}\left(\frac{eV_p}{kT_p}\right)^{1/2}}$$

Since $\left(1-\text{erf}\, X^{1/2}\right)\exp X \simeq (\pi X)^{-1/2}$ (for $X > 2$),

and since $\frac{2}{\pi^{1/2}}\left(\frac{eV_p}{kT_e}\right)^{1/2} >> 1 > \left(\frac{\pi eV_p}{kT_e}\right)^{-1/2}$

and $\frac{2}{\pi^{1/2}}\left(\frac{eV_p}{kT_p}\right)^{1/2} >> 1 > \left(\frac{\pi eV_p}{kT_p}\right)^{-1/2}$

we obtain $$\frac{J_p}{J}\quad\frac{m_p T_p}{m\ T_e}\quad\frac{T_p}{T}^{1/2} \qquad (11)$$

or $$\frac{J_p}{J_\epsilon} = \left(\frac{m_\epsilon}{m_p}\right)^{1/2} \qquad (12)$$

This is the familiar relationship.

We also find that for $T_e = 1500^\circ K = T_p$, $J_e = 10$ amps/cm^2 and $V_p = 1.5$ volts, that the cathode sheath will be about 0.005 cm. thick, a reasonable value as evidenced by visual observation of the discharge. This also supports the validity of the assumption of no collisions in the emitter sheath.

4.5 PLASMA REGION

Inside of the plasma region there is effectively no free charge (i.e., total charge = 0) so that $\rho_\epsilon = \rho_p = n$. The electron flow density $\vec{\Gamma}_\epsilon$ and the ion flow density $\vec{\Gamma}_p$ are governed by the flow equations

$$\vec{\Gamma}_\epsilon = -n \mu_\epsilon \vec{E} - \nabla (D_\epsilon n)$$
$$\vec{\Gamma}_p = n \mu_p \vec{E} - \nabla (D_p n)$$

and the continuity equations

$$\nabla \cdot \vec{\Gamma}_\epsilon = zn \simeq 0$$
$$\nabla \cdot \vec{\Gamma}_p = zn$$

where the subscripts ϵ and p refer to electrons and ions, respectively, E is the electric field, u the mobility and D the diffusion coefficient. z is the number of ions generated per second per electron and, according to Johnson (RCA Rev. 16: 498, 1955), it is given by

$$z = 0.625 \times 10^6 \, T_\epsilon^{1/2} \, a \, p \, (V_i + 2kT_\epsilon/e) \exp(-eV_i/kT_\epsilon)$$

where the quantity a is defined in equation 4.1 on page 79 of Cobine (Gaseous Conductors, Dover, N.Y., 1958), p is the vapor pressure in torr and V_i is the ionization potential of the vapor. Johnson derives this expression by assuming a one-step ionization of the gas by the high energy tail of a maxwellian distribution of the impinging electrons. Since our measurements indicate that the electrons in the plasma of our discharge are almost entirely maxwellian or very closely maxwellian, this expression is valid.

Since our measurements show no appreciable variation of the potential along the x-axis, the longitudinal component of the electric field must be zero. However, the electron temperature does change so that the electron diffusion coefficient D_ϵ cannot be removed from under the differentiation sign at least in the x direction. By further making the assumptions that the radial flow of electrons is zero under dynamic equilibrium, that D_p is constant and that z can be represented by an average z throughout the region, depending on an average electron temperature $\bar{T}_\epsilon$, we obtain an expression for the minimum $\bar{T}_\epsilon$ required to maintain the discharge

$$f(\bar{T}_\epsilon) = 0.625 \times 10^6 \, \bar{T}_\epsilon^{-1/2} \left(V_i + \frac{2k\bar{T}_\epsilon}{e}\right) \exp -\left(\frac{eV_i}{k\bar{T}_\epsilon}\right) = \frac{\mu_p k}{ape}\left[\frac{5.784}{r_1^2} + \frac{9.87}{l^2}\right]\frac{T_p}{\bar{T}_\epsilon}$$

and for the concentration

$$n = C_1 J_o(2.405\, r) \cos\left(\pi x/l + C_2\right)$$

where r_1 is the outside radius of the plasma, l is the length of the plasma and C_1 and C_2 are constants.

The observed electron concentration distribution agrees quite well with the cosine distribution given by the above equation. The radial distribution is close to the Bessel function found. Further, by inserting values appropriate to our discharge it is found that $C_2 \simeq \pi/2$ and thus the maximum concentration of electrons (and ions) should occur near the center of the plasma. Again this corresponds to the position of the maximum as determined by the measurements. By inserting the best available values we obtain

$$f(\bar{T}_\epsilon) = .5064 \left[\frac{5.784}{r_1^2} + \frac{9.870}{l^2}\right]\frac{T_p}{\bar{T}_\epsilon}$$

Since, as mentioned previously, the visible discharge appears to be confined almost exclusively within a cylinder with a radius equal to the radius of the emitter (.3 cm) and a length equal approximately to the emitter to collector separation, we can put r_1 = .15 cm. and l = .25 cm. corresponding to TC-158. If we then assume that $T_p/\bar{T}_e$ is about 0.1 we find that

$$T = 8100^{\circ}K$$

This value agrees remarkably well with the value 7900°K actually found near the center of the discharge considering all the assumptions made in the derivation of the equation.

The equation also shows that the temperature should decrease when the separation and/or the emitter area is increased. Again this decrease is noted. If we place r = .32 cm and ℓ = .44 cm, the values corresponding to those present in the metal-ceramic cell, we find

$$T = 7000^{\circ}K.$$

Actually the measured temperature is about 5500°K. This result indicates that whereas a large part of the ionization can be explained simply by the high energy tail of the maxwellian distribution, other processes must be present. However, the enhancing effects of resonance entrapment and of molecular ion formation as discussed previously undoubtedly explain the required remainders.

4.6 COLLECTOR SHEATH

The collector sheath must supply conditions which match the edge of the plasma with the surface of the collector. Thus there must be a retarding field present in the sheath in order to permit the proper number of electrons to escape from the plasma to correspond to the measured current. This retarding field must arise from a potential drop V_c which is given by

$$V_c = \frac{kT_\epsilon}{e} \ell n \frac{\rho_\epsilon \bar{v}_\epsilon}{4 \Gamma_\epsilon}$$

where $\bar{v}_\epsilon$ is the average velocity of the electrons and all the values in the right side of the equation refer to the collector edge of the plasma. By our measurements in TC-158 we have

$$T_\epsilon = 5600^\circ K$$

$$\rho_\epsilon = .57 \times 10^{13} \text{ cm}^{-3}$$

$$J_\epsilon = e \Gamma_\epsilon = 4.5 \text{ amps/cm}^2$$

and $\bar{v}_\epsilon = 6.21 \times 10^5 \, T^{1/2} = 4.65 \times 10^7$ cm/sec.

Thus we find

$$V_c = .41 \text{ volt.}$$

The considerations discussed above are illustrated in Figure 39 which shows the potential diagram for electrons which is present in our thermionic converters according to the measured values. The actual values for the quantities shown in Figure 39 in the case of the particular glass cell used with the adjustable probe are

$\phi_e = 2.2$ volts (corresponding to $J_e = 10$ amps/cm^2)

$V_m = 0.1$ volt

$V_e = 1.3$ volts

$V_c = 0.4$ volt

$V = 0.1$ volt

According to Figure 39 we see that the plasma drop must be $V_e - V_c = 0.9$ volt. The collector work function $\phi_c - \phi_e - V - JR_p = 1.2$ volts.'

For the metal-ceramic probe cell TC-230 we have

$$T_e = 5000^oK$$

$$\rho_e = 0.8 \times 10^{13} \text{ cm}^{-3}$$

$$J_e = 6.5 \text{ amps/cm}^2$$

and thus $$V_c = 0.3 \text{ volt.}$$

Since V is 0.2 volt and V_e is 1.0 volt and assuming the other values are the same as for TC-158, the plasma drop V_d is $V_e - V_c = 0.7$ volt. The collector work function ϕ_c is given by

$$\phi_e - V_d - V = 2.2 - 0.7 - 0.2 = 1.3 \text{ volts.}$$

These estimates of collector work function indicate strongly that the collector surface is a complex one and not simply pure cesium upon clean molybdenum. The emitter evaporants in conjunction with outgassing reaction compounds produce multi-atom attraction forces at the collector surface.

4.7 ENERGY BALANCE

We have shown that the electron temperature, electron concentration, and space potential distribution agree fairly well with a simply physical picture. One further point must be discussed. This is the energy balance in an operating thermionic device. As discussed earlier, the heat applied to the emitter raises the electrons from their Fermi level inside the emitter to the potential at the surface, and supplies them with an additional amount of energy equal to $2kT_e$. Heat is lost from the emitter by radiation and conduction.

The maximum output from the cell per electron is equal to $(\phi_e - \phi_C)e$. However, in the plasma additional energy is lost by radiation and diffusion of the ions. This energy is equivalent to perhaps a few tenths of a volt. A more serious loss is due to the fact that at the collector edge of the plasma the electrons are at a much higher temperature than at the emitter surface. Thus, the average kinetic energy in the direction of the collector at the emitter is $2kT_e$. At the collector it is $2kT_C$ where T_C is the electron temperature at the collector. Thus a potential drop equal to $2k(T_C - T_e)$ must be supplied in the arc to take care of this loss. Since T_e was 1500^oK, in the case of glass cell TC-158 this will amount to $2k(4100^oK) = 0.7$ volt, while for metal-ceramic cell TC-230 it is $2k(3500^oK) = 0.6$ volt. Since an 0.9 volt arc drop was found in the first case and 0.7 volt in the second, 0.2 volt and 0.1 volt, respectively, are available for other arc losses. Thus the energy balance appears to check quite well.

SECTION 5. EMITTER WORK FUNCTIONS AND PATCH EFFECTS

5.1 Work Functions

Our major interest in the work functions of the emitter and collector is focused on their ultimate effect on diode output. The most obvious effects are on the electron emissivity of the emitter and on the output voltage of the converter.

The work function is basically a measure of the energy of electrons at the emitter surface. Therefore, in order to understand its significance we must study the energy of electrons both inside and outside of materials. There are two basic approaches: the macroscopic or thermodynamic method and the microscopic or statistical-mechanical method. The thermodynamic approach has the advantage that no particular model or physical assumptions need be made. Variables are defined in experimentally measurable terms and appropriate equations are derived by purely mathematical methods. Herring and Nichols (Revs. Mod. Physics 21: 185, 1949) define quantities $\bar{\mu}$ and μ which they call the electrochemical and the chemical potentials respectively:

$$\bar{\mu} = (\partial F/\partial n)_{T,v} \qquad (1)$$

$$\mu = \bar{\mu} + e\,\phi \qquad (2)$$

where F is the Helmholtz free energy, n is the electron concentration, e is the electron charge and ϕ is the electrostatic potential. μ has the advantage over $\bar{\mu}$ in that it is independent of surface and external conditions. These variables can then be used to derive useful equations.

The statistical approach, on the other hand, requires specific assumptions to be made about the internal states (i.e., it needs a physical model). However, it permits a much better insight into the actual processes involved. In order to apply the statistical-mechanical method each electron

is assumed to be specified by six variables or "coordinates", three spatial coordinates and three momentum coordinates.

From Heisenberg's Uncertainty Principal (i.e., relating to Planck's quantum hypothesis) a "point" in phase space must have a volume of h^3. Furthermore, since electrons have spins of one-half unit, their wave functions must possess certain symmetry properties. This leads to Pauli's exclusion principle: Each quantum energy level can be occupied by one and only one particle with a half-integral spin. However, since there are two possible orientations of the spin of an electron and the spin orientation does not affect the magnitude of an energy level, each energy level can hold two electrons. Inside of a solid where the energy levels are discrete and there are large numbers of electrons present, then, even at absolute zero, high energy levels must be populated by electrons. In summary, half-integral spin particles must obey Fermi-Dirac statistics. Other particles obey Bose-Einstein statistics.

The result of these considerations is that electrons inside of a solid do <u>not</u> have a Maxwellian distribution of energy, but rather, the probability that a state of energy ϵ is occupied is given by the expression

$$\frac{1}{\exp\left(\frac{\epsilon - \mu}{kT}\right) + 1},$$

where μ here is known as the Fermi level which is the energy level with an occupation probability of one-half. It must be noted that in a vacuum, electrons are essentially free particles; hence, their energy levels become

continuous, and the Pauli exclusion principle is meaningless. Thus, in a vacuum, the electrons can possess a Maxwellian distribution.

We can now define the "true work function" ϕ as the difference between the electrostatic potential energy of an electron just outside the surface of a solid ($-O_a$) and its Fermi level just inside the surface ($\bar{\mu}/e$):

$$\phi = -O_a - \bar{\mu}/e \tag{3}$$

Since the Fermi levels of two conductors in contact must be equal, their "contact potential" is equal to the difference in their work functions. The output of a thermionic converter depends on the contact potential between collector and emitter; therefore, the determination of the work functions is of utmost importance in the theoretical analysis of these devices.

For the case of a plane emitter with a perfectly smooth surface and a uniform work function which emits electrons with a Maxwellian distribution, the familiar Richardson equation can be derived.

$$j_s = A \quad T^2 \quad e^{e\phi/kT} \tag{4}$$

where j_s = saturation current density

$$A = \frac{4\pi mk^2e}{h^3} = 120 \text{ amp/cm}^2\text{T}^2$$

A somewhat more sophisticated derivation gives an equation of the following form:

$$j_s = A\,(1-r)T^2e^{e\phi/kT} \tag{5}$$

where r is a reflection coefficient. Unfortunately, this reflection coefficient is very difficult to determine, but indications are that it is generally very close to zero; hence, the simpler Richardson equation is quite adequate if its restrictions are duly noted.

It is known that the work function varies linearly with temperature:

$$\phi = \phi + \alpha T \tag{6}$$

Thus, we can write the Richardson equation in the form:

$$j_s = A^* T^2 \, e^{e\phi/kT} \qquad (7)$$

where $A^* = A \, e^{\alpha e/k}$ (or more exactly $A(1-r)e^{\alpha e/k}$

This form is applied very frequently. However, it appears more profitable for us to apply the original Richardson equation since we are mostly interested in the actual work function at operating temperature, and this permits a more direct comparison of different emitters.

Another phenomenon which must be considered is the well-known Schottky Effect (Nottingham, Thermionic Emission, Encyclopedia of Physics 21:1, 1956). It is apparent from the definition of the true work function that if the potential outside the surface of an emitter is changed the true work function also changes. Thus, if an electric field is applied, the work function will be reduced by an amount proportional to the square root of the electric field. If a plot is made of the logarithm of the collected current versus the square root of the electric field, , a straight line should be obtained once the space-charge limited region is passed. This line has the equation (Millman and Seely, Electronics, McGraw-Hill, 1951, p. 151)

$$\log_{10} I = \log_{10} I_{th} + \frac{0.190 \, \mathcal{E}^{1/2}}{T} \qquad (8)$$

Thus the slope of the line is $0.190/T$. Such a "Schottky Plot" can give valuable information and will be discussed again in the next section.

5.2 "Patch Effects"

Actual emitters very rarely possess uniform surfaces with a constant work function. A surface with "patches" of different work functions next to each other would give rise to electric fields which would seriously affect emission. In the case of closed-spaced devices, such patches could be considered to be equivalent to numerous diodes connected in parallel and would

decrease the efficiency of a converter considerably (Weigmann and Gummick, Closed-Spaced Thermionic Converter Effects, AIEE Pacific General Meeting, Aug. 1960).

In the case of diodes where the interelectrical spacing is large in comparison with the size of the patches, Herring and Nichols (Revs. Mod. Physics, 21: 185, 1949) show that when small fields are present the Schottky plot will be a straight line with the same slope as a uniform surface with the following work function:

$$\bar{\phi} = \sum f_i \ \phi_i$$

where f_i is the fraction of the surface occupied by a material with a work function of ϕ_i. $\bar{\phi}$ is the effective work function of the composite surface. With higher fields this relationship no longer holds true. However, Schottky plots with high fields present can yield valuable information as to the exact character of a surface. Unfortunately in vapor diodes, externally applied, high fields cause extensive ionization effects which mask such surface phenomena.

In the case of dispenser cathodes the surface is rather rough and fields are present due to this roughness, causing a greater slope to the Schottky lines (J. Ap. Phys. 28: 2, 12, 1957). L-cathodes in a vacuum have a surface consisting of a complete barium monolayer on top of a nearly complete monolayer of oxygen. For impregnated cathodes in a vacuum the same is almost true except that there is emission from the impregnant at the ends of the pores (Brit. J. Ap. Phys. 8: 27, 1957). Thus, the basic surface is not quite as patchy. The effect of cesium on such a surface is reported in the following section.

5.3 Effects of Adsorbed Gases

The classic experiments of Langmuir (Taylor and Langmuir Phys. Rev. 44: 423, 1933) and Becker (Becker, Trans Amer. Chem. Soc. 55: 153, 1929) on the effects of the adsorption of cesium and barium on tungsten have provided the physical model of the adsorption process by which resulting changes in the metal work function can be calculated to a high degree of accuracy.

Electropositive elements, such as cesium and barium, tend to give up their valence electrons to the base refractory metal, forming an electric dipole layer with the positive end of the dipole standing outward from the surface of the metal. An electron in the metal will gain an amount of energy $\Delta V = 2\pi\sigma\mu$ (where σ is the surface density of adsorbed ions, and μ is the dipole moment of the layer) in going through the dipole layer. The quantity ΔV represents the amount by which the work function of the metal has been lowered for a given coverage σ. The effects of other factors such as van der Waals interaction and interactions between adsorbed ions on the surface are responsible for a ten to fifteen percent energy contribution to $\Delta V'$, the measured decrease in work function (DeBoer, Electron Emission and Adsorption Phenomena, Cambridge 1934). An electronegative element, on the other hand, tends to form a dipole layer with the negative end of the dipole standing outward from the surface of the metal. An electron within the metal would lose energy in traversing the dipole layer, so that the effective metal work function is increased. Since the positive ions in the metal remain in relatively fixed positions however, the strength of the dipole layer is less than in the case of adsorption of the electropositive elements, so that electropositive positive elements are held more strongly to the metal surface than are electronegative elements.

A layer of adsorbed cesium or barium then, lowers the work function, while an adsorbed layer of oxygen raises it. It is, however, an experimentally determined fact that the simultaneous adsorption of oxygen and cesium or barium lowers the work function more than the adsorbed layer of cesium or barium alone does. This phenomenon can be explained by assuming that the oxygen and cesium atoms are adsorbed next to each other (rather than in successive layers) on the surface. The presence of the oxygen atom or ion increases the surface binding energy of the cesium making it easier for electrons within the metal to escape. Use of this phenomenon is made in the construction of impregnated cathodes, in which layers of oxygen and barium are present on the cathode surface. The interaction of cesium with the adsorbed layers of oxygen barium appears to enhance the emission. There is not, at this time, sufficient experimental data on which to base a more sophisticated theory of multicomponent adsorption which is needed to explain the observed phenomena.

5.4 Experimental Results

An analysis of the available emission data and I-V characteristics of cesium-filled test cells showed that the effective work function of the cesium covered impregnated tungsten varies essentially linearly with the emitter temperature, within the range of temperatures of interest, 1400-1600°K. Figures 40 and 41 show plots for two cylindrical cells for which a relatively large amount of experimental data was available. The data shows that the effective work function, ϕ_E, is well represented by

$$\phi_E = \phi_{1500} + 1.04 \times 10^{-3} (T-1500) \qquad (1)$$

where ϕ_{1500} is the effective work function at 1500°K. At a cesium temperature of 200°C, $\phi_{1500} = 2.17$ volts. According to Stout (Proc. Fourth Nat. Conf.

on Tube Techniques, 178, NYU Press, 1959) the vacuum emission of the impregnated tungsten emitter is

$$\phi = 2.25 + 3.2 \times 10^{-4} (T-1500) \qquad (2)$$

If the cesium pressure is varied the work function varies as

$$\phi_E = \phi_{200} - 1.9 \times 10^{-3} (t-200) \qquad (3)$$

where ϕ_{200} is the effective emitter work function at a cesium temperature t = 200°C. (See Figure 41)

It is quite apparent that the variation in work function is due to a varying coverage of the emitter by cesium. By using equation (24), noting that the work function of pure cesium $\phi_{cs} = 1.81 - 2.59 \times 10^{-5}T$, and assuming that the sub-layer of the impregnated cathode is a uniform surface, we find that $f_{cs} = 0.17$ for T = 1500°K and $t_{cs} = 200°C$. This agrees reasonably well with the value 0.20, coverage of pure tungsten at such a cesium pressure.

If we extrapolate the equations to find the emitter temperature at which the cesium coverage would be zero, we set equation (25) equal to equation (26) and obtain T = 1629°K (t = 200°C). This is near the temperature range within which the equations should be valid. Thus, it indicates that at 1629°K and a cesium temperature of 200°C there would be practically no cesium on the surface. If we set equation (25) equal to equation (27), we find that at T = 1126°K (t = 200°C), $f_{cs} = 1$. Thus, if the equations are valid at this low temperature, a complete monolayer of cesium would cover the basic emitter.

We see from the above that under operating conditions (T = 1500°K; t = 200°C) our emitter will be covered by approximately one-fifth of a monolayer of cesium. If the temperature of the emitter is increased to about 1630°K, there would be no effective cesium present on the surface, while the emitter would have to be kept well below 1200°K before a complete monolayer would be formed.

SECTION 6. RECOMMENDATIONS

The pulsed Langmuir Probe techniques developed here should be extended to other practical geometries beyond that of the planar diode. The use of the probe as a thermionic diagnostic tool in device development can also place experimental programs on a firmer basis by making the microscopic plasma characteristics immediately available during any parametric study. Furthermore, the development of miniature probe fabrication techniques for closer spaced diodes might be seriously considered for comparison with the higher temperature cesiated refractory metal family of diodes.

The results of future investigations on electron cross-sections should be applied to the spectrographically determined distribution of excited cesium atoms to calculate an electron temperature. Then comparisons with probe determined electron temperatures would be meaningful. In addition, such probe and spectrographic data should be taken simultaneously from the same device to avoid drift complications.

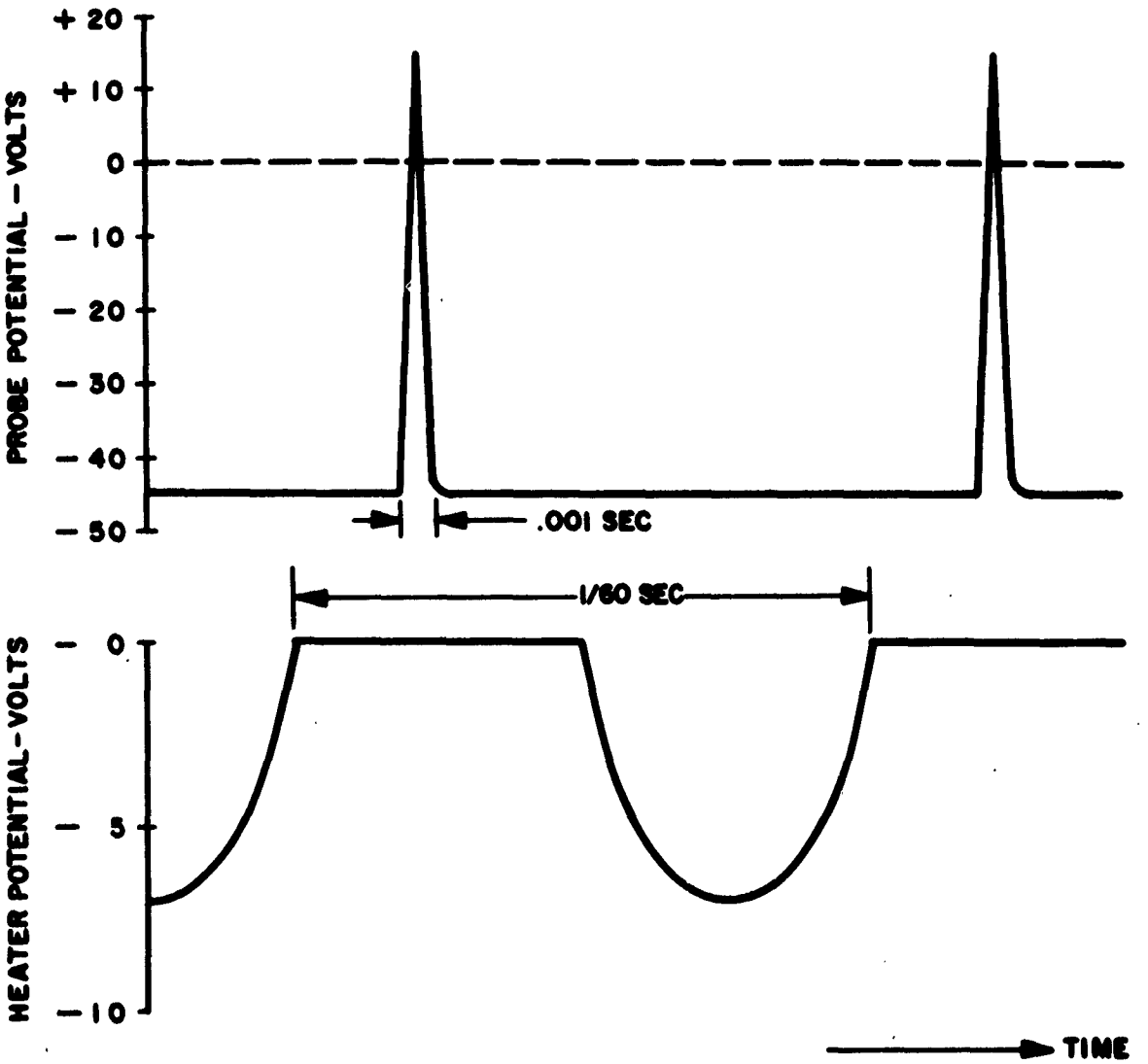

FIGURE 1
TEMPORAL RELATIONSHIP BETWEEN PROBE PULSE AND HEATER VOLTAGE

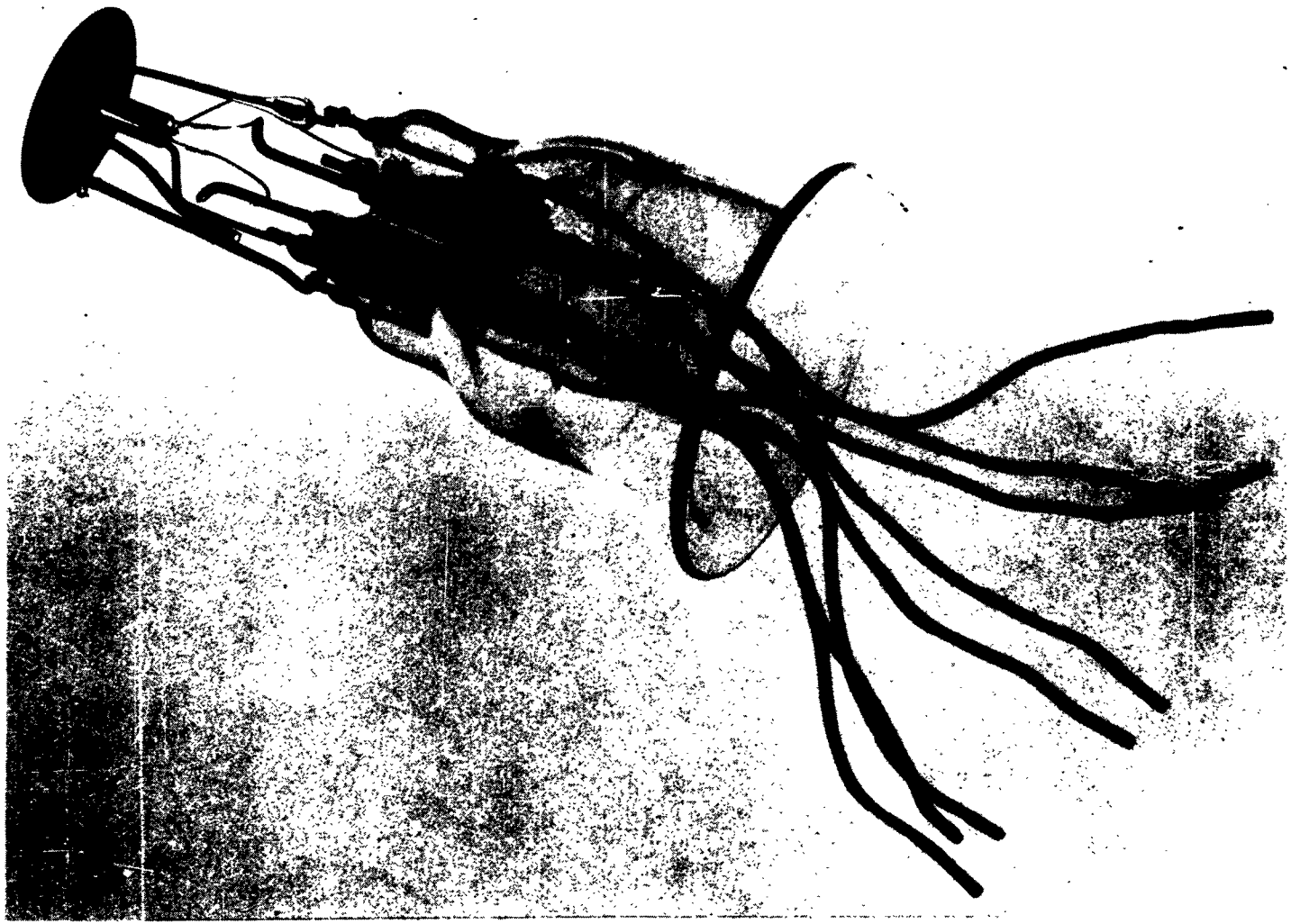

FIGURE 2. RADIAL PROBE ASSEMBLY FOR TC-94

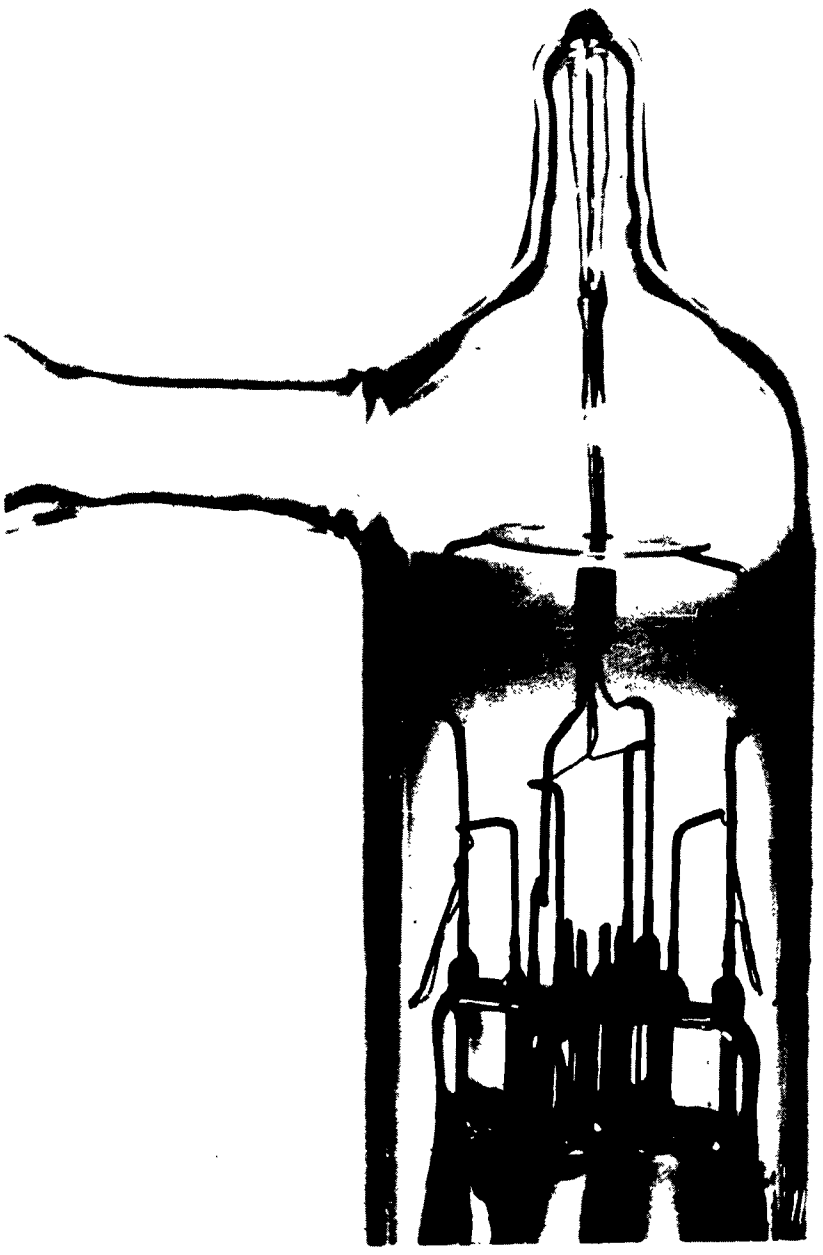

TEST CELL #106 - AXIAL PROBE ASSEMBLY, PARALLEL PLATE GEOMETRY

FIGURE 3

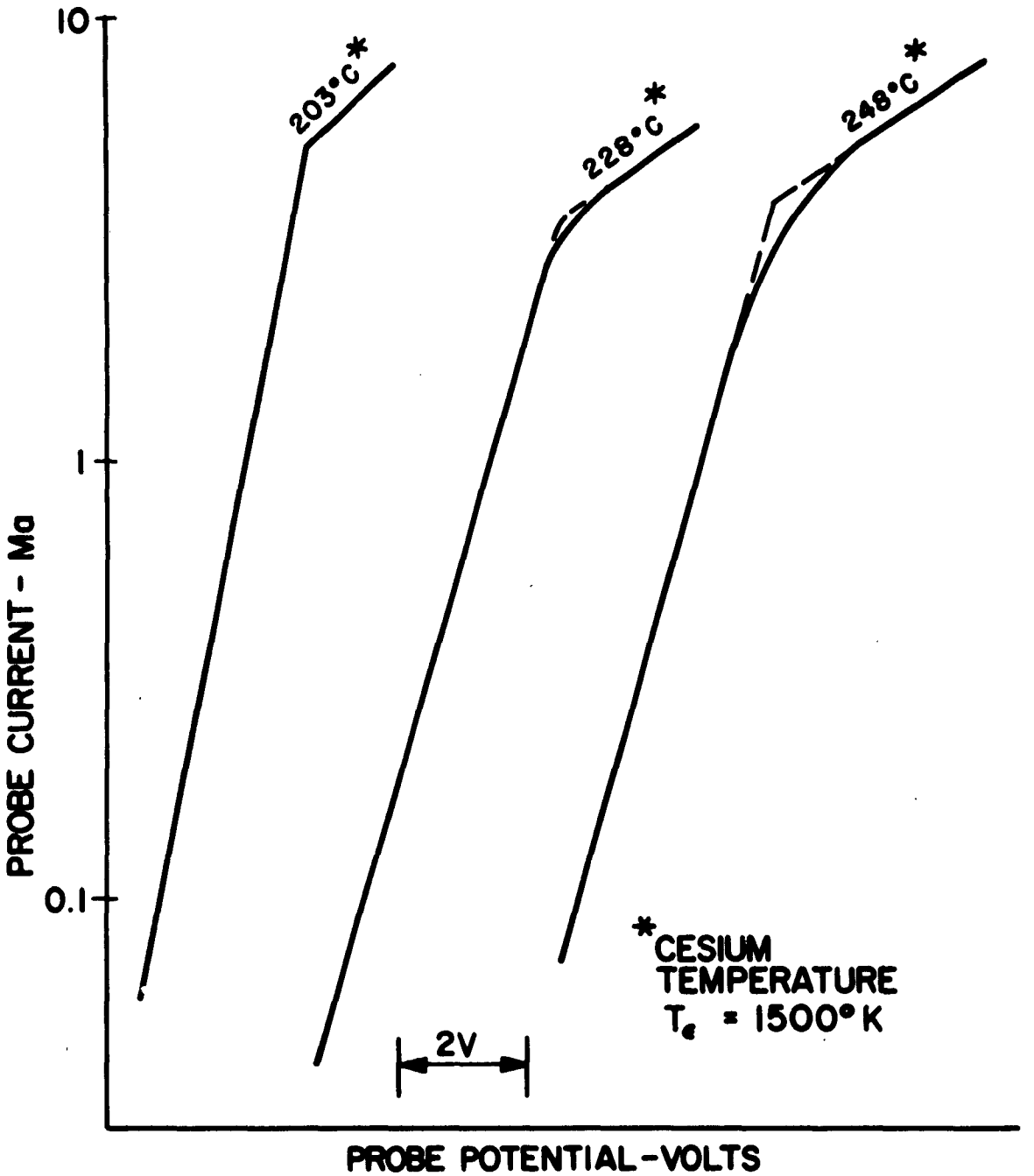

FIGURE 4
PROBE CHARACTERISTICS OBTAINED WITH FIXED PROBE CELL TC-106.
EMITTER TEMPERATURE, T_e = 1500 °K.

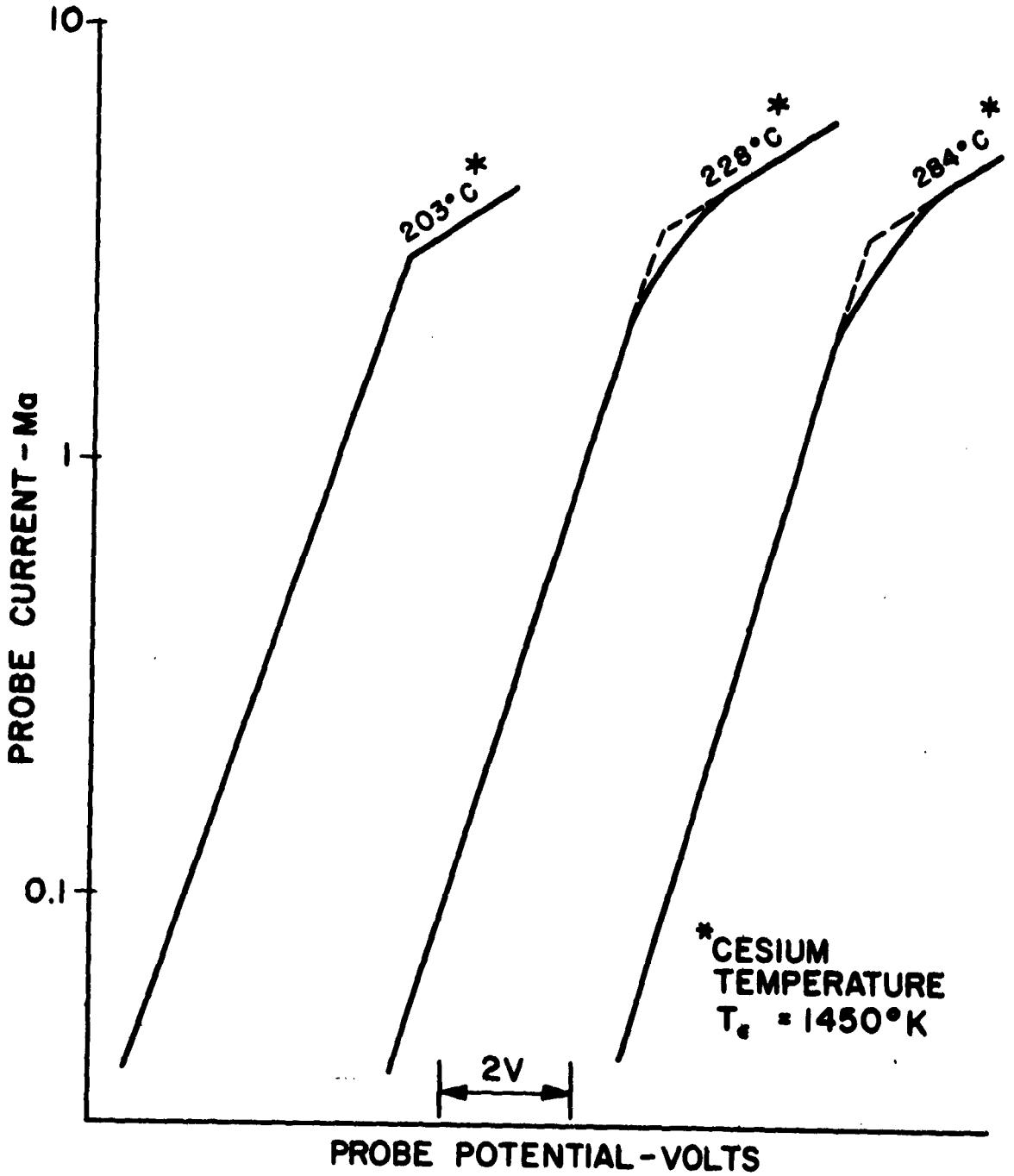

FIGURE 5
PROBE CHARACTERISTICS OBTAINED WITH FIXED PROBE CELL TC-106.
EMITTER TEMPERATURE, T = 1450°K.

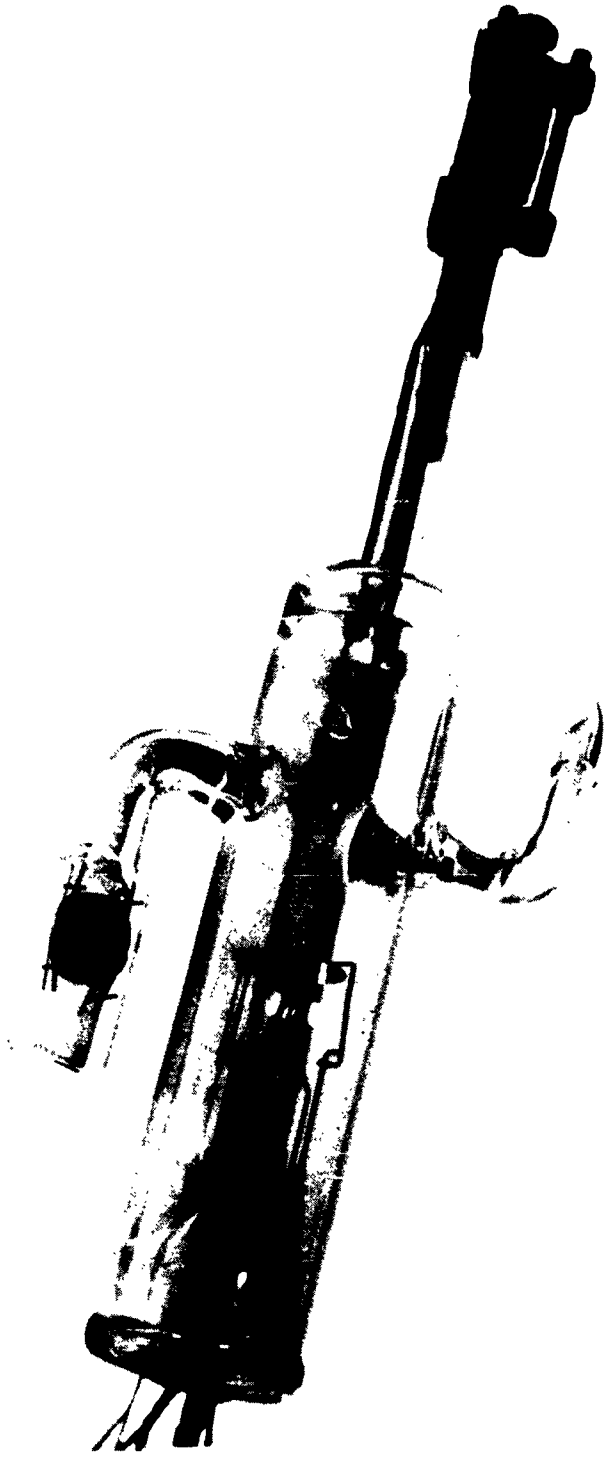

FIGURE 6 ADJUSTABLE LONGITUDINAL PROBE TUBE

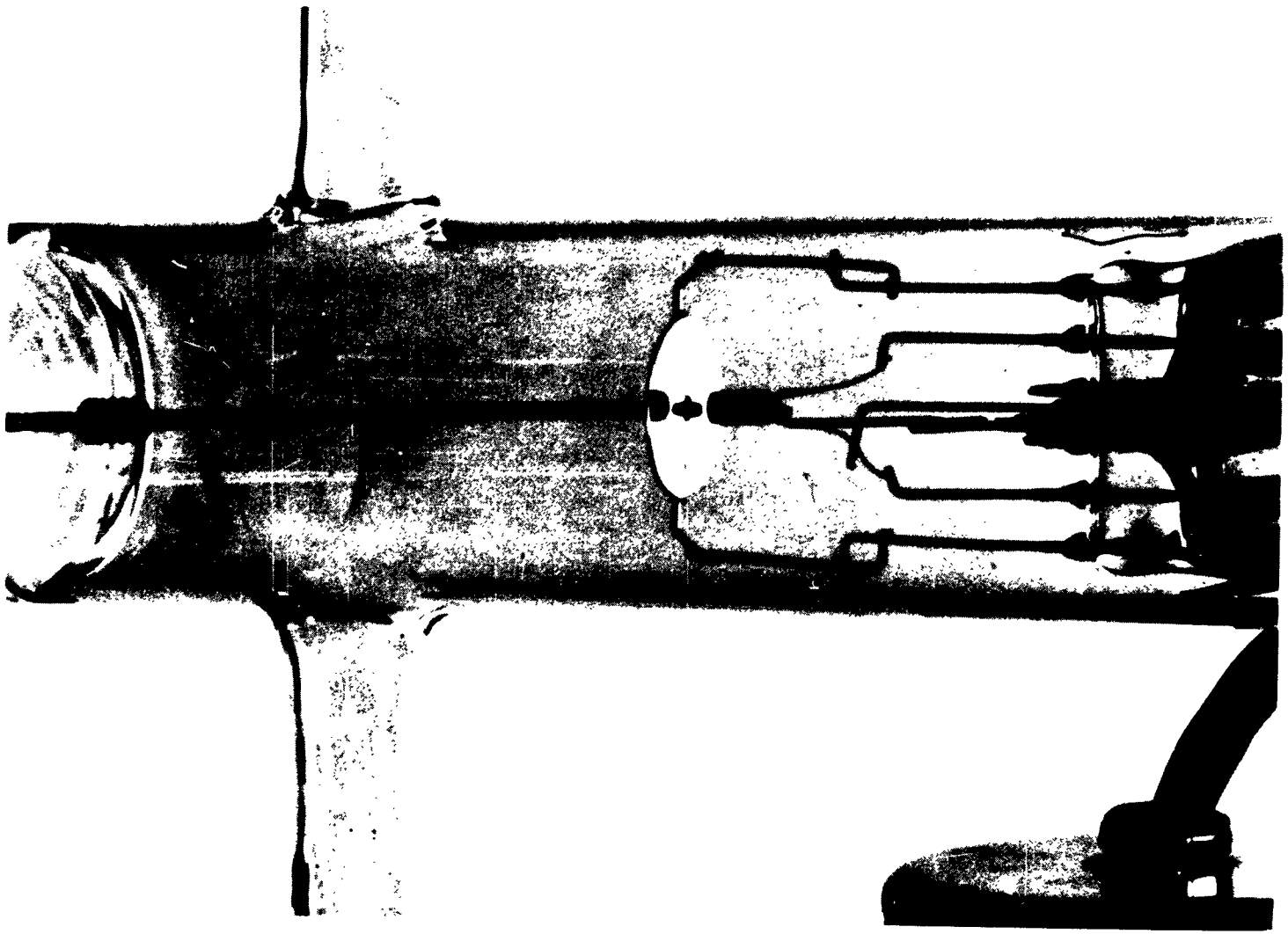

FIGURE 7. DETAILS OF PROBE ASSEMBLY IN ADJUSTABLE LONGITUDINAL PROBE TUBE

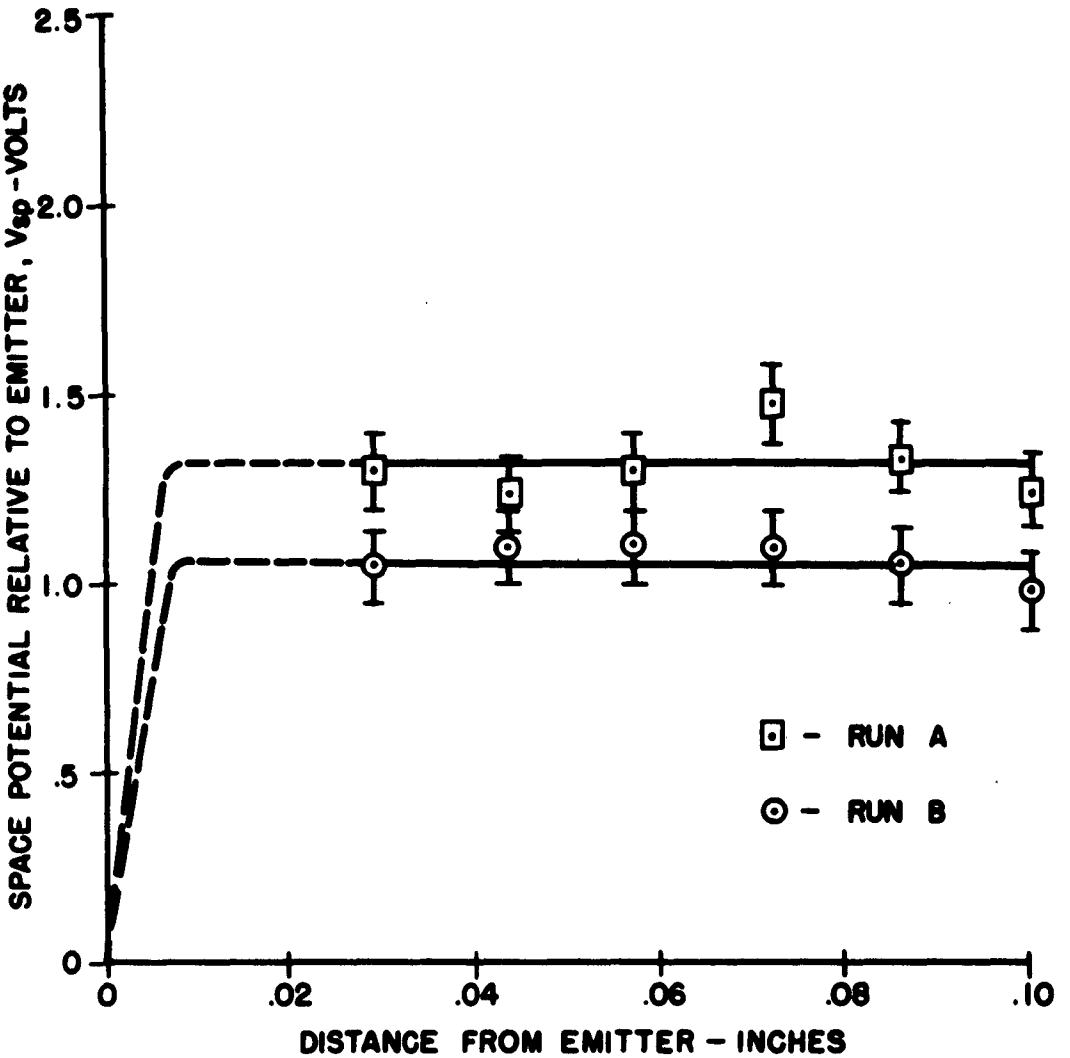

FIGURE 8
SPACE POTENTIAL VARIATION WITH POSITION IN TWO TYPICAL RUNS WITH TC-158

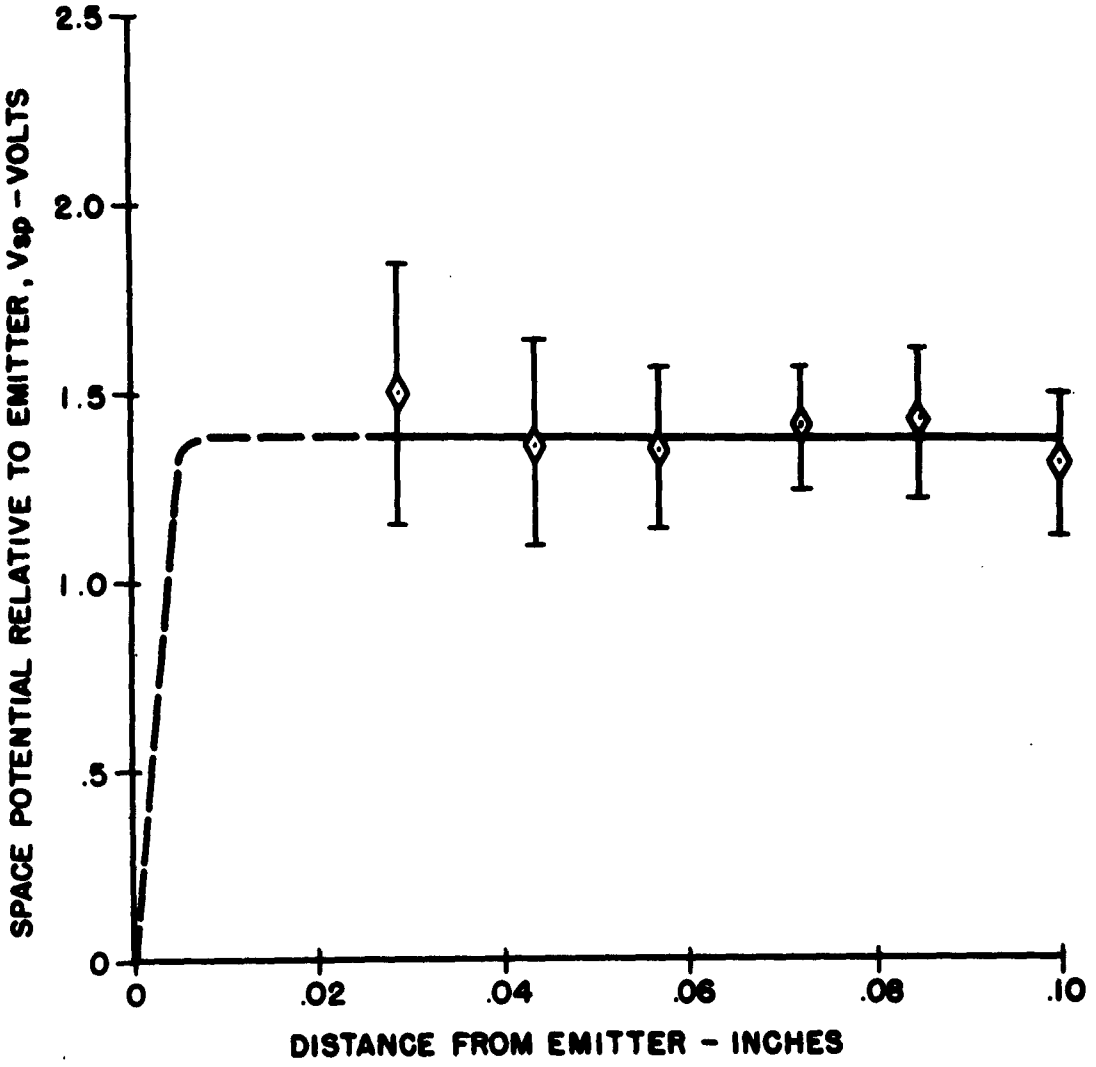

FIGURE 9
AVERAGE SPACE POTENTIAL VARIATION WITH POSITION IN TC-158.

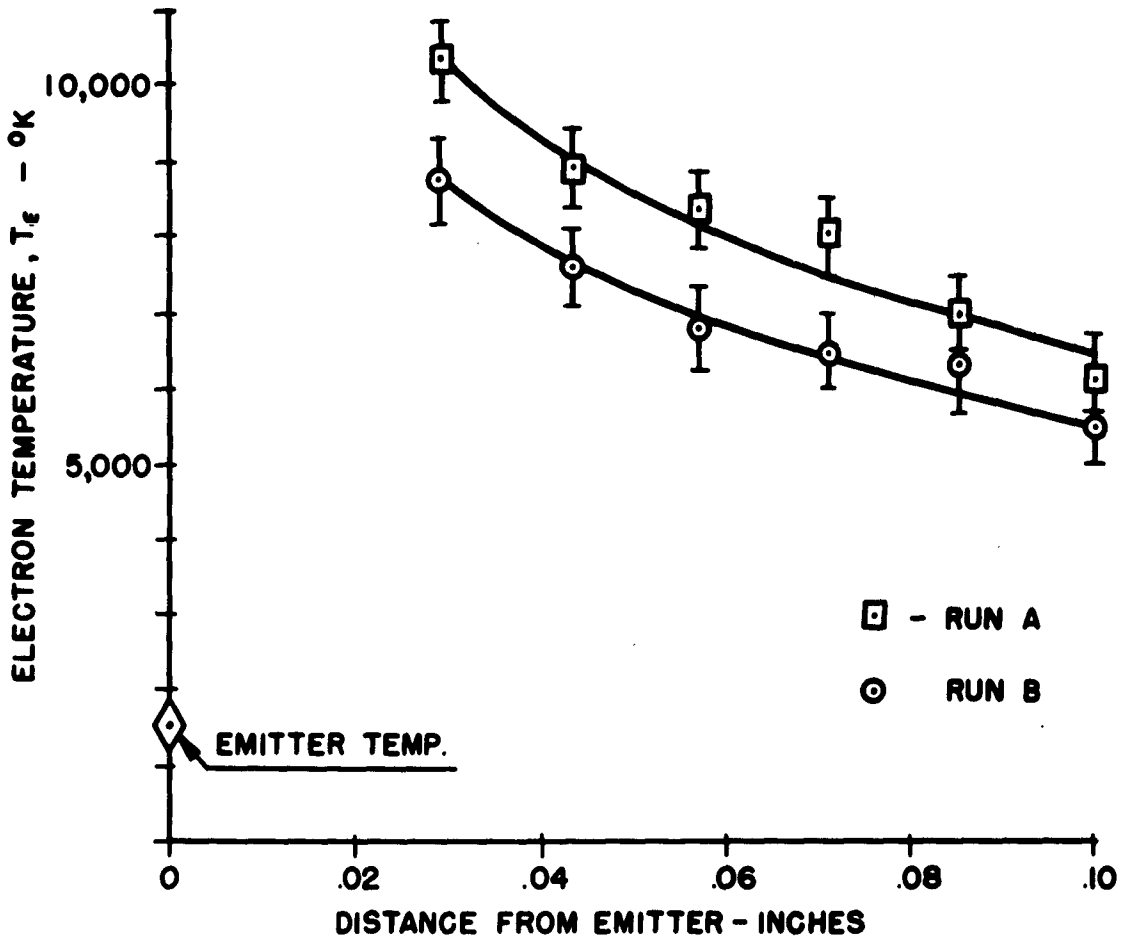

FIGURE 10
SPATIAL VARIATION OF ELECTRON TEMPERATURE IN TWO TYPICAL RUNS WITH TC-158.

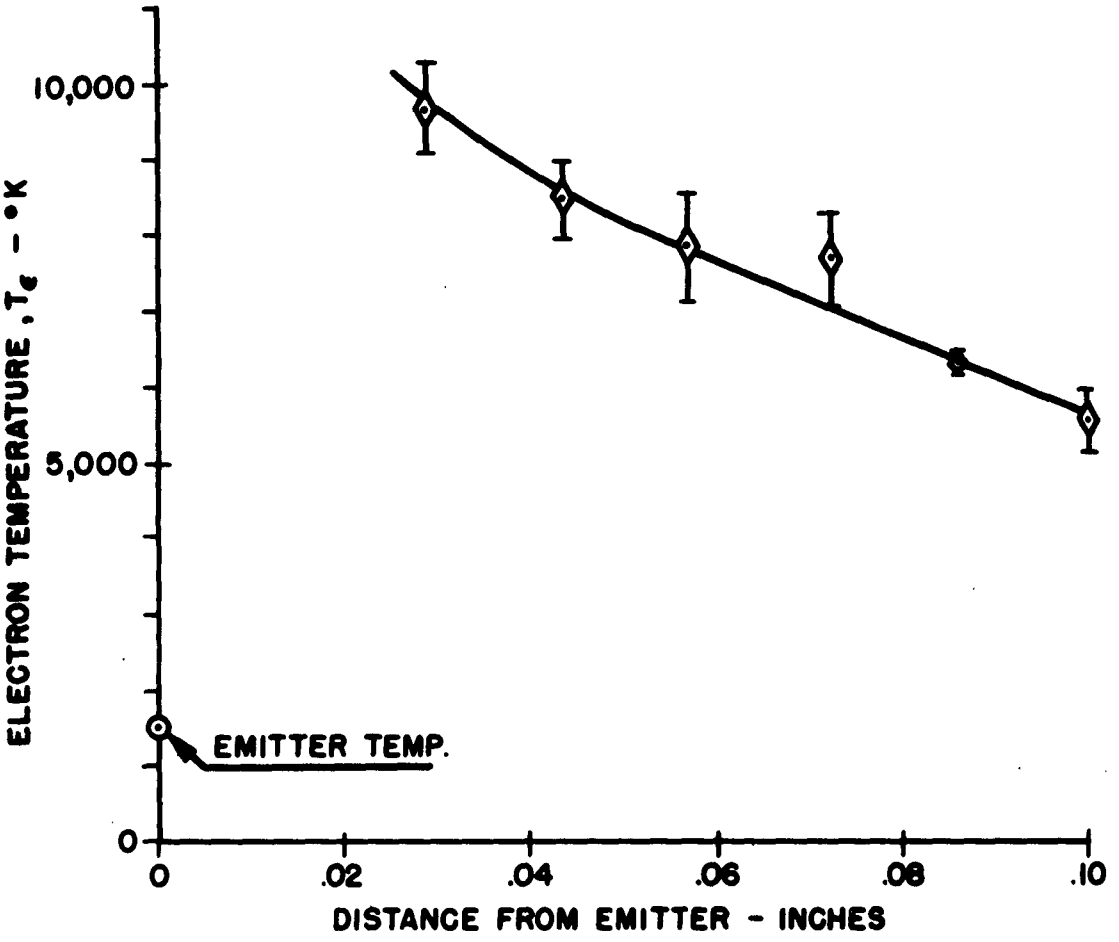

FIGURE II
AVERAGE SPATIAL VARIATION OF ELECTRON TEMPERATURE IN TC-158.

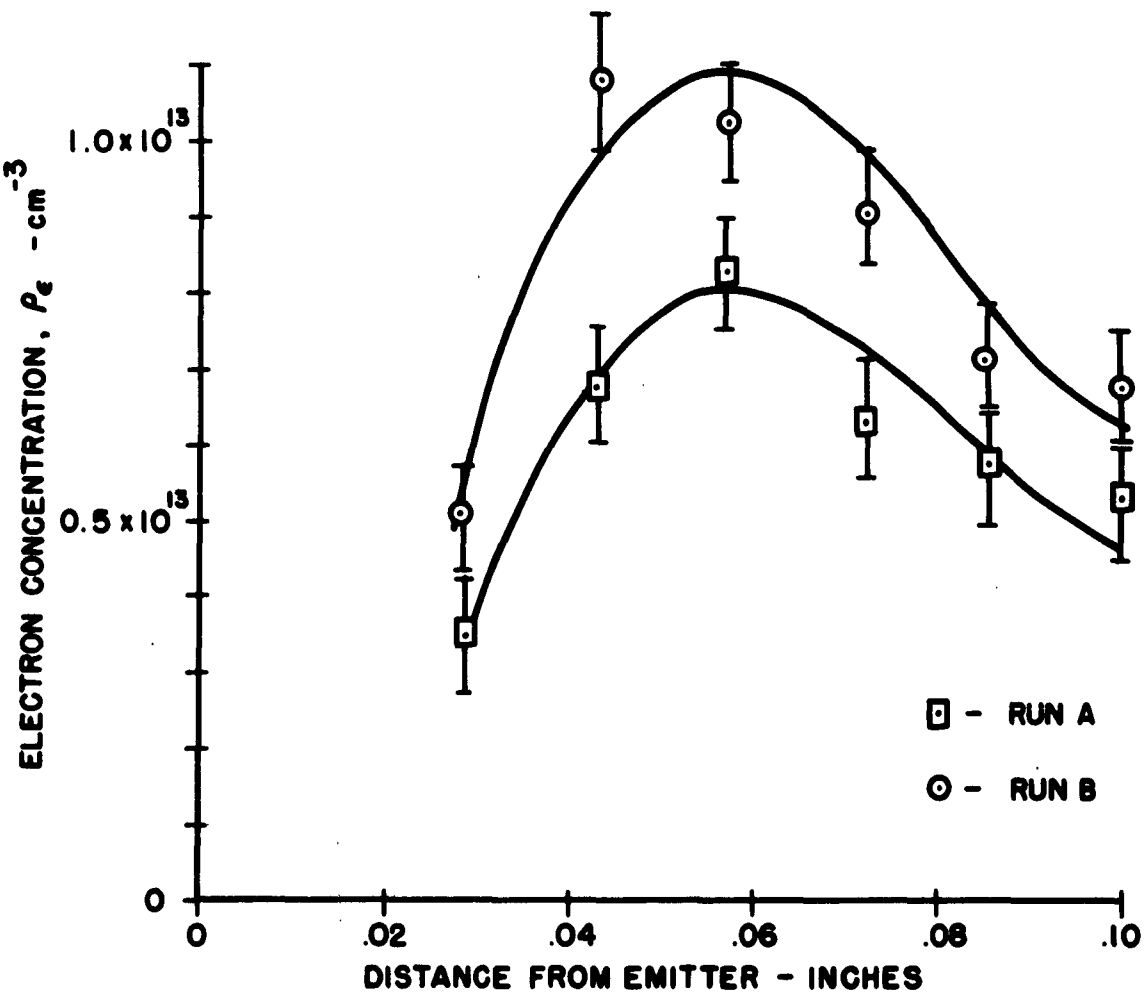

FIGURE 12
SPATIAL VARIATION OF ELECTRON CONCENTRATION IN TWO TYPICAL RUNS WITH TC-158.

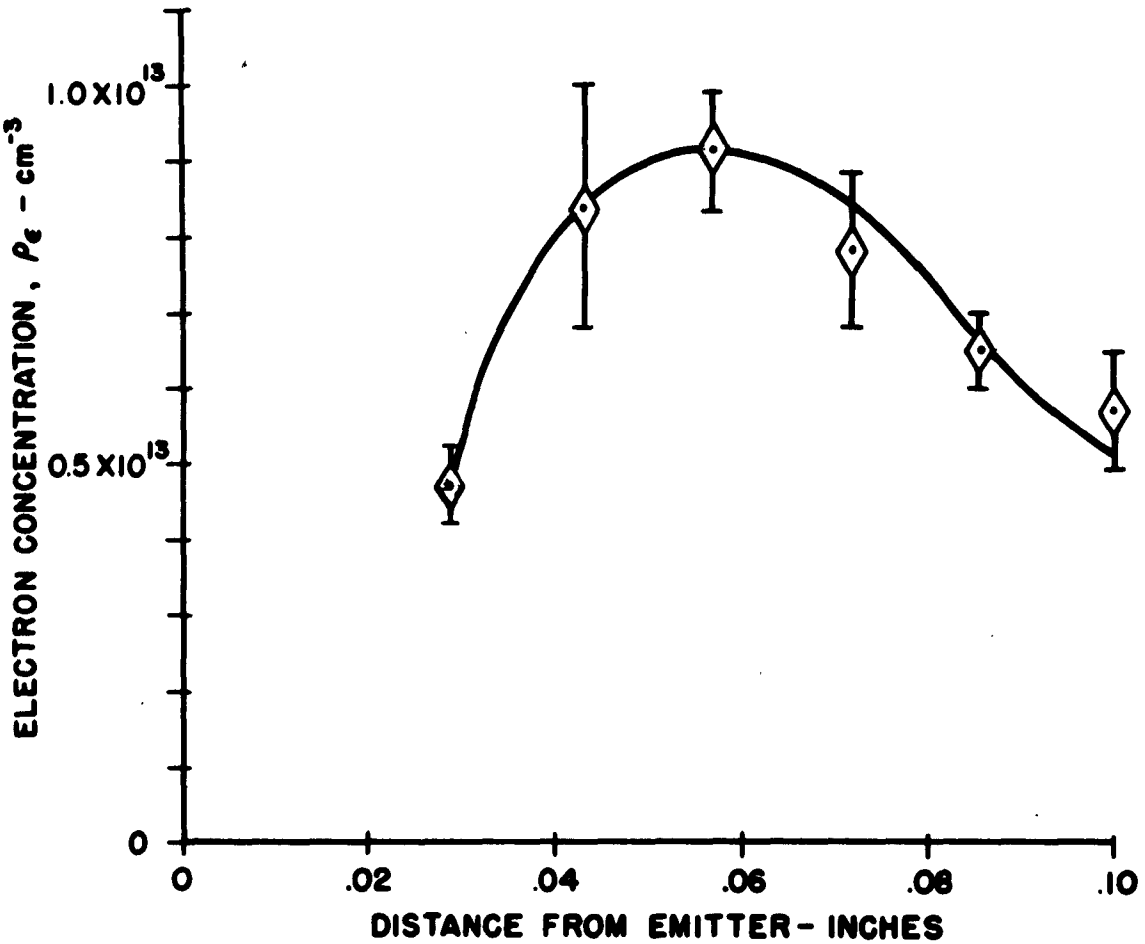

FIGURE 13
AVERAGE SPATIAL VARIATION OF ELECTRON CONCENTRATION IN TC-158.

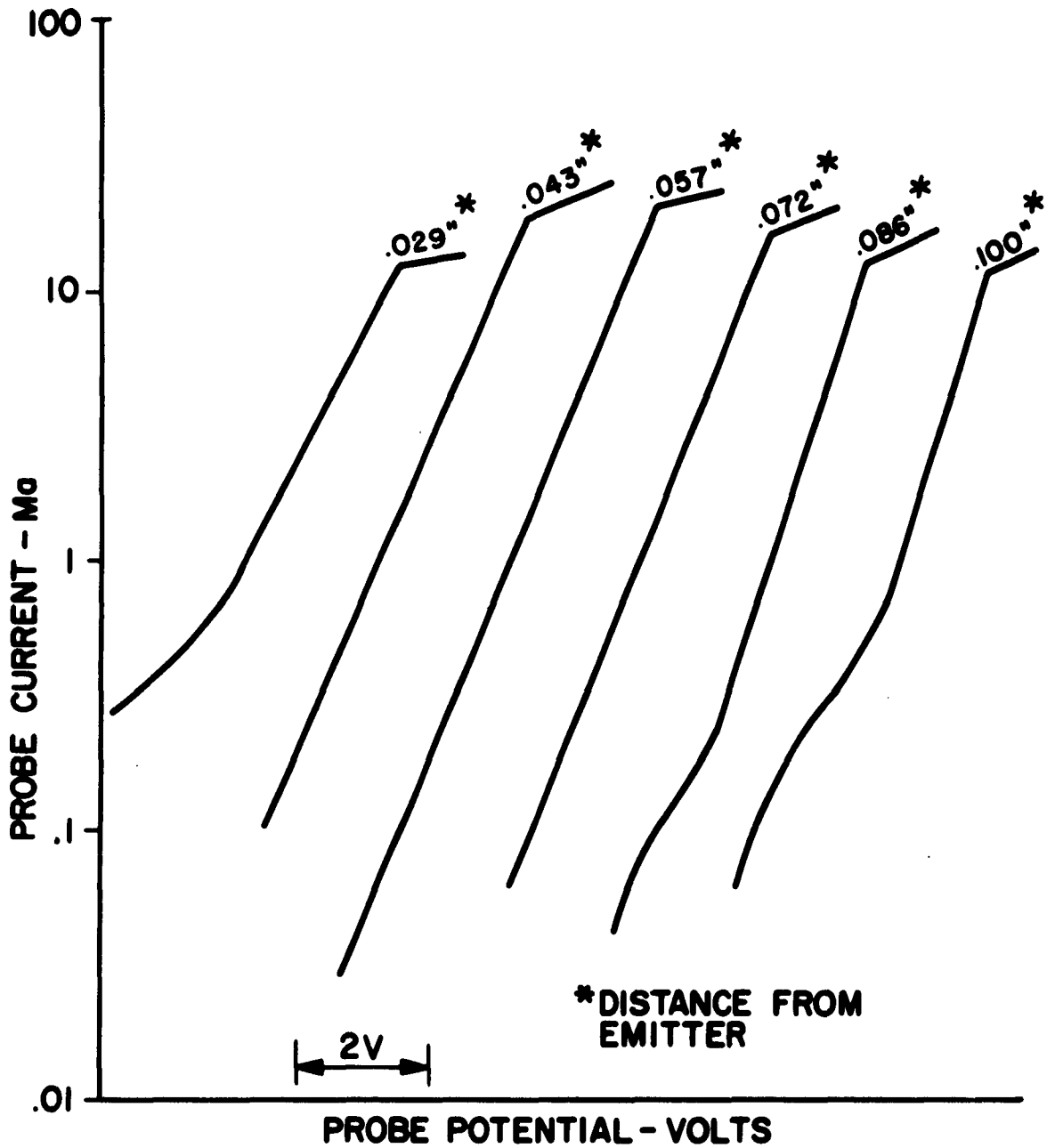

FIGURE 14
TYPICAL CHARACTERISTICS OBTAINED AT VARIOUS POSITIONS INSIDE OF ADJUSTABLE PROBE TEST CELL TC-158.

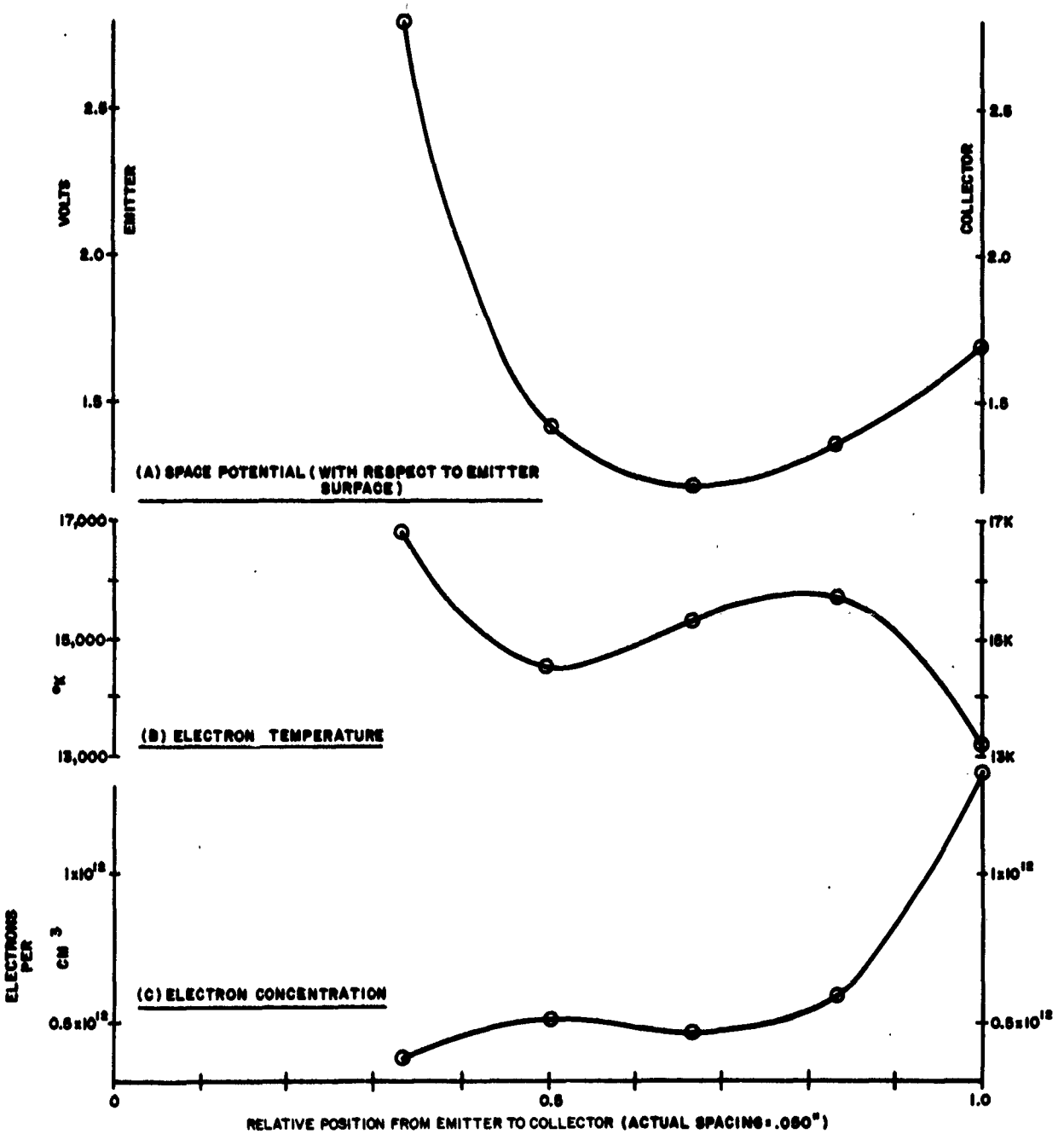

FIGURE 15. MEASURED PARAMETERS IN TC-150

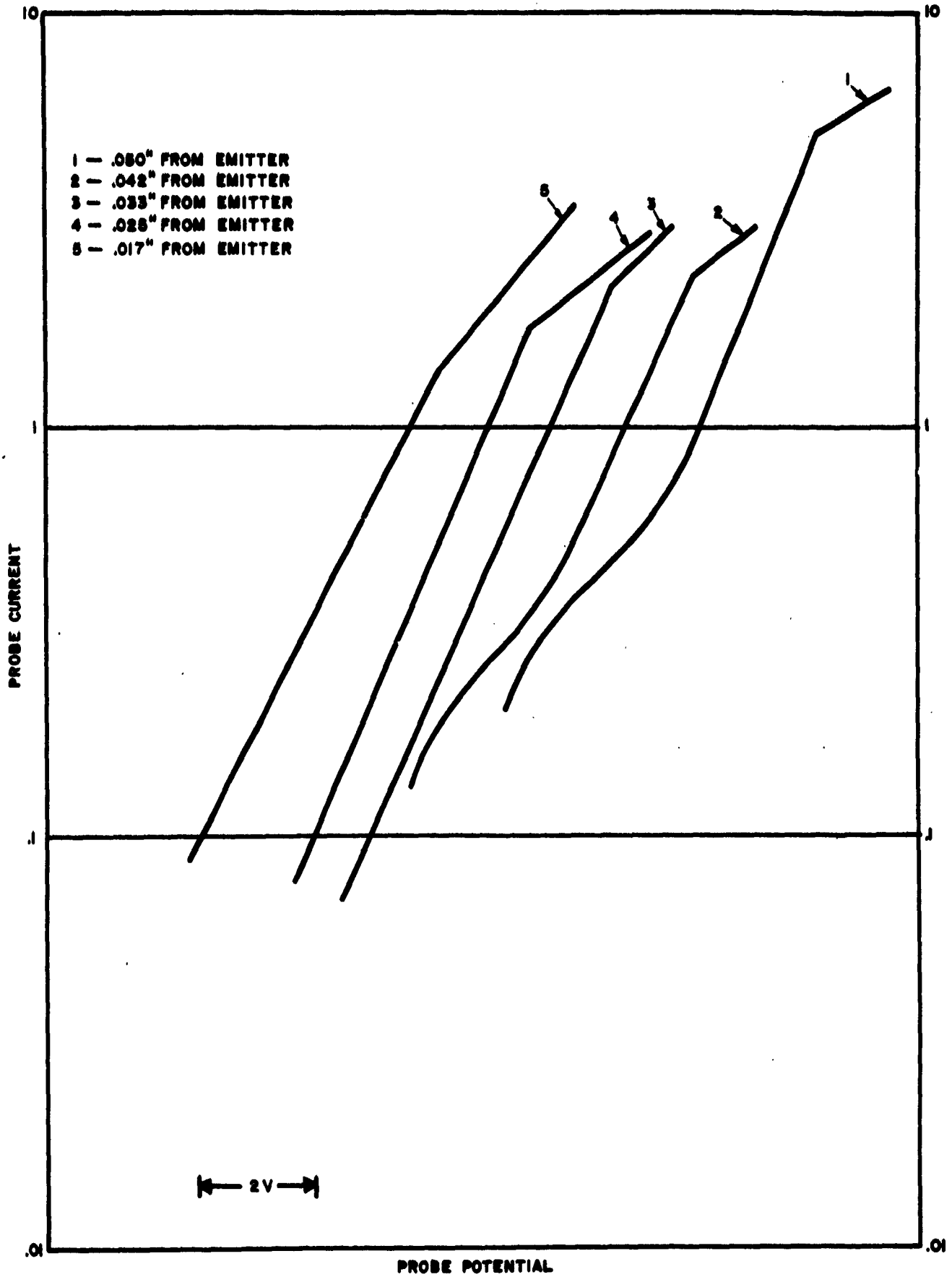

FIGURE 16 PROBE CHARACTERISTICS FOR TC-150

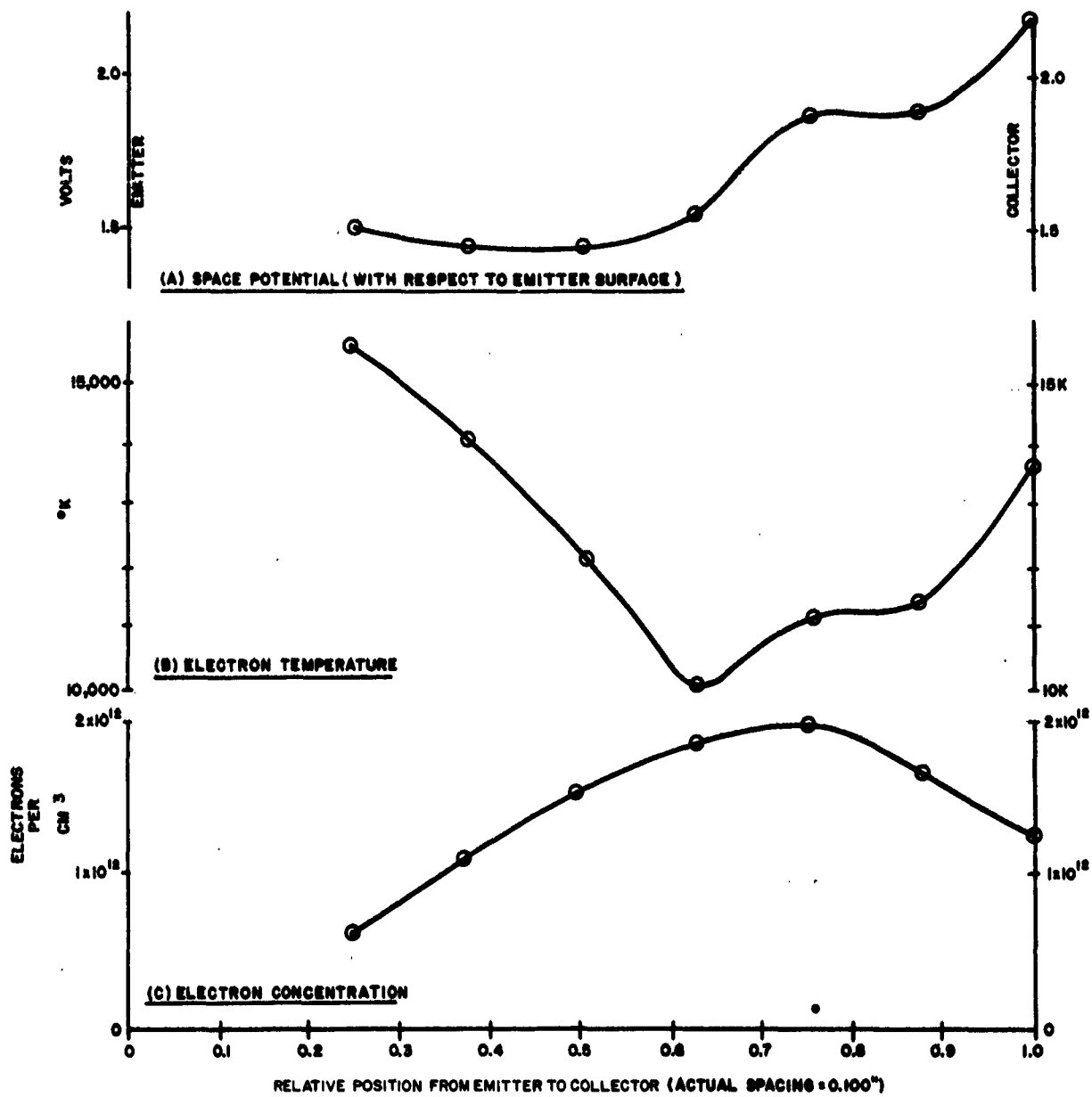

FIGURE 17. MEASURED PARAMETERS IN TC-155

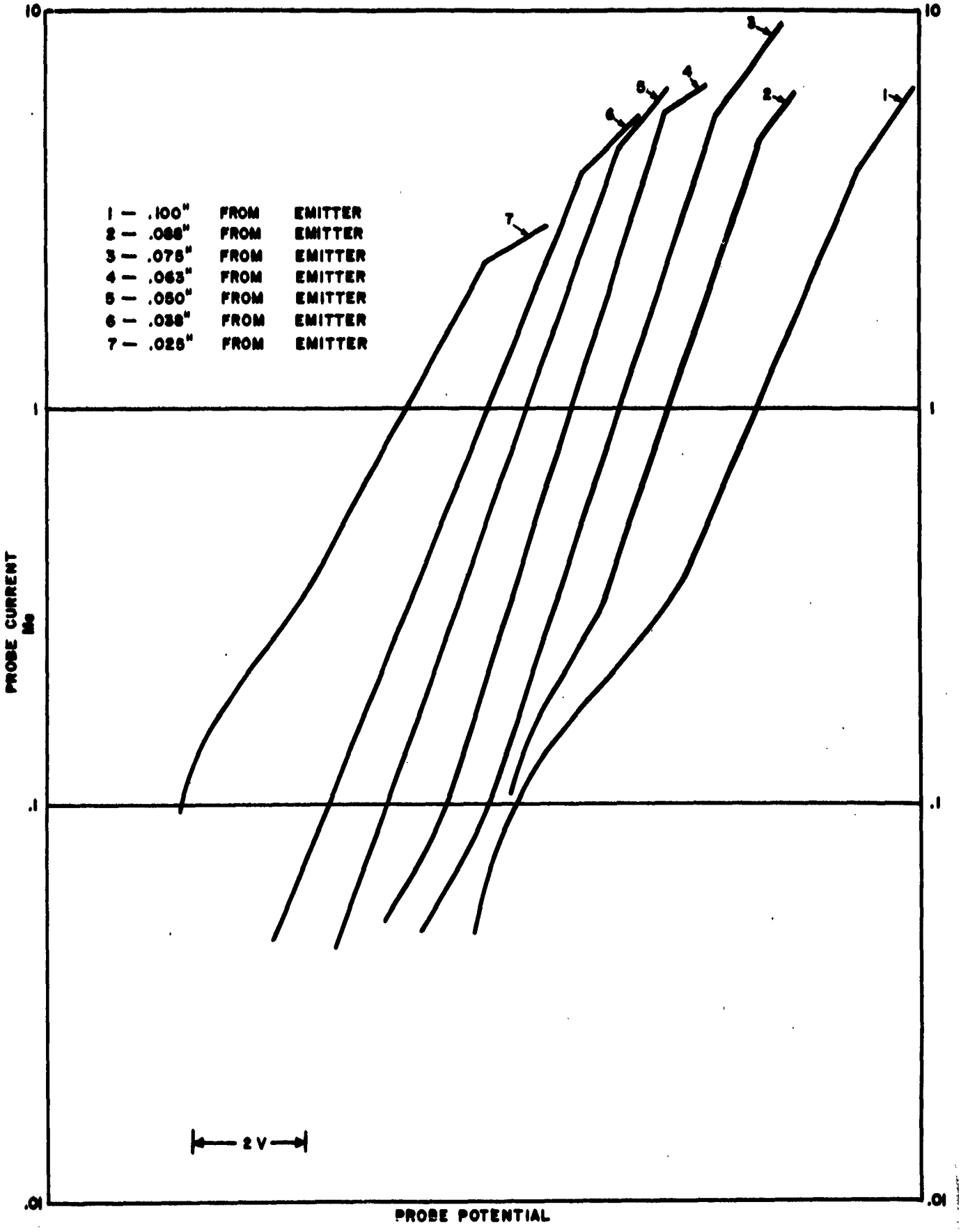

FIGURE 18 PROBE CHARACTERISTICS FOR TC—155

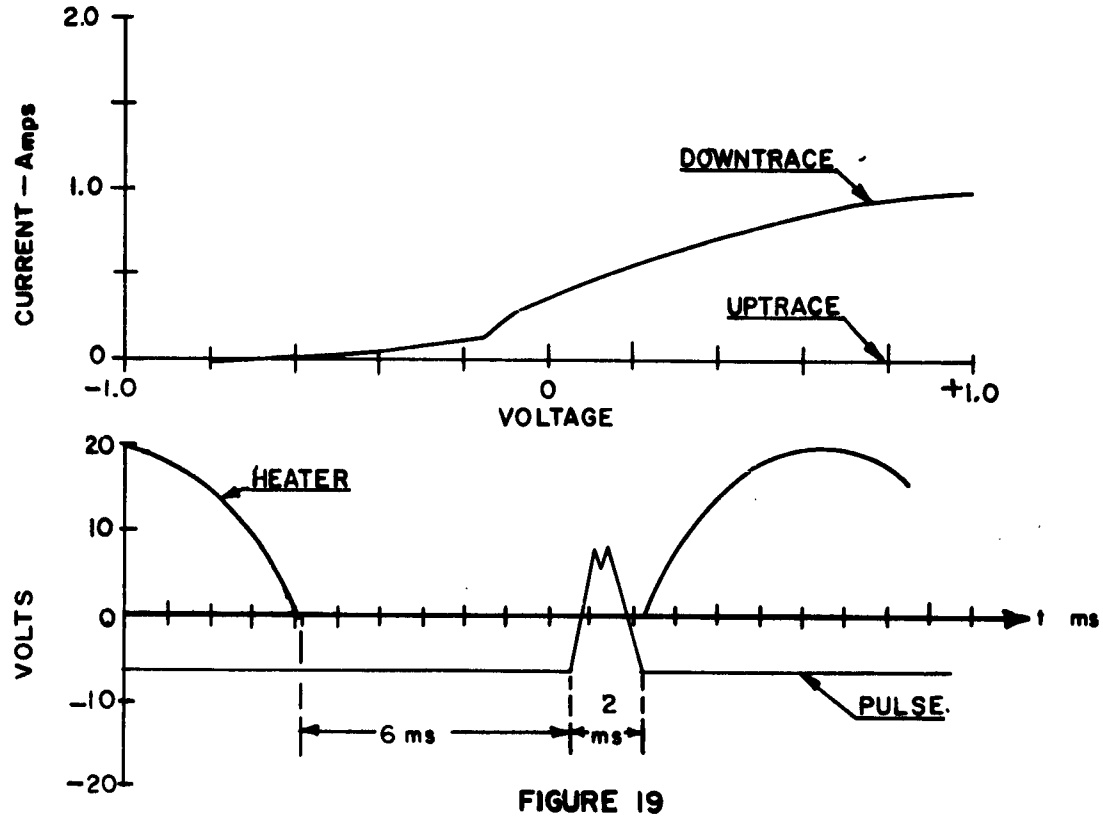

FIGURE 19

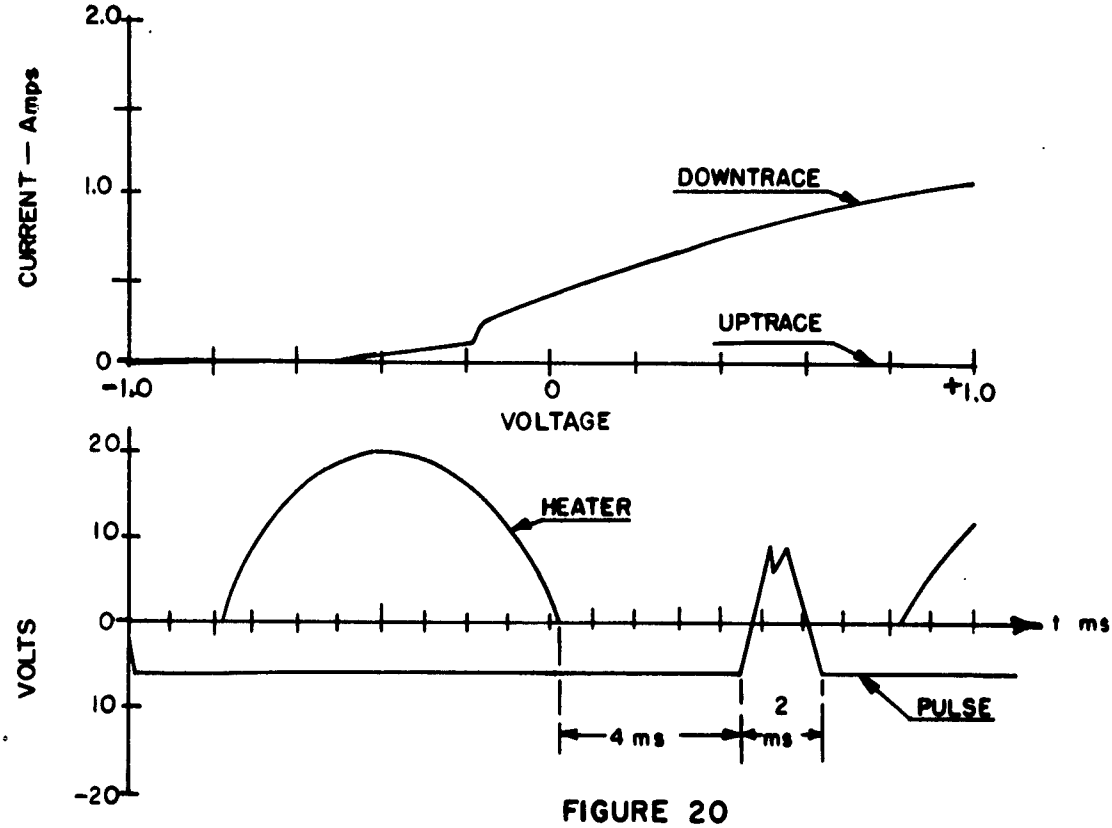

FIGURE 20

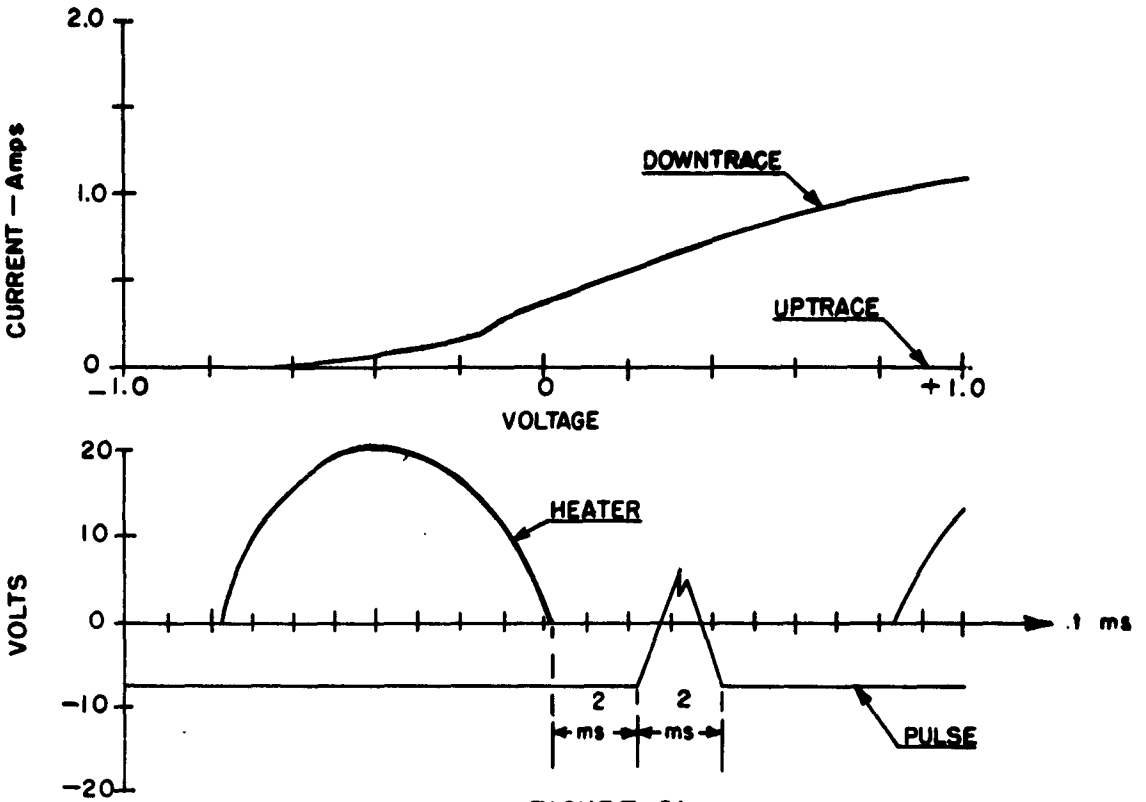

FIGURE 21

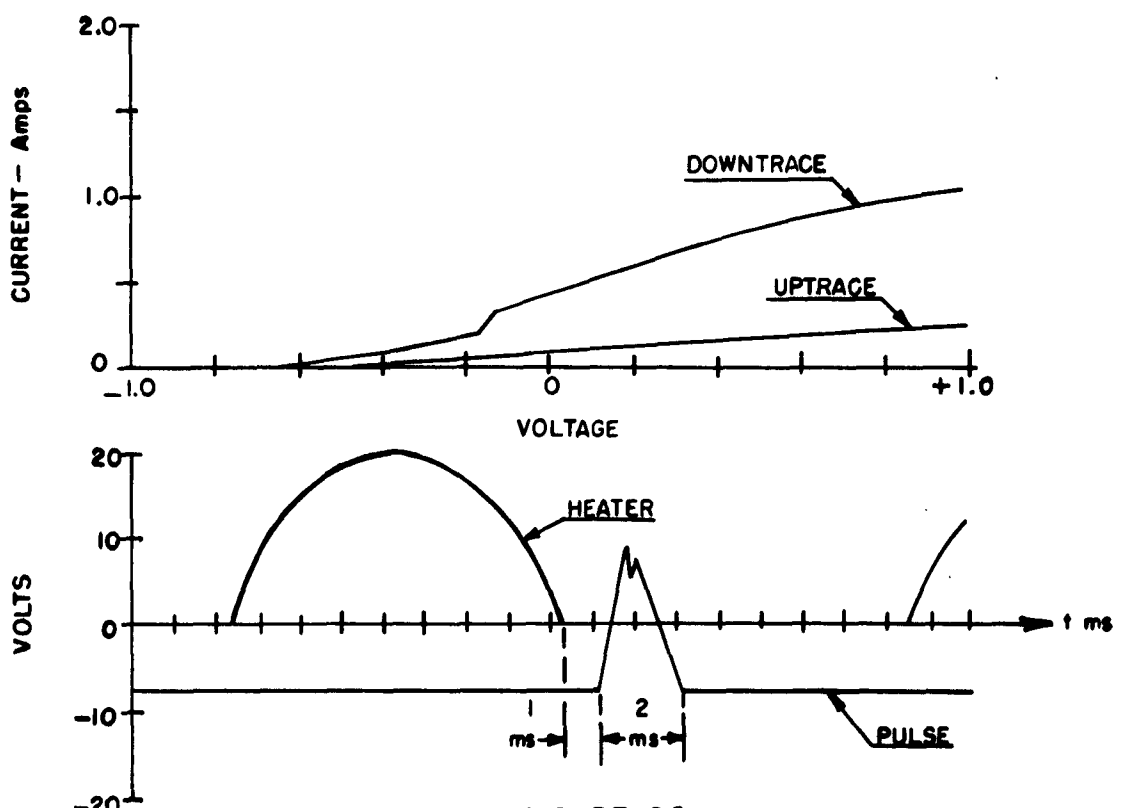

FIGURE 22

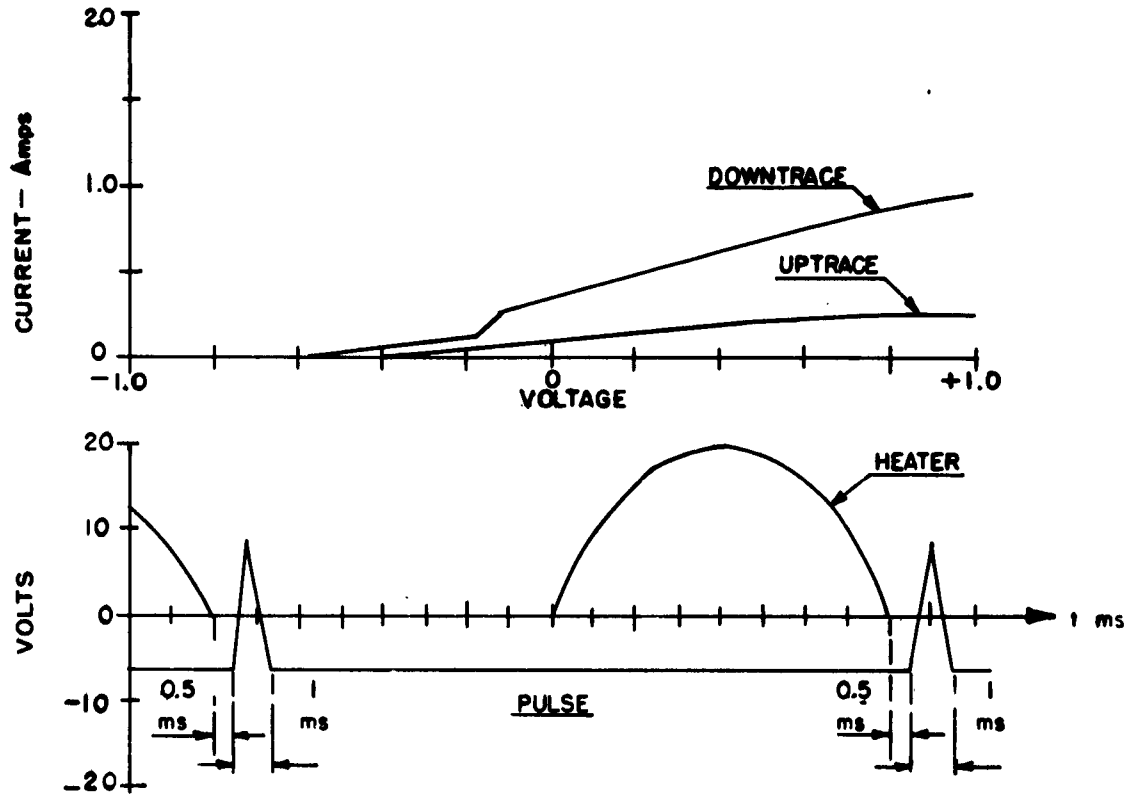

FIGURE 23

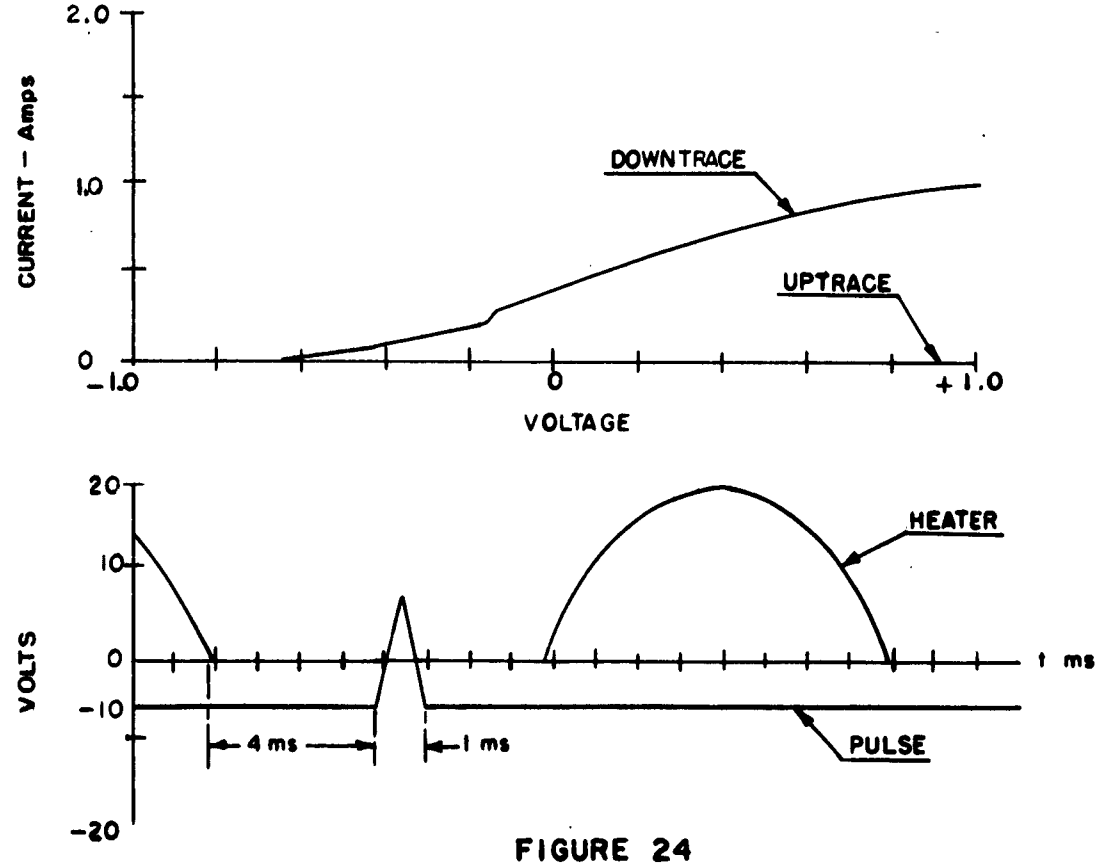

FIGURE 24

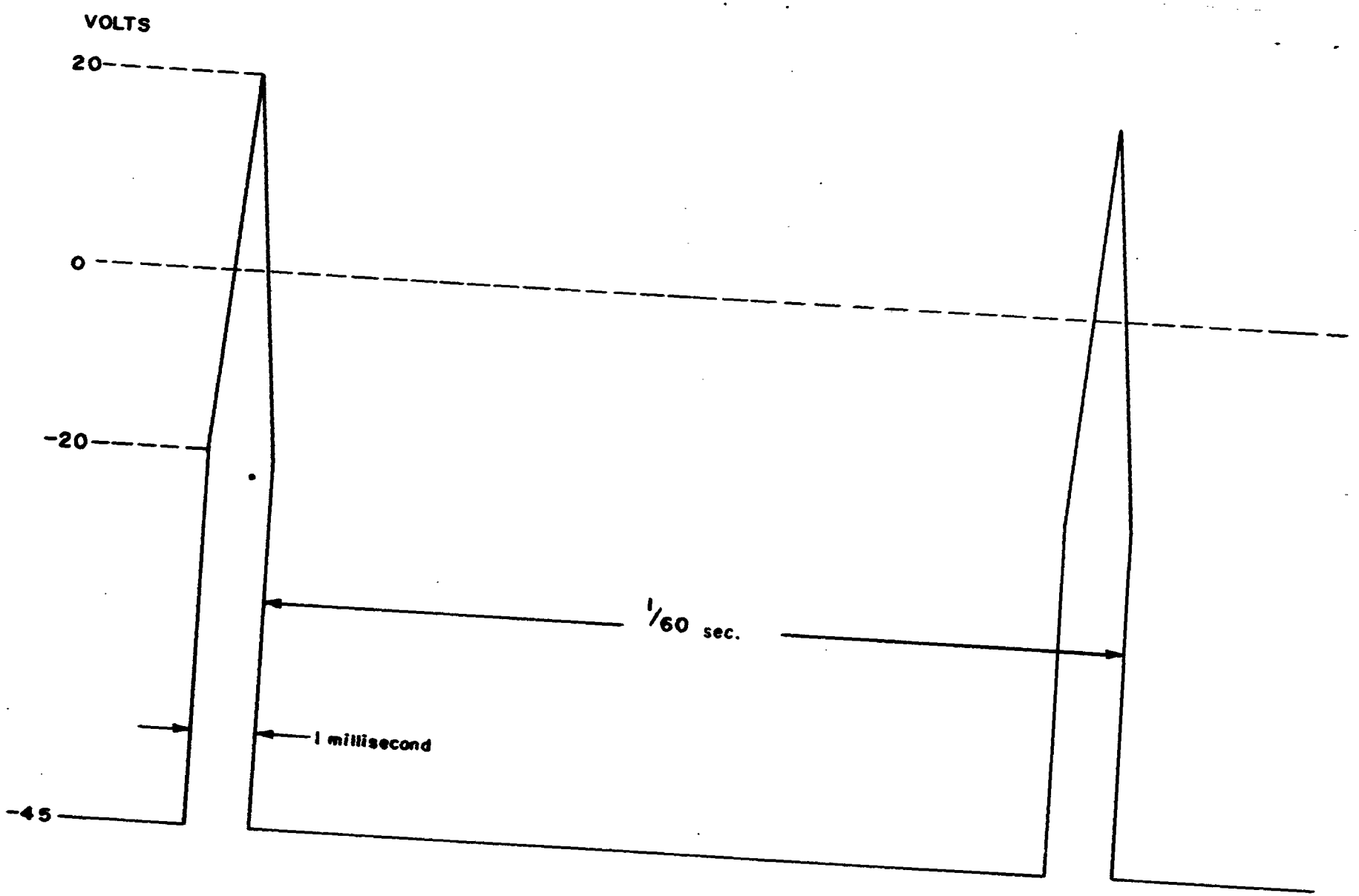

FIGURE 25 PULSE APPLIED TO PROBE

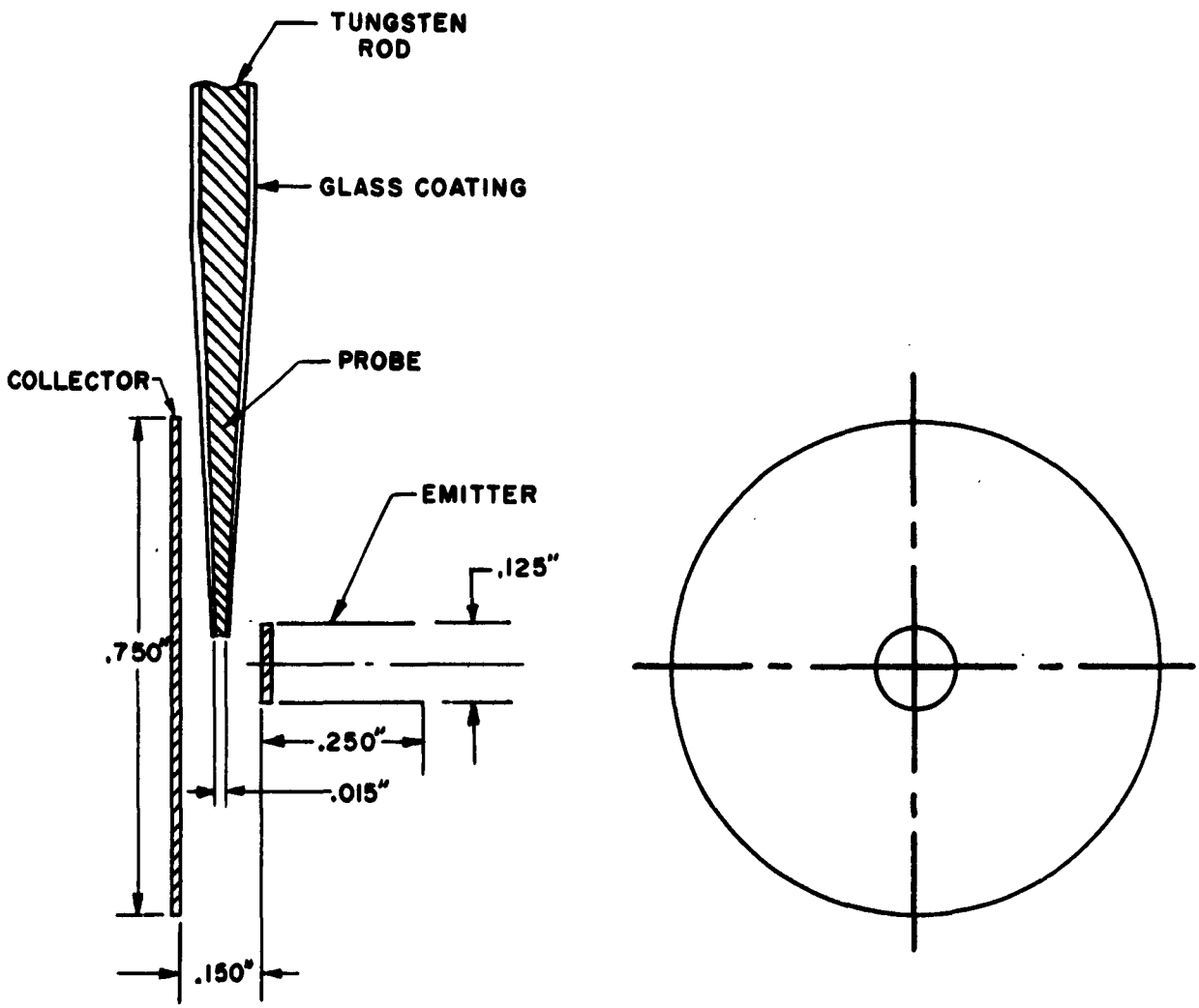

FIGURE 26

SCHEMATIC DIAGRAM OF RADIAL PROBE ASSEMBLY

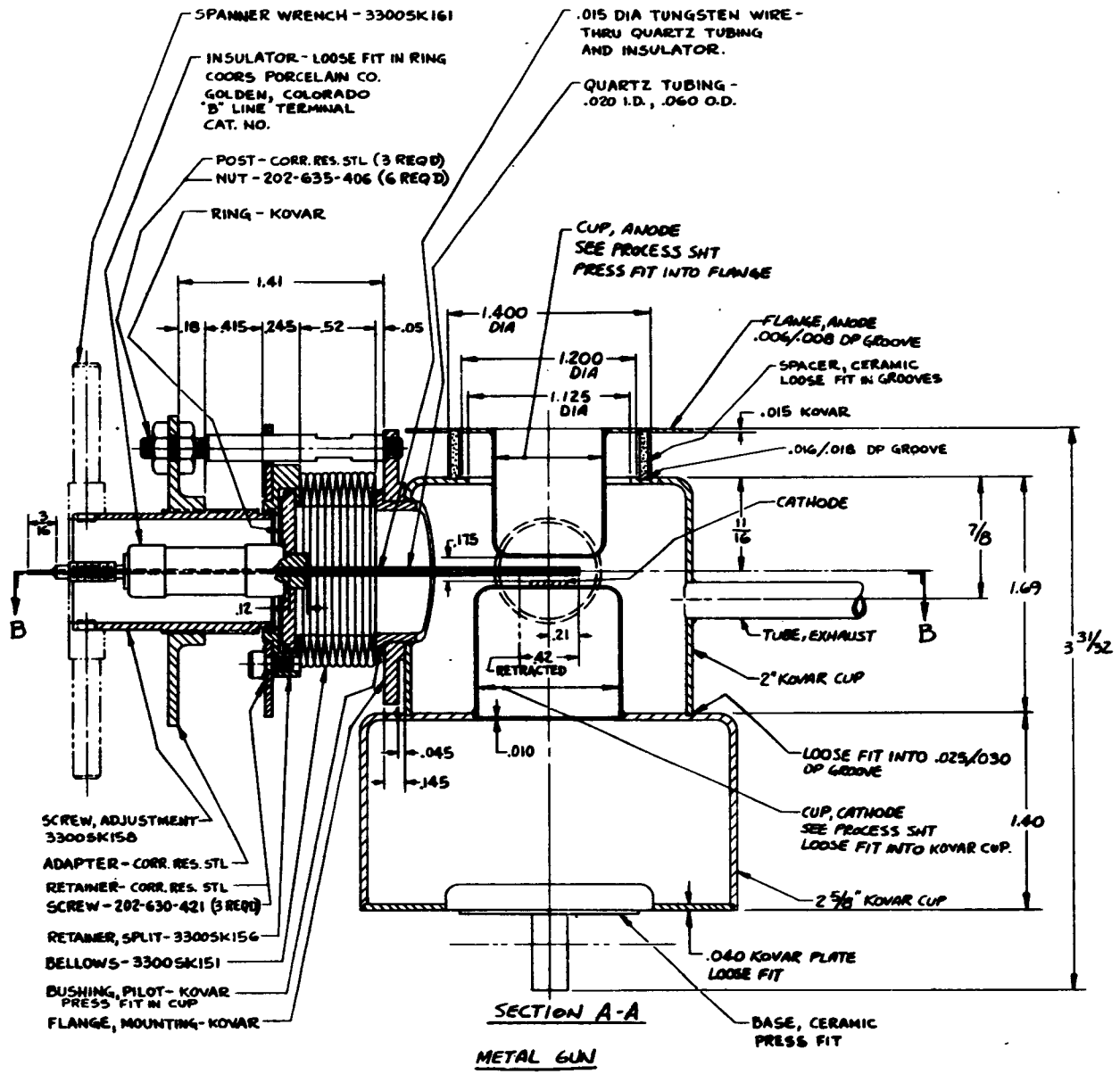

FIGURE 27. METAL CERAMIC ADJUSTABLE PROBE OPPOSED CUP GEOMETRY ASSEMBLY

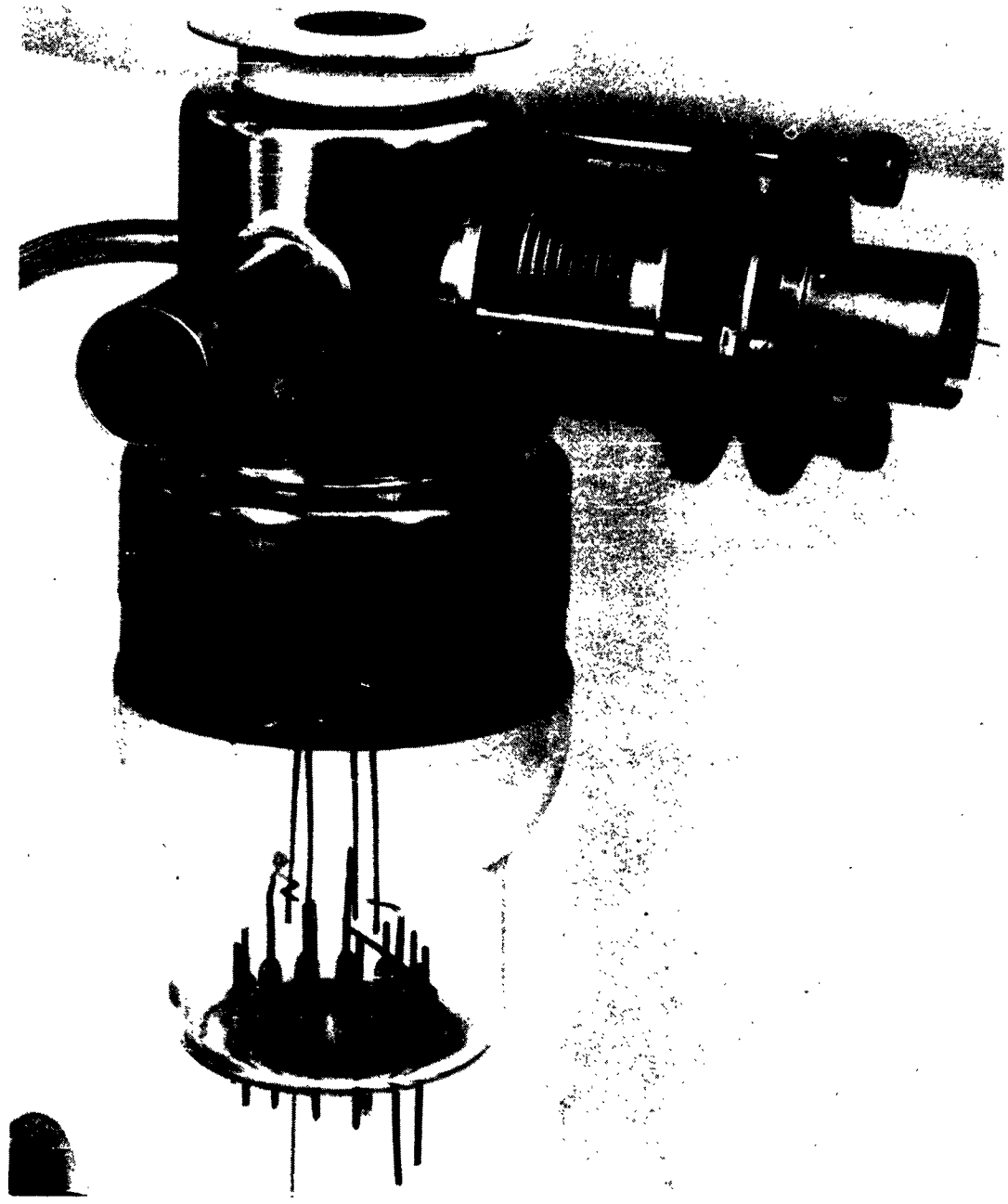

FIGURE 28

METAL CERAMIC ADJUSTABLE PROBE CELL TC- 230

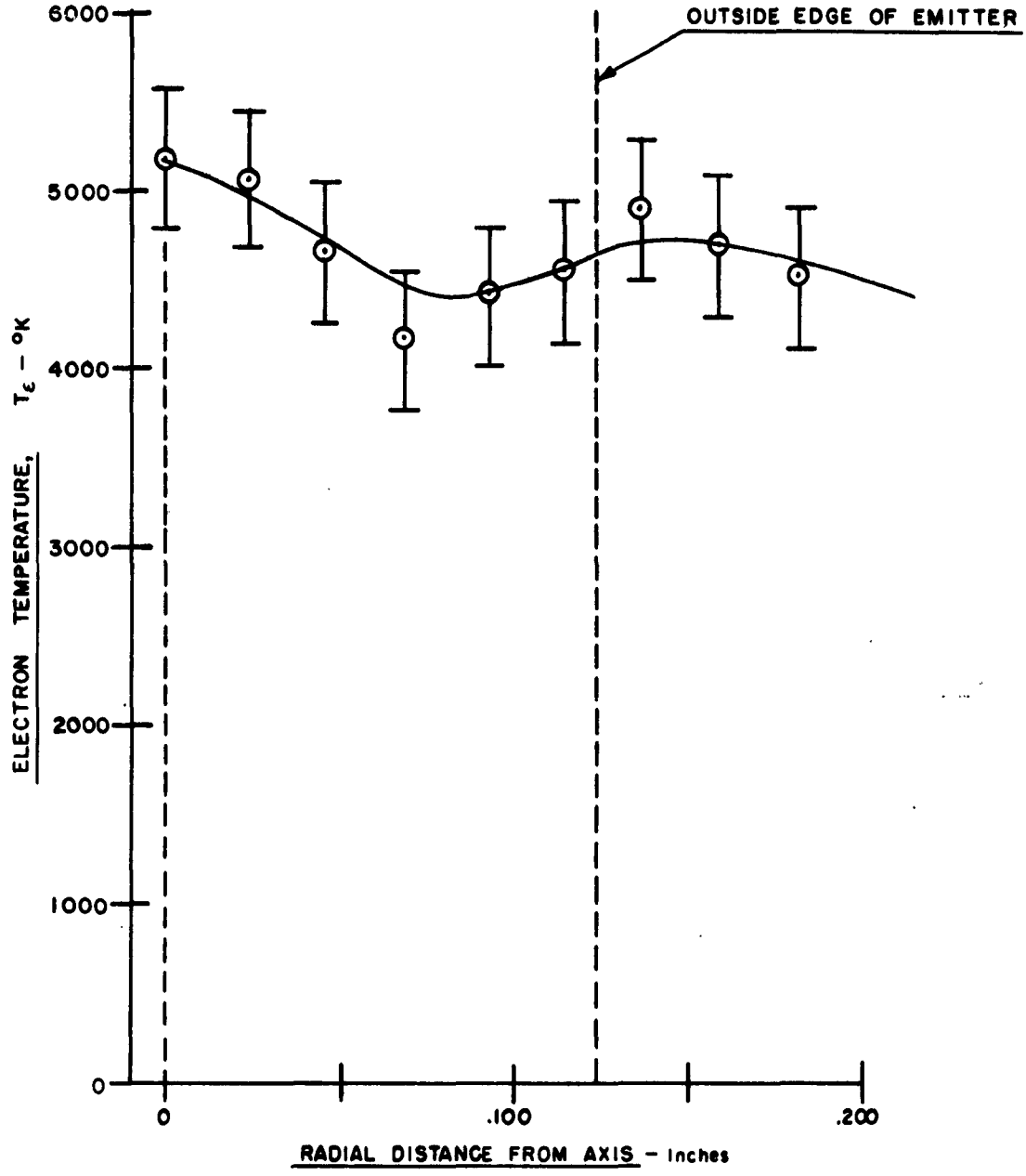

FIGURE 30

RADIAL VARIATION OF ELECTRON TEMPERATURE IN METAL-CERAMIC CONVERTER, TC-230

$\left(J = 6.5 \text{ AMPS} / \text{CM}^2\right)$

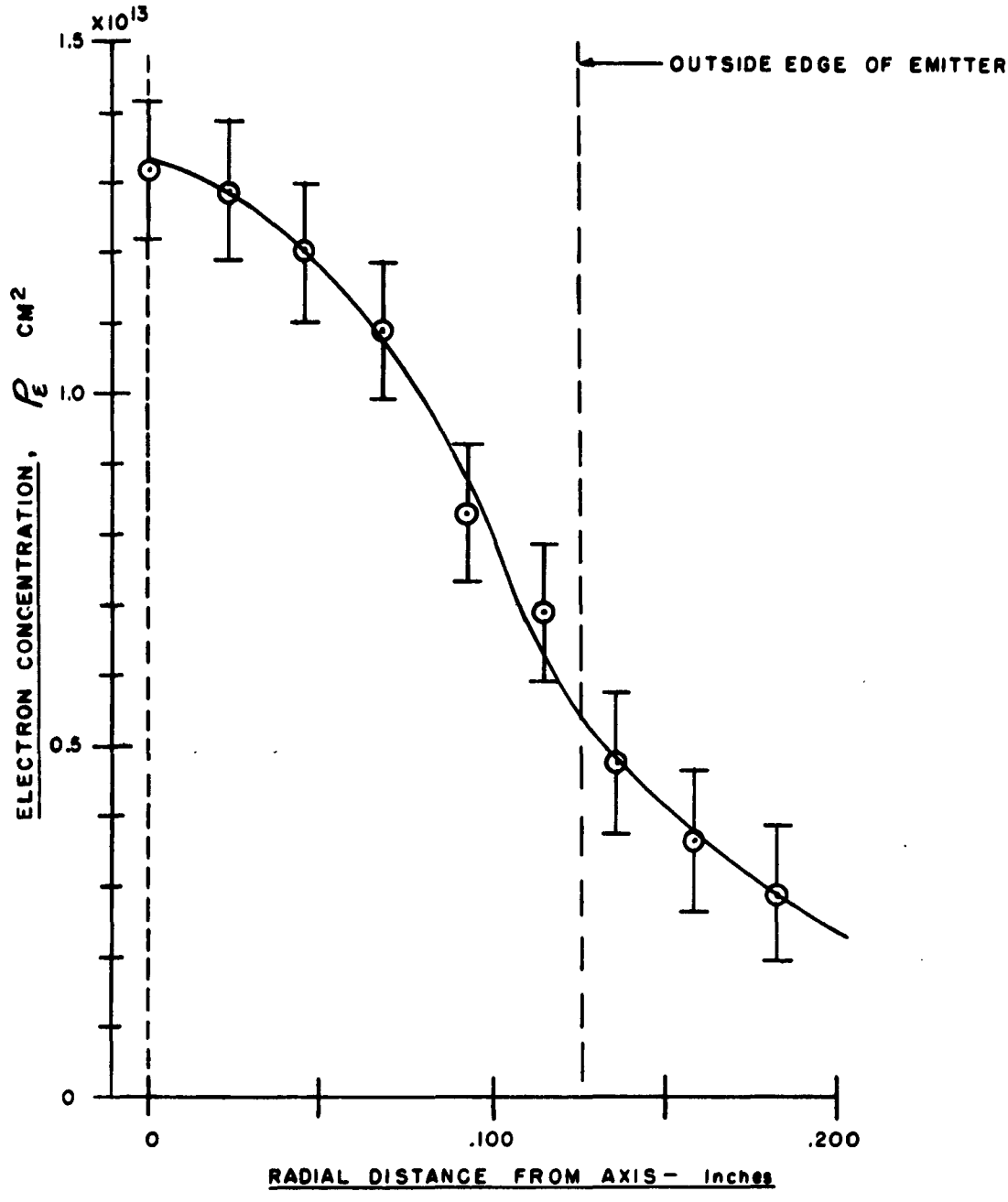

FIGURE 31

RADIAL VARIATION OF ELECTRON CONCENTRATION

IN METAL–CERAMIC CONVERTER, TC-230

(J = 6.5 AMPS CM^2)

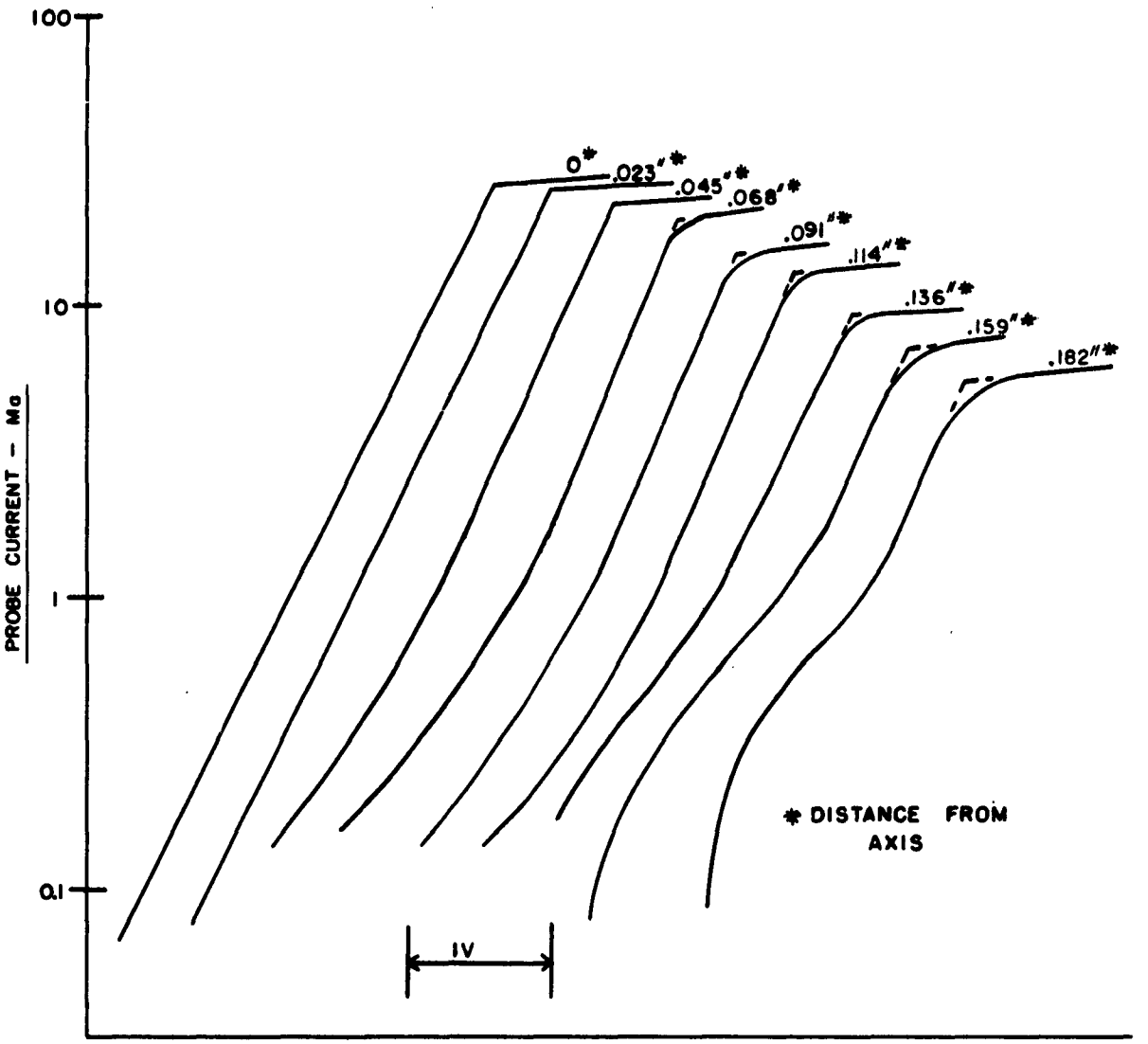

FIGURE 32

PROBE CHARACTERISTICS OBTAINED WITH METAL-CERAMIC CONVERTER TC-230 AT VARIOUS RADIAL DISTANCES FROM THE CENTRAL AXIS
(J = 6.5 AMPS / CM^2)

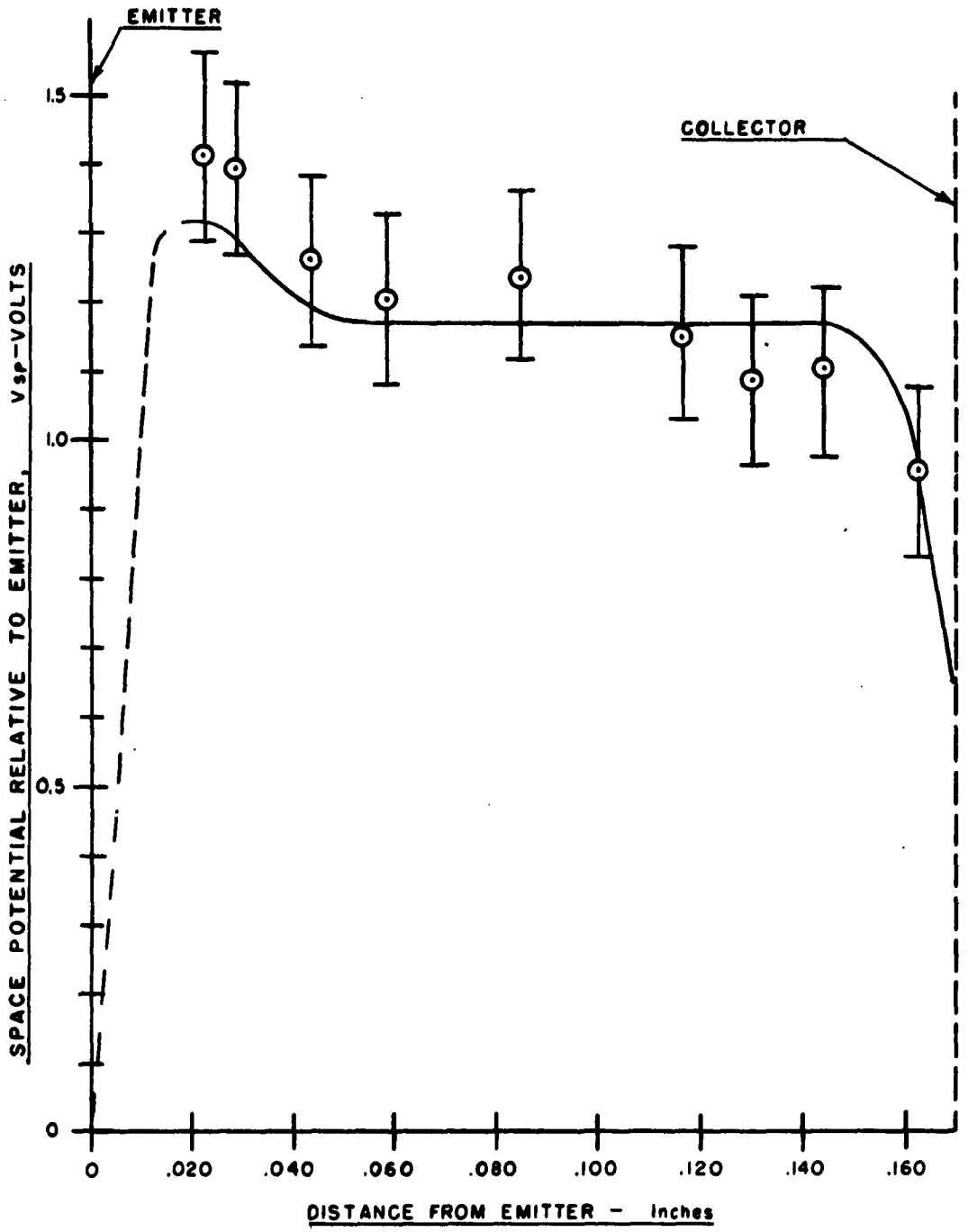

FIGURE 33

VARIATION OF SPACE POTENTIAL ALONG AXIS OF

METAL-CERAMIC CONVERTER, TC-230

$\left(J = 6.5 \text{ AMPS} / \text{CM}^2\right)$

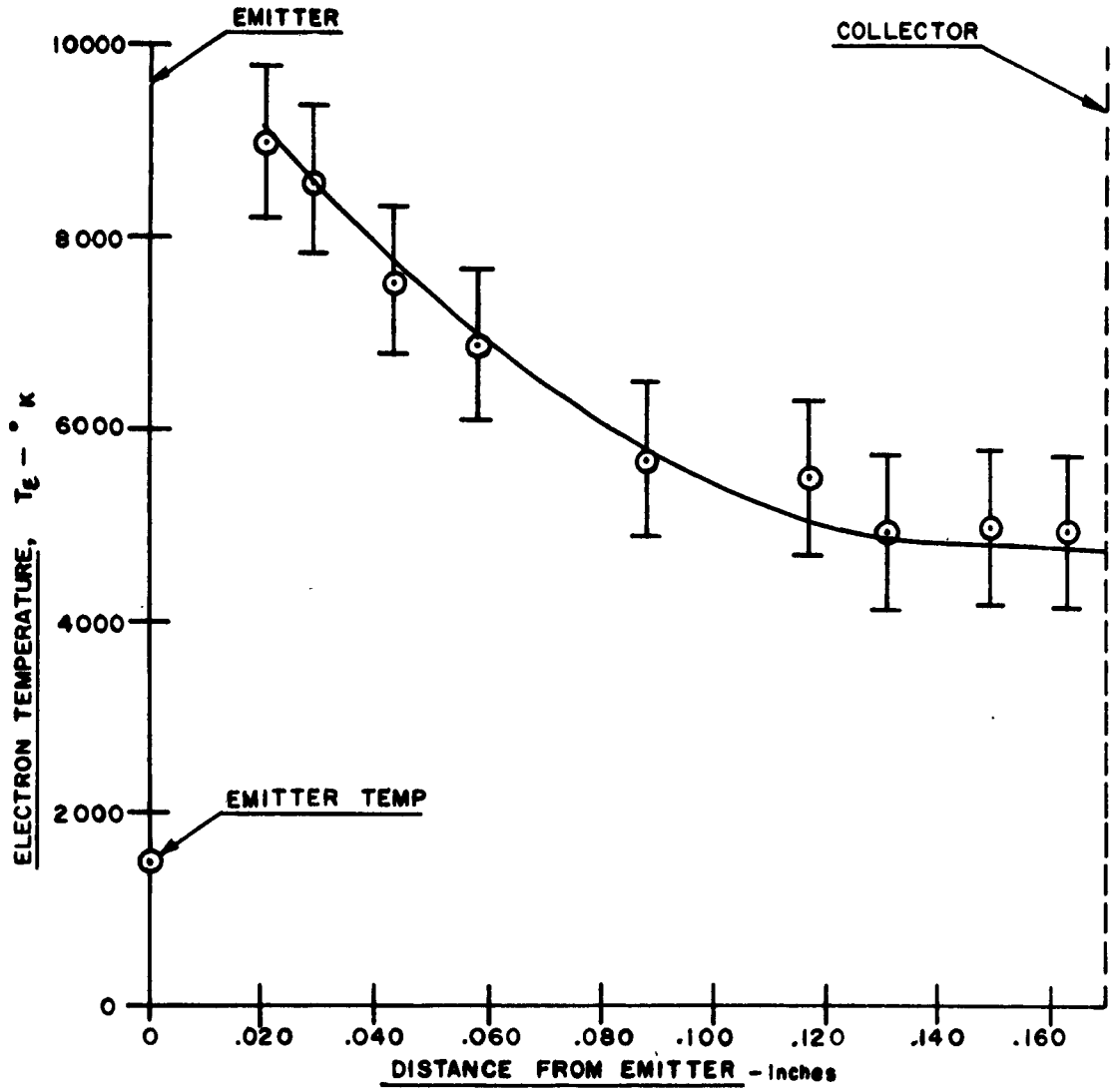

FIGURE 34

VARIATION OF ELECTRON TEMPERATURE ALONG AXIS OF METAL–CERAMIC CONVERTER TC–230

($J = 6.5$ AMPS/CM^2)

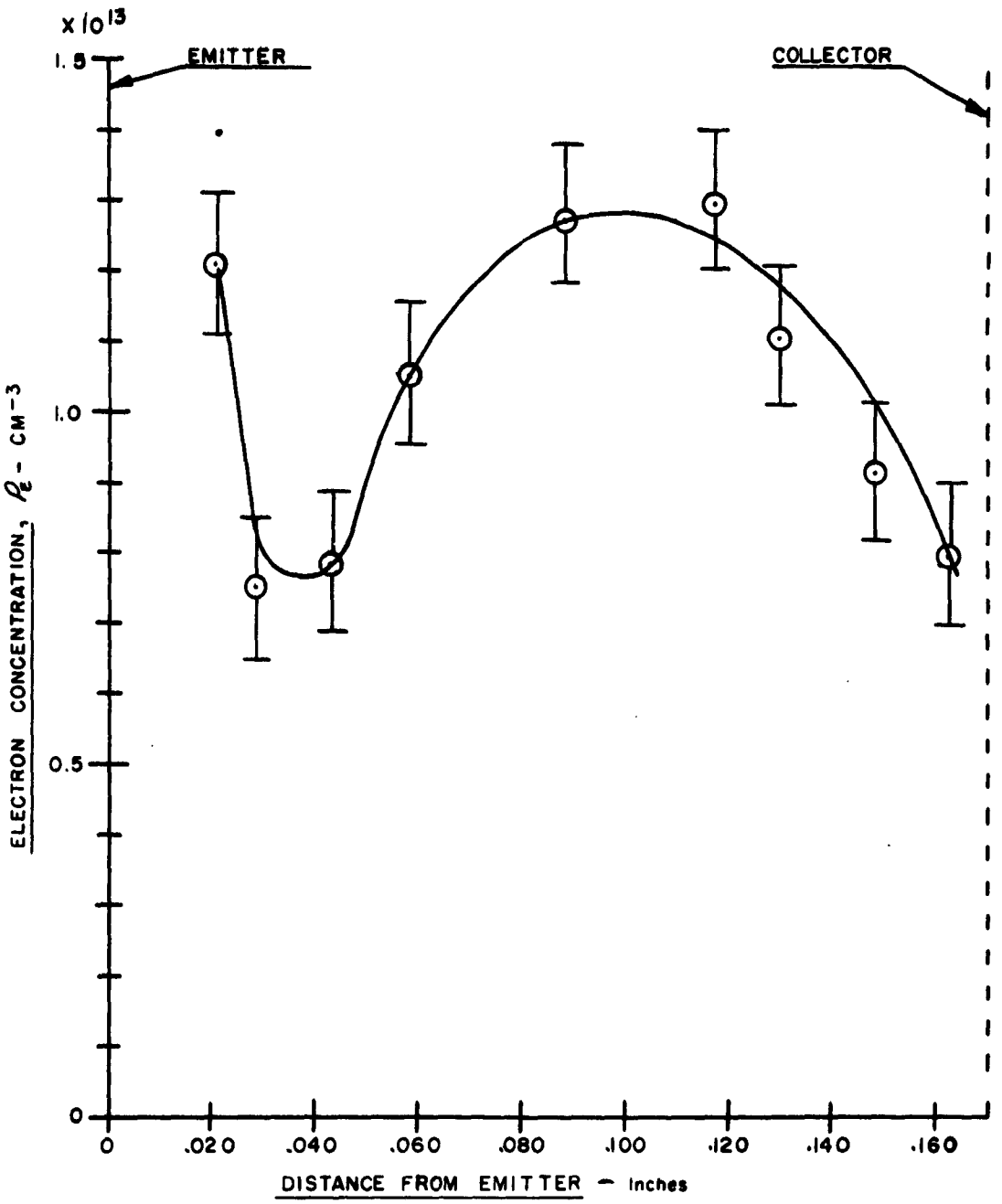

FIGURE 35

VARIATION OF ELECTRON CONCENTRATION ALONG AXIS OF METAL-CERAMIC CONVERTER, TC-230

$(J = 6.5 \text{ AMPS}/\text{CM}^2)$

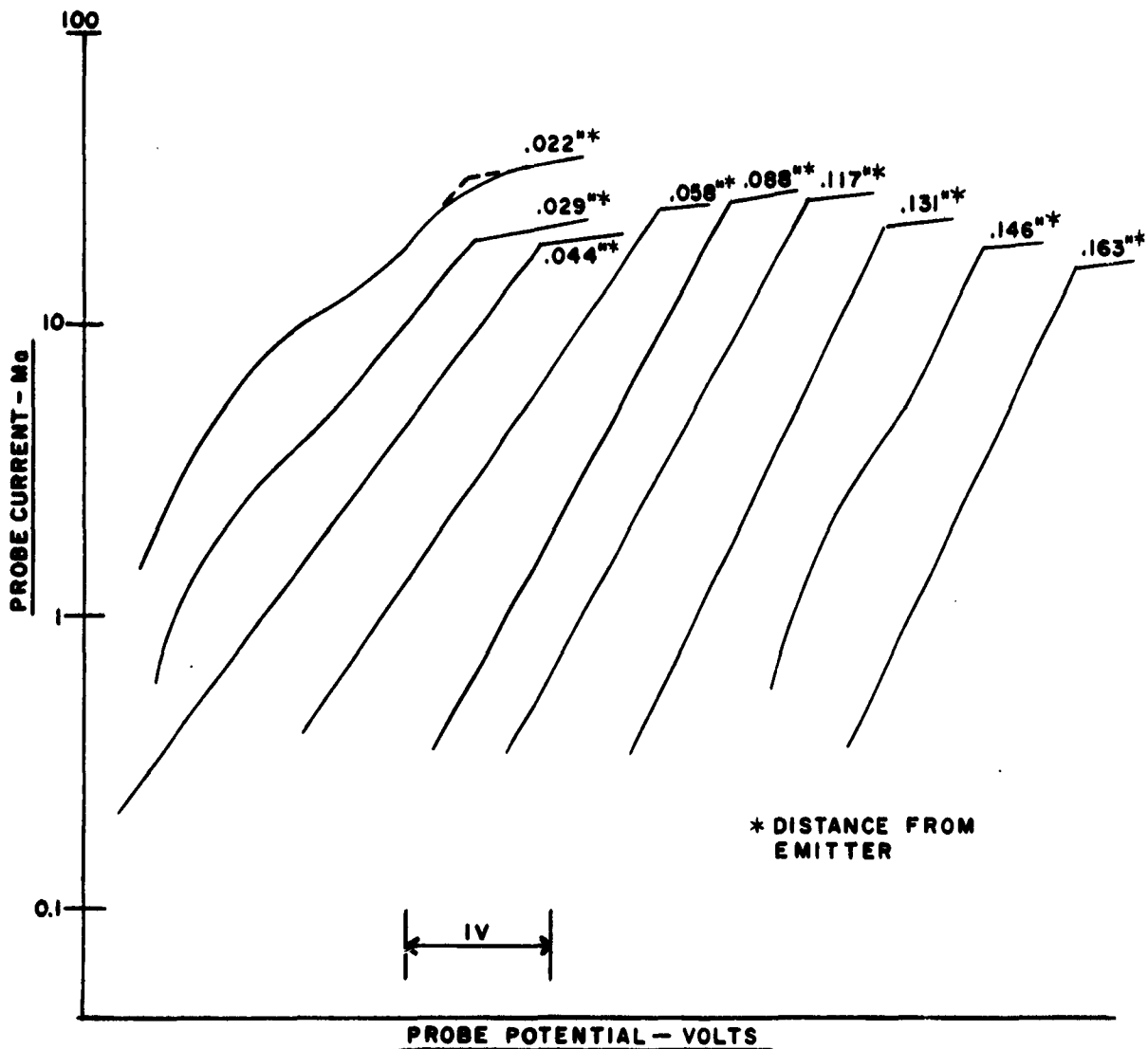

FIGURE 36

PROBE CHARACTERISTICS OBTAINED ALONG CENTRAL AXIS OF METAL-CERAMIC CONVERTER TC-230 ($J = 6.5$ AMPS / CM^2)

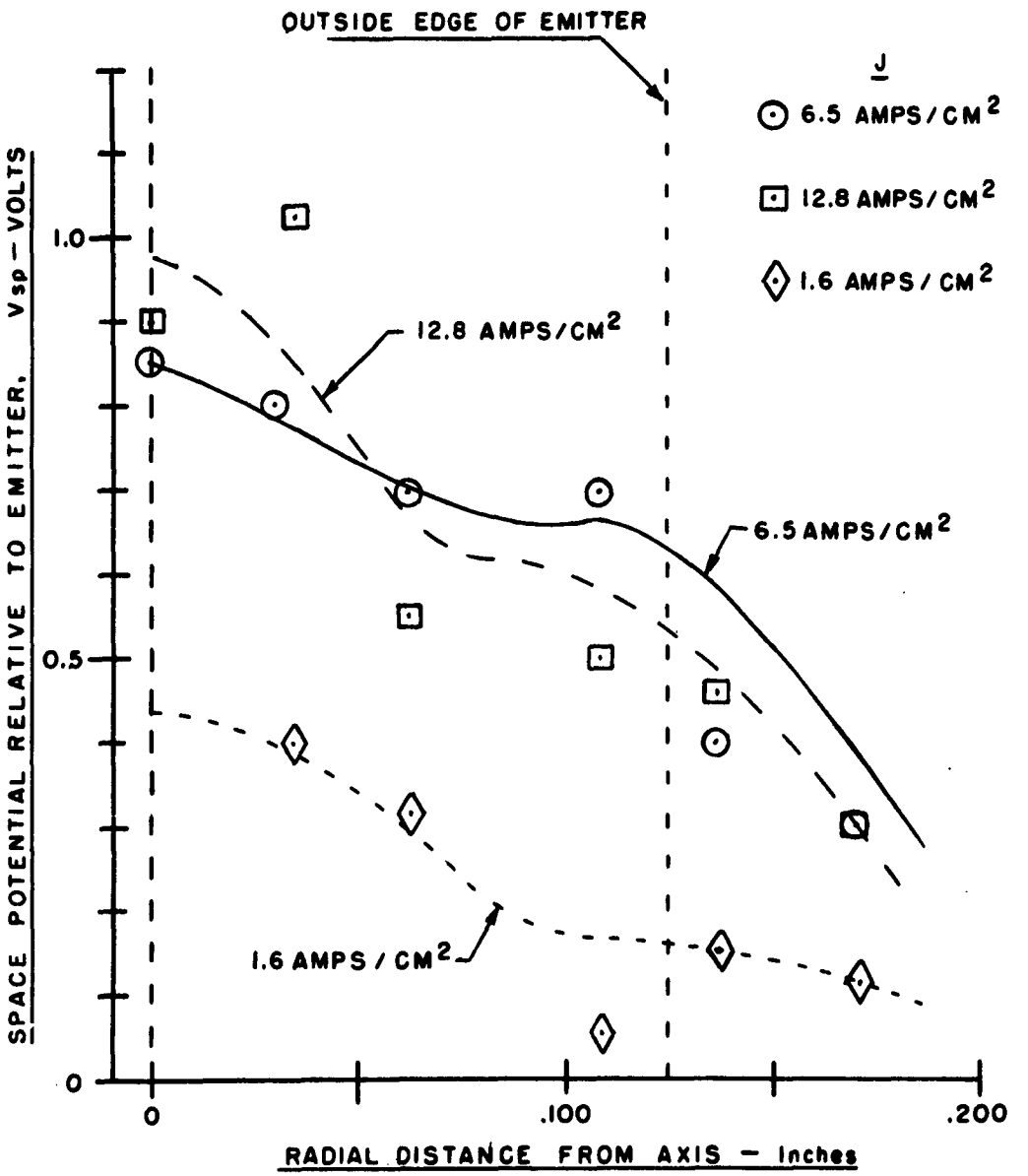

FIGURE 37

RADIAL VARIATION OF SPACE POTENTIAL FOR VARIOUS OUTPUT CURRENT DENSITIES IN METAL-CERAMIC CONVERTER, TC-230

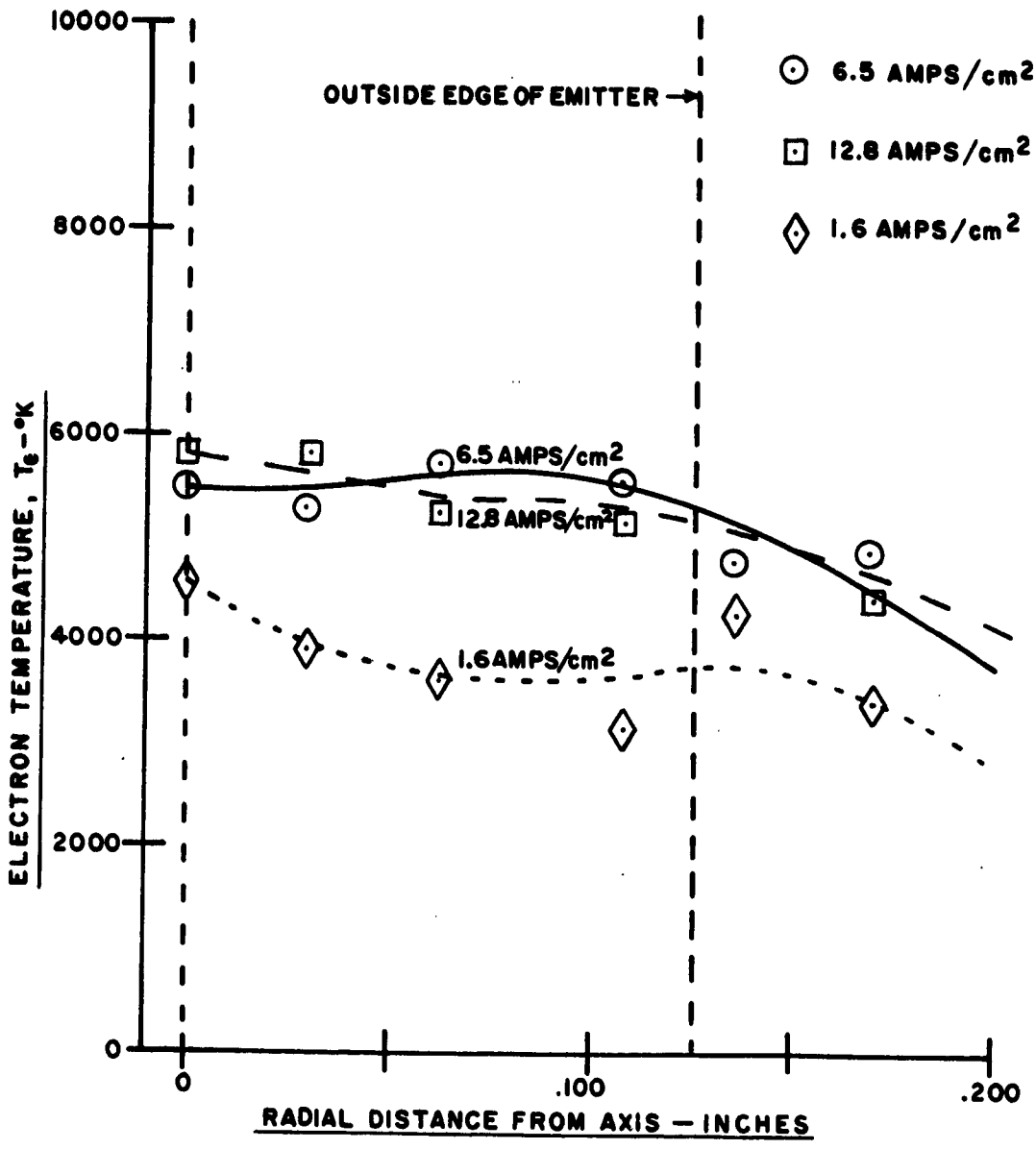

FIGURE 38

RADIAL VARIATION OF ELECTRON TEMPERATURE FOR VARIOUS OUTPUT CURRENT DENSITIES IN METAL-CERAMIC CONVERTER, TC-230

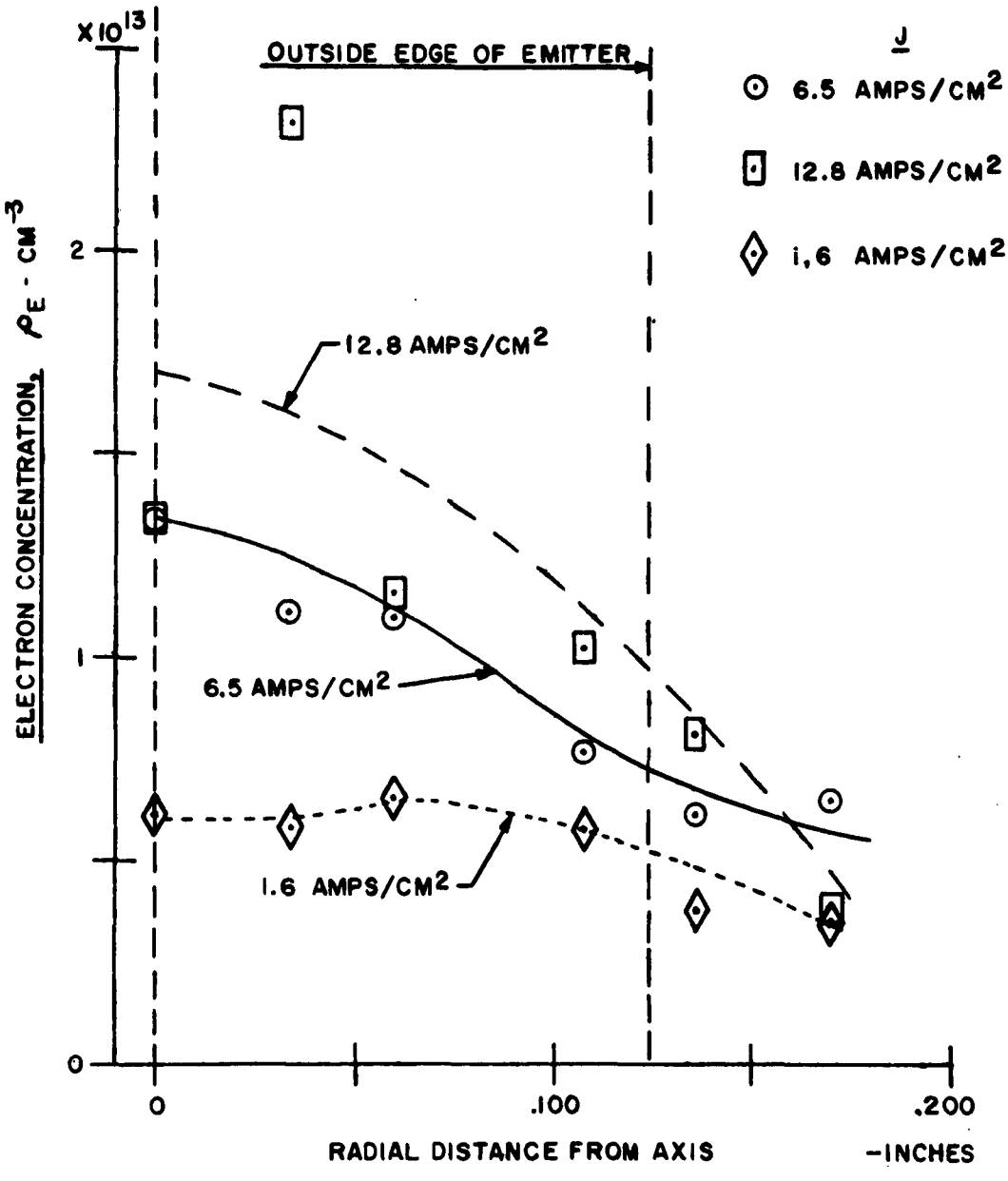

FIGURE 39

RADIAL VARIATION OF ELECTRON CONCENTRATION FOR VARIOUS OUTPUT CURRENT DENSITIES IN METAL-CERAMIC CONVERTER TC-230

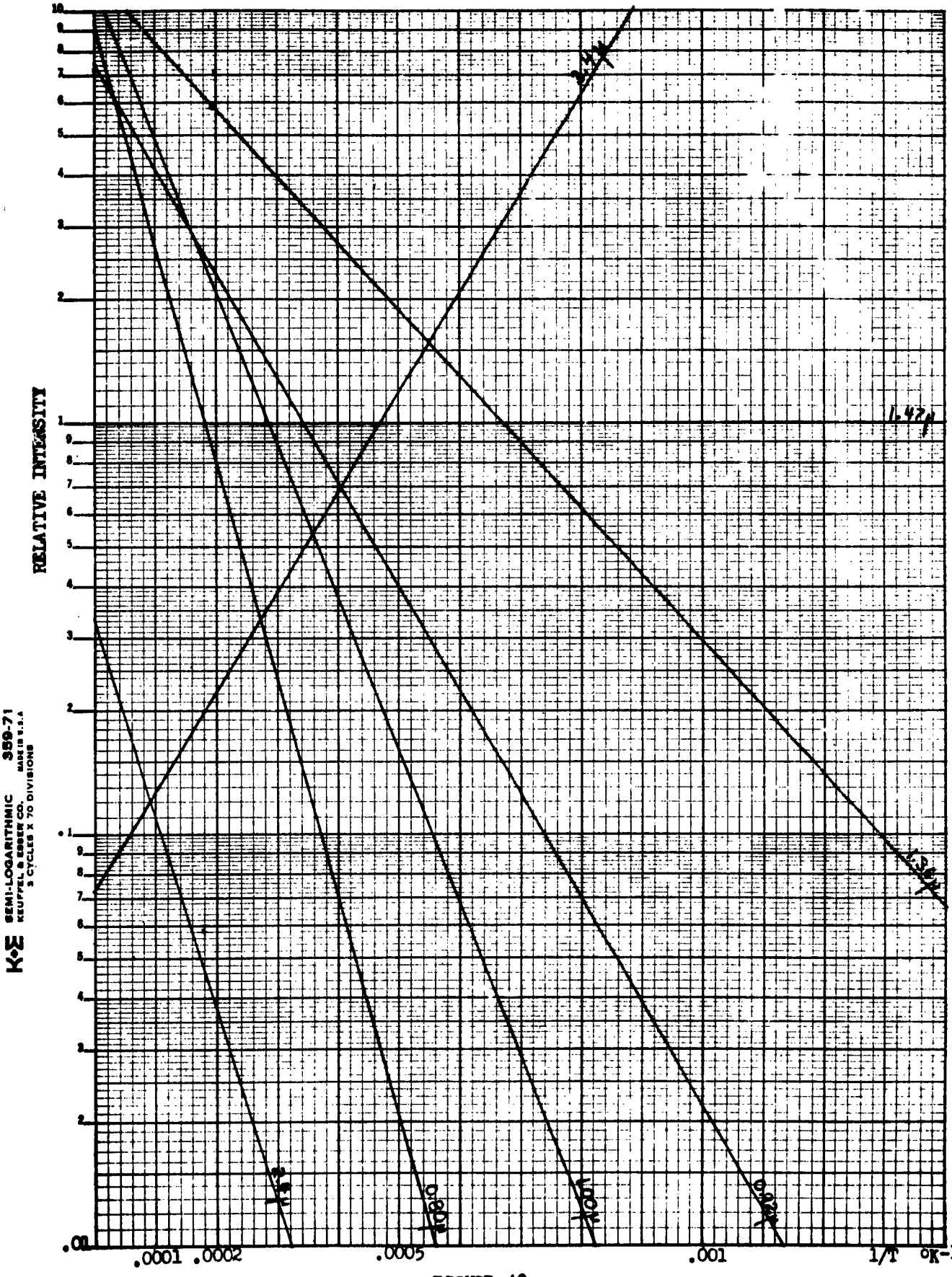
RELATIVE INTENSITY
K&E SEMI-LOGARITHMIC 359-71
KEUFFEL & ESSER CO. MADE IN U.S.A.
3 CYCLES X 70 DIVISIONS
2.3μ
1.47μ
1.25μ
0.98μ
0.80μ
0.62μ
.0001 .0002 .0005 .001
1/T °K-1

FIGURE 40

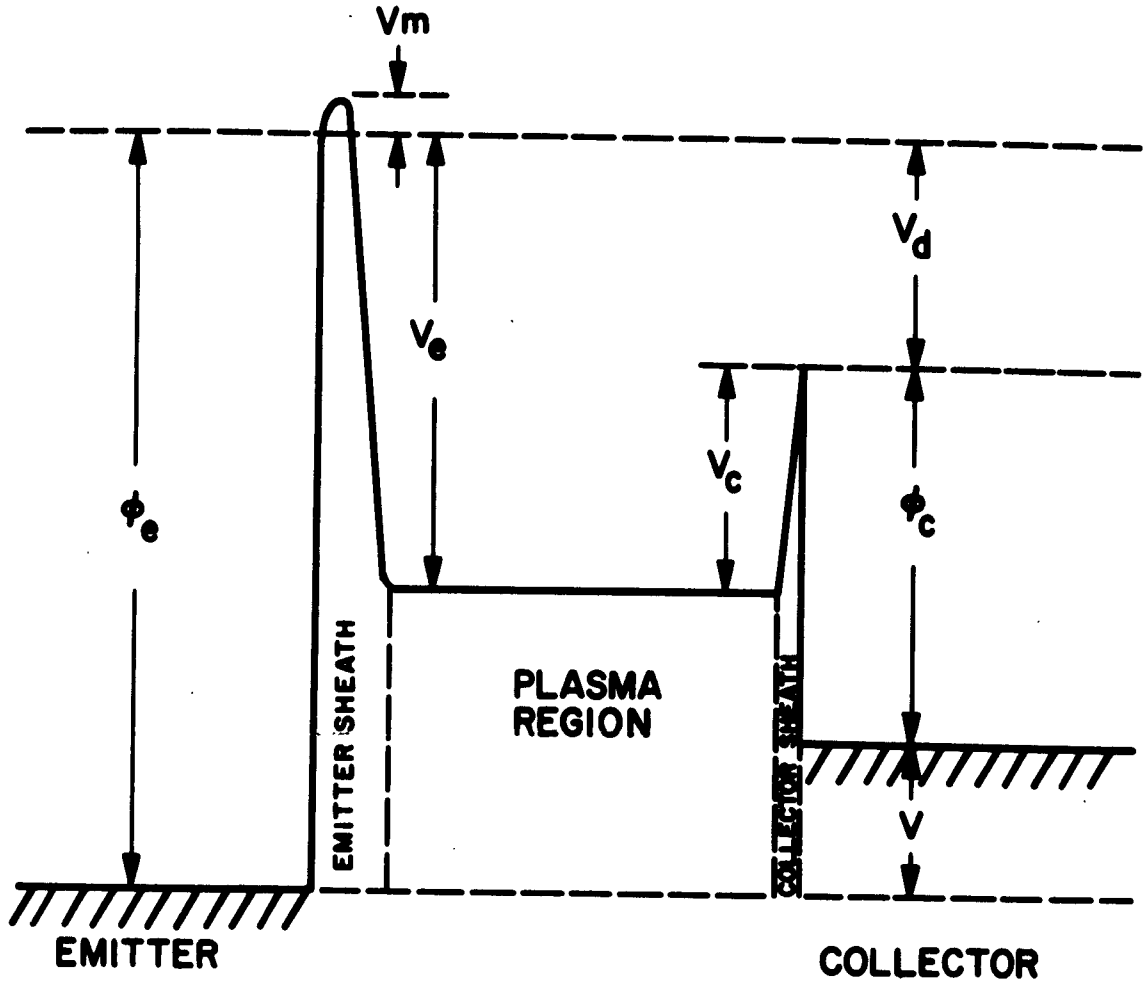

FIGURE 41
ELECTRON POTENTIAL DIAGRAM FOR THE LOW TEMPERATURE CESIUM VAPOR THERMIONIC CONVERTER.

TC-75

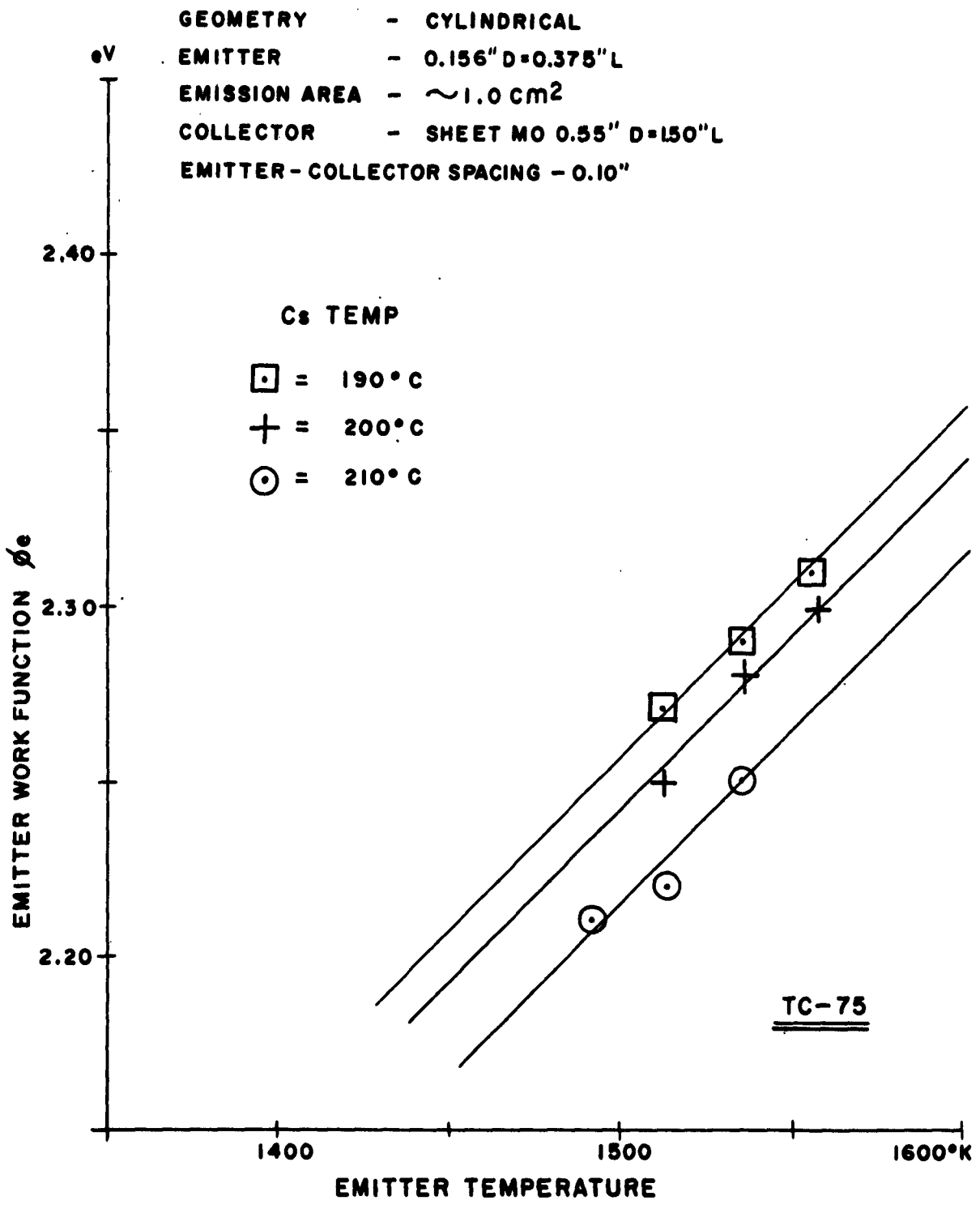

FIGURE 42

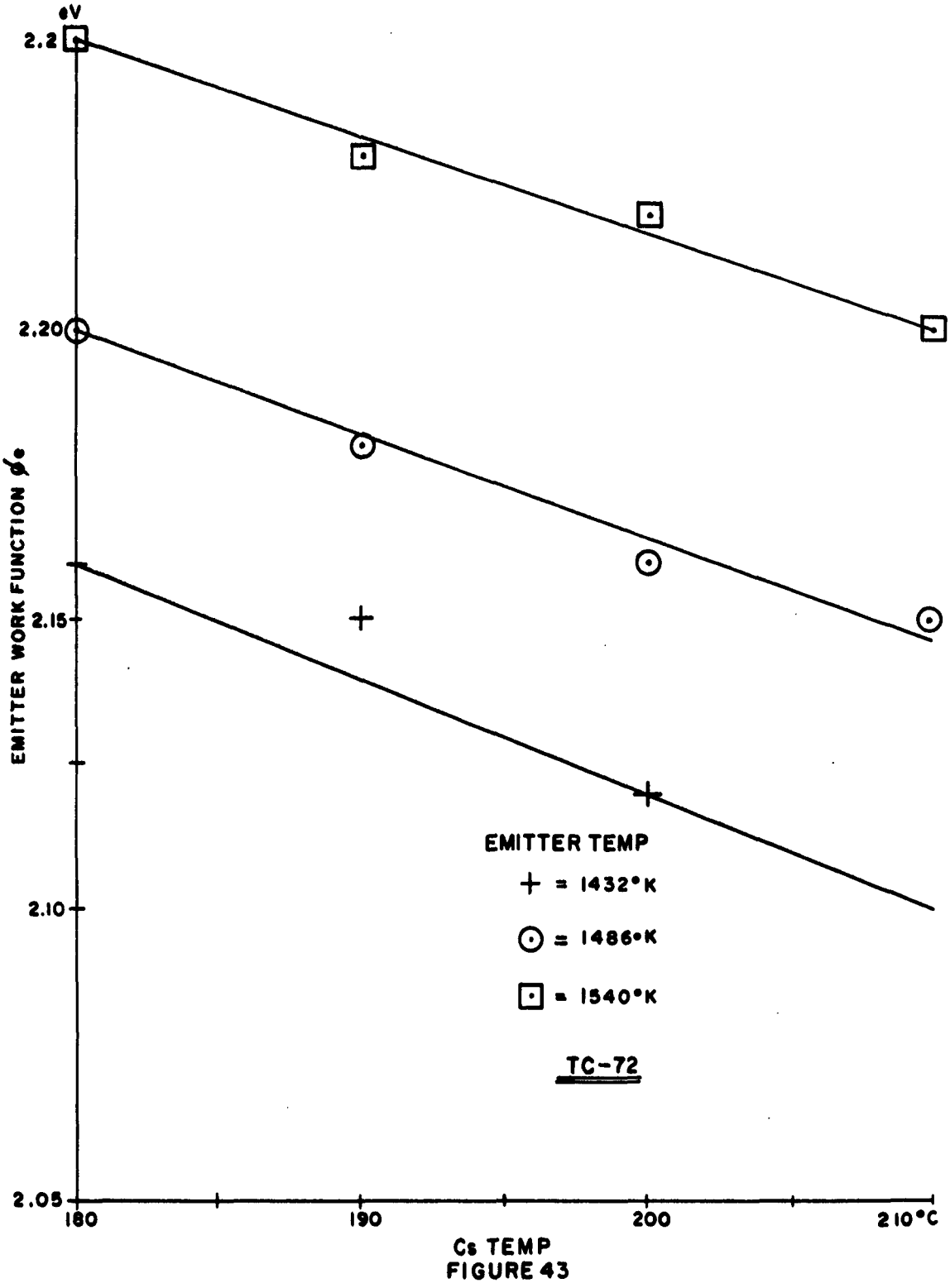
eV
2.2
2.20
2.15
2.10
2.05
EMITTER WORK FUNCTION ϕe
EMITTER TEMP
+ = 1432°K
⊙ = 1486°K
⊡ = 1540°K
TC-72
180
190
200
210°C
Cs TEMP
FIGURE 43

DISTRIBUTION LIST

	No. Copies
Office of Naval Research Power Branch (Code 429) Department of the Navy Washington 25, D.C.	4
Cognizant ONR Area Branch Office	1
U.S. Naval Research Laboratory Technical Information Division Washington 25, D.C.	6
U.S. Naval Research Laboratory Washington 25, D.C. Attn: Code 6430	1
Commanding Officer Office of Naval Research Branch Office Box 39 Navy #100 Fleet Post Office New York, N.Y.	2
Office of Technical Services Department of Commerce Washington 25, D.C.	1
Armed Services Technical Information Agency Arlington Hall Station Arlington 12, Virginia	10
National Aeronautics and Space Administration 1520 H Street, N.W. Washington 25, D.C. Attn: James J. Lynch	1
National Aeronautics and Space Administration Lewis Research Center 2100 Brookpark Road Cleveland 35, Ohio	
Attn: Frank Rom	1
Roland Breitwieser	1
Bernard Lubarsky	1
Chief of Naval Operations (OP-07G) Department of the Navy Washington 25, D.C.	1

DISTRIBUTION LIST (cont'd)

	No. copies
Commandant, U.S. Marine Corps Code CSY - 3 Headquarters, Marine Corps. Washington 25, D.C.	1
Chief, Bureau of Ships Department of the Navy Washington 25, D.C. Attn: Code 342B Code 1500, Mr. Wm. Hewitt Code 456B, Mr. V. Gardner Code 335	 2 1 1 2
U.S. Atomic Energy Commission Division of Reactor Development Washington 25, D.C. Attn: Auxiliary Power Branch Direct Conversion Branch Army Reactor and Water Systems Branch	 1 1 1
U.S. Atomic Energy Commission San Francisco Operations Office 211 Bancroft Way Berkeley 4, California Attn: Reactor Division	 1
Aeronautical Systems Division ASRMFP-2 Wright Patterson Air Force Base Ohio	 1
Air Force Cambridge Research Center (CRZAP) L.G. Hanscom Field Bedford, Massachusetts	 1
Power Information Center University of Pennsylvania Moore School Building 200 South 33rd Street Philadelphia 4, Pennsylvania	 1
Director of Special Projects (SP-001) Department of the Navy Washington 25, D.C.	 10

DISTRIBUTION LIST (cont'd)

	No. copies
Los Alamos Scientific Laboratory P.O. Box 1663 Los Alamos, New Mexico Attn: Dr. George M. Grover	1
Argonne National Laboratory 9700 South Cass Avenue Argonne, Illinois Attn: Aaron J. Ulrich	1
Director, Advanced Research Projects Agency The Pentagon Washington 25, D.C. Attn: Dr. John Huth	1
U.S. Army Signal R and D Laboratory Fort Monmouth, New Jersey Attn: Emil Kittil	1
Mr. A. J. Underwood Manager, General Motors Research Labs. 12 Mile and Mound Road Warren, Michigan Attn: Dr. F. Jamerson	1
Atomics International P.O. Box 309 Canoga Park, California Attn: Dr. R.C. Allen	1
General Atomic P.O. Box 608 San Diego 12, California Attn: Dr. R. W. Pidd	1
Aracon Laboratories Virginia Road Concord, Massachusetts Attn: Dr. S. Ruby	1
Ford Instrument Company 31-10 Thomson Avenue Long Island City, N. Y. Attn: T. Jarvis	1

DISTRIBUTION LIST (cont'd)

	No. copies
Armour Research Foundations 10 W. 35th Street Chicago 16, Illinois Attn: Dr. P.W. Levinson	1
Jet Propulsion Laboratory California Institute of Technology 4800 Oak Grove Drive Pasadena, California	1
RCA Laboratories David Sarnoff Research Center Princeton, New Jersey Attn: Dr. Paul Rappaport	1
The Martin Corporation Baltimore 3, Maryland Attn: Dr. M. Talaat	1
Thermo Electron Engineering Corporations 85 First Avenue Waltham 54, Massachusetts Attn: Dr. George Hatsopoulos	1
Hughes Research Laboratories 3011 Malibu Canyon Road Malibu, California Attn: Dr. R. C. Knechtli	1
Thomson Ramo Wooldrige, Inc. 7209 Platt Avenue Cleveland 4, Ohio Attn: Wm. J. Leovic	1
General Electric Research Laboratory Schenectady, New York Attn: Dr. V.C. Wilson	1
The Marquardt Corporation ASTRO Division 16555 Saticoy Street Van Nuys, California Attn: A. N. Thomas	1

DISTRIBUTION LIST (cont'd)

	No. copies
Texas Instruments Inc. P.O. Box 5474 Dallas 22, Texas Attn: Dr. R.A. Chapman	1
University of Denver Colorado Seminary Denver Research Institute Denver 10, Colorado Attn: Dr. Charles B. Magee	1
Radio Corp. of America Electron Tube Division Lancaster, Pennsylvania Attn: F.G. Block	1
Electro Optical Systems, Inc. 125 N. Kinedo Avenue Pasadena, California Attn: A. Jensen	1
General Electric Company P.O. Box 846 Atomic Product Division Vallecitos Laboratory Pleasenton, California Attn: Robert Scott	1
General Electric Company Power Tube Division 1 River Road Schenectady 5, New York Attn: Mr. Wm. Miller	1
Consolidated Controls Corporation Bethel, Connecticut Attn: Mr. David Mends	1
Institute for Defense Analysis 1666 Connecticut Avenue, N.W. Washington, D.C. Attn: Mr. Robert Hamilton	1

Ford Instrument Co., Div. of Sperry Rand Corp. 31-10 Thomson Avenue, Long Island City 1, N.Y. LO-TEMP THERMIONIC PLASMA STUDY, by Wolfram Stenzel. 31 January 1963. 120 p. illus. (Task 099-356) (Final Report) (Contract Nonr 3416(00))

Unclassified Report

Measurements of electron temperature, electron concentration and space potential in the plasma region of low temperature thermionic converters were determined by means of a pulsed Langmuir probe technique. The spatial distributions of these parameters, in parallel plate geometry, were measured with the aid of movable probes within these operating converters. The experimental values are shown to be consistant with reasonable physical models. Spectroscopic measurements were made in both the visible and infrared regions and the validity and applicability of the results are discussed. Results obtained from converters, in which small amounts of oxygen were present in the discharge region, are explored. The effects of cesium and "patch effects" on the surface characteristics of impregnated tungsten emitters are discussed on the basis of a theoretical analysis and experimental results with numerous test cells.

UNCLASSIFIED

1. Thermionic emission

UNCLASSIFIED

Ford Instrument Co., Div. of Sperry Rand Corp. 31-10 Thomson Avenue, Long Island City 1, N.Y. LO-TEMP THERMIONIC PLASMA STUDY, by Wolfram Stenzel. 31 January 1963. 120 p. illus. (Task 099-356) (Final Report) (Contract Nonr 3416(00))

Unclassified Report

Measurements of electron temperature, electron concentration and space potential in the plasma region of low temperature thermionic converters were determined by means of a pulsed Langmuir probe technique. The spatial distributions of these parameters, in parallel plate geometry, were measured with the aid of movable probes within these operating converters. The experimental values are shown to be consistant with reasonable physical models. Spectroscopic measurements were made in both the visible and infrared regions and the validity and applicability of the results are discussed. Results obtained from converters, in which small amounts of oxygen were present in the discharge region, are explored. The effects of cesium and "patch effects" on the surface characteristics of impregnated tungsten emitters are discussed on the basis of a theoretical analysis and experimental results with numerous test cells.

UNCLASSIFIED

1. Thermionic emission

UNCLASSIFIED

Ford Instrument Co., Div. of Sperry Rand Corp. 31-10 Thomson Avenue, Long Island City 1, N.Y. LO-TEMP THERMIONIC PLASMA STUDY, by Wolfram Stenzel. 31 January 1963. 120 p. illus. (Task 099-356) (Final Report) (Contract Nonr 3416(00))

Unclassified Report

Measurements of electron temperature, electron concentration and space potential in the plasma region of low temperature thermionic converters were determined by means of a pulsed Langmuir probe technique. The spatial distributions of these parameters, in parallel plate geometry, were measured with the aid of movable probes within these operating converters. The experimental values are shown to be consistant with reasonable physical models. Spectroscopic measurements were made in both the visible and infrared regions and the validity and applicability of the results are discussed. Results obtained from converters, in which small amounts of oxygen were present in the discharge region, are explored. The effects of cesium and "patch effects" on the surface characteristics of impregnated tungsten emitters are discussed on the basis of a theoretical analysis and experimental results with numerous test cells.

UNCLASSIFIED

1. Thermionic emission

UNCLASSIFIED

Ford Instrument Co., Div. of Sperry Rand Corp. 31-10 Thomson Avenue, Long Island City 1, N.Y. LO-TEMP THERMIONIC PLASMA STUDY, by Wolfram Stenzel. 31 January 1963. 120 p. illus. (Task 099-356) (Final Report) (Contract Nonr 3416(00))

Unclassified Report

Measurements of electron temperature, electron concentration and space potential in the plasma region of low temperature thermionic converters were determined by means of a pulsed Langmuir probe technique. The spatial distributions of these parameters, in parallel plate geometry, were measured with the aid of movable probes within these operating converters. The experimental values are shown to be consistant with reasonable physical models. Spectroscopic measurements were made in both the visible and infrared regions and the validity and applicability of the results are discussed. Results obtained from converters, in which small amounts of oxygen were present in the discharge region, are explored. The effects of cesium and "patch effects" on the surface characteristics of impregnated tungsten emitters are discussed on the basis of a theoretical analysis and experimental results with numerous test cells.

UNCLASSIFIED

1. Thermionic emission

UNCLASSIFIED